D20

THE AERODYNAMIC CHALLENGES OF THE
DESIGN AND DEVELOPMENT OF THE SPACE SHUTTLE ORBITER

LEAD AUTHORS
James C. Young and Jimmy M. Underwood
NASA Johnson Space Center
Houston, TX

CO-AUTHORS
Ernest R. Hillje, Arthur M. Whitnah, Paul O. Romere,
Joe D. Gamble, and Barney B. Roberts
NASA Johnson Space Center
Houston, TX

George M. Ware, William I. Scallion,
Bernard Spencer, Jr. and James P. Arrington
NASA Langley Research Center
Hampton, VA

Deloy C. Olsen
Rockwell/Space Systems Group
Downey, CA

ABSTRACT

The major aerodynamic design challenge at the beginning of the United States Space Transportation System (STS) research and development phase was to design a vehicle that would fly as a spacecraft during early entry and as an aircraft during the final phase of entry. The design was further complicated because the envisioned vehicle was statically unstable during a portion of the aircraft mode of operation. The second challenge was the development of preflight aerodynamic predictions with an accuracy consistent with conducting a manned flight on the initial orbital flight.

This paper presents a brief history of the early contractual studies highlighting the technical results and management decisions influencing the aerodynamic challenges. The configuration evolution and the development of preflight aerodynamic predictions will be reviewed. The results from the first four test flights shows excellent agreement with the preflight aerodynamic predictions over the majority of the flight regimes. The only regimes showing significant disagreement is confined primarily to early entry, where prediction of the basic vehicle trim and the influence of the reaction control system jets on the flow field were found to be deficient. This paper concludes with an analysis of postflight results to attempt to explain these prediction deficiencies.

INTRODUCTION

A traditional phased approach was used in the programmatic design evolution of the Space Shuttle. The concept evaluation phase (Phase A) contractural studies were conducted in 1969. The Phase B concept definition phase extended over approximately 2 years beginning in mid 1970. The research and development phase (Phase C) and the production and flight test phase (Phase D) began with selection of Rockwell International as prime contractor in August 1972.

The following sections begin with background information which presents a brief review of the Phase A and B studies. The study results and management decisions which influenced the aerodynamic design are highlighted.

The remainder of the paper addresses the challenges facing the aerodynamic analyst at the beginning of Phase C & D, the approach used in attacking these challenges, and the success with which these challenges were conquered. The paper concludes with a review of the postflight analysis activity.

NOMENCLATURE

ACRONYMS

ADDB	Aerodynamic Design Data Book
AFFTC	Air Force Flight Test Center
AEDC	Arnold Engineering Development Center
ALT	Approach and Landing Test
ARC	NASA Ames Research Center
ASI	Aero Stick Input
ATP	Authority to Proceed
CDR	Critical Design Review
DFRC	Dryden Flight Research Center
EAFB	Edwards Air Force Base
ETR	Eastern Test Range
FCF	First Captive Flight
FCS	Flight Control System
FMOF	First Manned Orbital Flight
GN&C	Guidance, navigation, and control
JSC	NASA Johnson Space Center
KSC	NASA Kennedy Space Center
LaRC	NASA Langley Research Center (also LRC)
LTV	Ling-Temco-Vought Corporation
MSFC	Marshall Space Flight Center
NASA	National Aeronautics and Space Administration
OADB	Operational Aerodynamic Data Book
OFT	Orbital flight test
OML	Outer Moldline
OMS	Orbital Maneuvering System
OV	Orbital Vehicle
PDR	Preliminary Design Review
PRR	Program Requirements Review
PTI	Programmed Test Input
PWT	Propulsion Wind Tunnel
RCS	Reaction Control System
RSI	Reusable Surface Insulation
SEB	Source Evaluation Board
SRR	Systems Requirements Review
SSME	Space Shuttle Main Engine
STS	Space Transportation System
TAEM	Terminal Area Energy Management
TPS	Thermal Protection System
TWT	Transonic Wind Tunnel
UPWT	Unitary Plan Wind Tunnel
VAFB	Vandenberg Air Force Base
VKF	Von Karman Facility
WTR	Western Test Range

SYMBOLS

b	Reference wing span, ft
C_A	Axial force coefficient
C_D	Drag force coefficient
C_L	Lift coefficient
C_ℓ	Rolling moment coefficient
C_{ℓ_β}	Effective-dihedral parameter, per degree
$C_{\ell_{\delta_a}}$	Aileron roll-control effectiveness, per degree
$C_{\ell_{\delta_r}}$	Rolling moment coefficient derivative with respect to rudder, per degree
C_m	Pitching moment coefficient

C_{m_α} Longitudinal static stability parameter, per degree

$C_{m_{\delta_e}}$ Elevon pitch control effectiveness, per degree

C_N Normal force coefficient

C_n Yawing moment coefficient

C_{n_β} Directional-stability parameter, per degree

$C_{n_{\delta_a}}$ Yawing moment due to aileron deflection, per degree

$C_{n_{\delta_r}}$ Rudder yaw-control effectiveness, per degree

C_Y Side-force coefficient

C_{Y_β} Side-force coefficient derivative with respect to sideslip, per degree

$C_{Y_{\delta_a}}$ Side-force coefficient derivative with respect to aileron, per degree

$C_{Y_{\delta_r}}$ Side-force coefficient derivative with respect to rudder, per degree

C'_∞ Factor of proportionality in linear viscosity-temperature relation

cg   Center of gravity, inch

h   Altitude, ft

L/D   Lift-to-drag ratio

L_B Reference body length, 107.525 ft

M   Free-stream Mach number

MAC   Mean aerodynamic chord, also $\bar{c}$, 39.568 ft

$\dot{m}$ Mass flow, lbm/sec

$\dfrac{\dot{m}_j}{\dot{m}_\infty}$ RCS jet mass flow ratio

n_j Number of RCS jets firing

$\bar{q}$ Dynamic pressure, lb/ft^2

q_∞ Free-stream dynamic pressure, lb/ft^2

R_e Reynolds number

S   Reference area, 2,690 ft^2

V   Velocity

V_D Design touchdown speed

$\bar{V}'_\infty$ Viscous interaction parameter

x   Characteristic length, ft

$\bar{\chi}'$ Viscous interaction parameter

α Angle of attack, deg

β Angle of sideslip, deg

δ_a Aileron deflection angle, (left elevon − right elevon)/2, deg

δ_{BF} Bodyflap deflection, positive for trailing edge down, deg

δ_e Elevator deflection, positive for trailing edge down, (left elevon + right elevon)/2, deg

δ_R Rudder deflection, deg

δ_{SB} Speedbrake deflection, deg

Λ Sweep angle, deg

λ Taper ratio

ρ Mass density of air

ϕ Momentum parameter (lbf)

ϕ Bank angle, deg

$\dfrac{\phi_j}{\phi_\infty}$ RCS jet stream momentum ratio

X_{cp} Longitudinal center of pressure, inch

$RM_{JI_{SFJ}}$ Rolling moment interaction due to side firing jets

$YM_{JI_{SFJ}}$ Yawing moment interaction due to side firing jets

$SF_{JI_{SFJ}}$ Side force interaction due to side firing jets

$PM_{JI_{SFJ}}$ Pitching moment interaction due to side firing jets.

$RM_{JI_{DFJ}}$ Rolling moment interaction due to down-firing jets

Δ Incremental value

SUBSCRIPTS

j Jet exit conditions
∞ Free-stream conditions
s Spanwise shock location

BACKGROUND

The Space Transportation System (STS) was initiated with the "Phase A" conceptual design contracts in 1969. These contracts studied various methods of producing a completely reusable spacecraft system capable of a runway landing. A typical concept is shown in figure 1. The results of the Phase A studies led to the selection of a two-stage, completely reusable vehicle as the focus for "Phase B" contractual studies. The majority of the studies addressed a first stage manned "flyback" booster in combination with an Orbiter second stage as shown in figure 2. Subsequent to staging, the flyback booster utilized air breathing engines to return to the launch site for a runway landing. The Orbiter would continue the launch phase until low earth orbit was achieved. Following a typical on-orbit mission of 5 to 7 days, the Orbiter would re-enter the Earth's

atmosphere at a high angle of attack (up to 60°), ultimately landing on a runway much like a conventional airplane. Midway through Phase B, estimates of system development costs indicated that the peak yearly funding requirements for the parallel development of two manned, fully reusable vehicles would not be a viable programmatic approach. During this time, the second stage fuel tanks were removed from the Orbiter to minimize the impact of any Orbiter weight growth during program development.

In the final months of Phase B, a parallel-burn concept was selected. This concept consisted of the simultaneous burn of both the solid rocket boosters (SRB) and the three liquid-fueled Space Shuttle main engines (SSME). The two SRBs assisted lift-off and the initial ascent flight. The SSMEs, fed by an expendable external tank (ET), continued to burn until near orbital insertion. The orbital maneuvering system (OMS) engines provided the additional delta-velocity required for orbital insertion. Figure 3 shows a Rockwell configuration, which is typical of the four parallel-burn configurations proposed for the Phase C & D contract.

As a result of the Phase B efforts, the Shuttle configuration shown in figure 4 was selected for the design and development phase. It was a partially-reusable vehicle with a parallel-burn propulsion system consisting of recoverable SRB's and an expendable ET used to supply fuel to the three main engines of the completely reusable Orbiter.

In addition to defining the concept for the Phases C & D contract, Phase B studies resulted in several programmatic decisions which significantly influenced the aerodynamic design of the Space Shuttle Orbiter.

The most significant Phase B decision was the selection of the reusable surface insulation (RSI) system rather than a hot-structure system for protection from entry heating. This RSI design

dictated that the initial entry angle of attack (α) should be as high as possible (30° to 50°) to minimize re-entry heating. The U.S. Air Force requirement of a 1100-nautical mile (2037-kilometer) crossrange dictated that α be 30° or lower in order to achieve the required hypersonic L/D. To

reduce re-entry heating, thereby increasing lifetime of the RSI, an α profile of 40° was chosen for those missions not requiring the high crossrange.

Another Phase B decision affecting the future aerodynamic design was to provide for a completely computer-controlled, automated entry. This permitted the design of an entry flight control system (FCS) to artificially provide the required vehicle stability and the proper handling qualities. Traditionally, a relatively large empennage is required to provide the requisite vehicle directional stability. However, augmentation of the aerodynamic stability through the FCS permits the design of a smaller empennage, thus providing a significant reduction in vehicle weight.

Initially in Phase B there was not a design landing velocity on which to size the wing, the major weight driver of the Orbiter. As a consequence, it was difficult to make relative weight comparisons among the various contractor designs. Midway through the Phase B effort, NASA defined a subsonic "design" velocity which was to be used to size the Orbiter wing. This design velocity, later referred to as the design landing velocity, was defined as the trimmed velocity at an angle of attack equivalent to tail scrape angle at touchdown. A design velocity of 165 knots (306 km/hr) was chosen since man-in-the-loop simulations indicated this velocity produced actual touchdown velocities of 180-190 knots (334-352 km/hr). Touchdown velocities of this magnitude were well within the state of the art in landing gear systems. This criteria was used throughout the remainder of the development program.

As an end item product for Phase B each contractor was required to estimate the amount of the Phase C & D wind tunnel testing that would be required for detail design and development. In reviewing these estimates, it became obvious that the aerodynamicist would be faced with properly analyzing, verifying, and documenting the largest wind tunnel development program ever undertaken. Using these contractor estimates, NASA established the Source Evaluation Board (SEB), a total baseline wind tunnel program of 32,000 hours. Proposals of the four contractors called for programs ranging from 27,000 to 50,000 hours. The actual program ultimately accumulated 46,000 hours for the Phase C & D effort.

Although not directly related to the aerodynamic design, two program management decisions were made at the beginning of Phases C & D which significantly affected the magnitude of the challenge to the aerodynamicists. The first decision was to baseline the Orbiter systems configuration at the Authority To Proceed (ATP) milestone. Thereafter, the only design changes permitted were those which were required to fix critical system design problems. The Orbiter systems baseline included not only the vehicle outer mold line (OML) configuration, but guidance, navigation, and control (GN&C) systems and other subsystems. The second decision was to fly a manned, orbital mission on the initial flight of the Space Shuttle system. This philosophy of permitting only mandatory design changes (which became known as "make-work") significantly influenced the management of the aerodynamic and FCS development.

THE CHALLENGES

Strongly influenced by the economic and programmatic decisions previously discussed, three major aerodynamic challenges emerged.

The first challenge was the aerodynamic design of a spacecraft/aircraft that could fly through the entire atmospheric flight regime. The design had to satisfy the conflicting requirements of a spacecraft-like re-entry and a aircraft-like runway landing. It was to be the first winged vehicle to fly through the hypersonic speed regime, providing the first real test of experimental and theoretical technology of high speed flight. No design precedents existed to help establish the design requirements of such a vehicle. Yet, the design had to satisfy the conflicting aerodynamic characteristics of the various flight regimes as well as satisfying the requirements of a completely automated, multi-mode flight control system.

The second challenge was the preflight prediction of the aerodynamic characteristics of a complex vehicle with an accuracy consistent with establishing sufficient confidence to conduct the first orbital flight with a manned vehicle. This required the identification of the proper aerodynamic similarity parameters and overcoming the unknowns of the hypersonic wind tunnel facilities. It called for the efficient conduction and analysis of the most extensive wind tunnel program ever undertaken. And finally, in order to ensure consistency of design, it required careful configuration management of a continuously evolving aerodynamic data base to ensure that at any one point in time all systems and subsystems were using the same set of aerodynamics.

Finally, the third challenge was the technical management of the aerodynamic subsystem, which consisted of the following elements:

a. Integrating and focusing the efforts of a diverse number of organizations from the NASA, DOD, and industry aerodynamic communities.
b. Obtaining the support and ensuring the efficient utilization of virtually every major wind tunnel facility in the United States.
c. Ensuring the proper and timely interface with the other Space Shuttle systems and subsystems.

This paper will primarily address the first two challenges, which are technical. Although the third challenge, technical management, is indirectly addressed, more insight into this challenge may be found in reference 1.

THE APPROACH

The Approach Section reviews the rationale the aerodynamic analyst used in attempting to conquer the aerodynamic challenges. The section begins with a review of the design criteria used to configure the Orbiter. Following this initial section, the program schedule will be delineated. The section concludes with an extensive review of the aerodynamic development.

ORBITER AERODYNAMIC CRITERIA

Aerodynamic criteria[2] for the final selected configuration dictated that the vehicle perform as both a spacecraft and an aircraft during re-entry (figure 5). Accordingly, the external features must be carefully configured to (1) provide the protection and versatility required for orbital and atmospheric flight and (2) the aerodynamic performance, stability, and control necessary for an unpowered descent and landing. The aerodynamic lines must ensure acceptable performance for the hypersonic-to-subsonic speed range and provide the required crossrange and touchdown velocity.

Aerodynamic requirements, as shown in table 1, were developed from analysis of the re-entry phase of the mission. The angle of attack during initial entry was established by the RSI temperature requirement. The center of gravity (cg) requirement resulted from a NASA survey of potential payload users. Aerodynamic static stability was not required, since the design criteria permitted stability augmentation by the FCS to meet aircraft flying qualities criteria. Early entry flight simulations identified a FCS requirement for longitudinal static stability of no more than 2% L_B (5.44 % MAC) unstable at the aft cg. These requirements defined the aerodynamic design criteria for pitching moment characteristics. The subsonic lift-to-drag ratio (L/D) was set by the minimum value necessary for a safe landing.

The final Orbiter configuration, as shown in figure 6, evolved from a series of program and technical refinements directed to achieve the vehicle yielding the best combination of performance and cost. This evolution is discussed further in a later section. Figure 7 presents the general sizing criteria for the various components of the Orbiter. The double-delta wing planform, combined with a fuselage of moderately low fineness-ratio (approximately five), minimizes the interference heating effects, provides the required hypersonic crossrange, and possesses an acceptable trim and stability range over the flight Mach number range.

The subsonic design velocity was increased to 171 knots (88 m/sec) in order to reduce the Orbiter wing size thereby reducing vehicle weight. The leading edge sweep angle ($\Lambda = 45^o$) and aspect ratio (2.265) were selected on the basis of aerothermodynamic trade studies to provide the design touchdown speed for a cg at the forward limit with minimum wing size. This optimized the wing leading edge thermal protection system for a reuse cycle of 100 flights before major rework.

The fuselage was designed to accommodate a variety of payloads and to house the crew. It also was designed to contain the propulsion systems for launch and orbital maneuvering as well as provide a support structure for the main engines. The size of the payload bay was a contract specification. The size of the base of the fuselage was dictated by the packaging of the SSME's. The forward fuselage was dictated by packaging of the crew compartment. Nose camber and cross section, along with upward sloping forebody sides, were selected to improve hypersonic pitch trim and directional stability. And in conjunction with wing-body blending, to reduce entry heating on the body sides. Reaction control system (RCS) jets for entry attitude control and orbital maneuvering engines were incorporated in pods located in the aft body fairings. The orbital maneuvering system (OMS) pods

were sized for the OMS tankage. The bodyflap, originally sized to provide thermal protection for the SSME's during entry, is now also used as the primary pitch trim device.

The vertical tail was sized to provide a low speed C_{n_β} of 0.0013 at an angle of attack of 13° about a center of gravity located at the aft limit. It has a reference area of 413.25 ft^2 (38.39 m^2) including the rudder/speedbrake. The section profile consists of a 5° half-angle double-wedge airfoil. The rudder is split along the Orbiter plane of symmetry to provide directional stability augmentation in the hypersonic/supersonic flight regimes, and to apply drag modulation for the subsonic flight phase, approach, and landing.

DEVELOPMENT APPROACH

The Development Approach will initially address the development schedule followed by a review of the configuration evolution.

DEVELOPMENT SCHEDULE

Major program milestones for Phase C & D are illustrated in figure 8. They start with the ATP in August 1972 and culminate with initial operational capability in 1982. The Orbiter concept at ATP was a blended delta wing vehicle based on precontract studies and configured to meet initial Space Shuttle Program requirements. As a result of a continuing assessment of system requirements and technical refinements early in the contract, the Orbiter concept was modified to reduce weight and decrease program and operating costs.[3] Refinements in the aerodynamic configuration led to a double-delta planform incorporating a more efficient lifting surface than the blended delta. The System Requirements Review (SRR) in August 1973, finalized the technical requirements for the Space Shuttle systems (i.e., the total vehicle, its elements, and their ground systems) and approved the design approach of the vehicle and associated support equipment. The Preliminary Design Review (PDR) cf the first Orbiter vehicle (OV-101) and subsystems for the approach and landing flight test (ALT) program were completed in February 1974. The PDR of the second Orbiter Vehicle (OV-102) followed in March 1975. OV-101 rollout from final assembly in Palmdale, California, took place in September 1976. The ALT Program consisted of three parts: (1) Orbiter/747 mated; (2) tailcone-on Orbiter alone; and (3) tailcone-off Orbiter alone. The vehicle was mated to the Boeing 747 carrier aircraft at the Dryden Flight Research Center (DFRC), Edwards Air Force Base, and the first captive flight was completed in February 1977. The first ALT flight of OV-101 from the Boeing 747 took place on August 12, 1977. A detailed review of the ALT program is presented in reference 4. In March 1978, OV-101 was delivered to the Marshall Space Flight Center (MSFC), Alabama, for ground vibration testing.

Fabrication and assembly of OV-102, the first orbital vehicle, began in 1975, and the Critical Design Review (CDR) was conducted in July 1977. Rollout of OV-102 was accomplished in March 1979, with delivery to Kennedy Space Center, Florida occurring a few weeks later. The first manned orbital flight was conducted in April 1981. The official Orbital Flight Test (OFT) program was established as the first four flights (STS-1 thru -4) with the initial operational capability starting with STS-5 in November 1982. However, aerodynamic flight test maneuvers are planned through STS-17.

CONFIGURATION EVOLUTION

Stability, control, and performance requirements for the Orbiter vehicle are, for the most part, established by the entry phase of the mission. On the other hand, design airload conditions are primarily driven by the ascent phase.

Design issues keyed to achieving the proper aerodynamic balance to provide stability, control, and center of gravity envelope during the entry flight regime are: (1) wing design, (2) wing-body integration, and (3) integration of aerodynamic and flight control requirements. Wing design was key because of its influence on vehicle weight, thermal environment, aerodynamic stability, buffet characteristics, and gliding and landing performance capability. Wing-body integration was important in obtaining a balanced aerodynamic configuration capable of trim and control over the entire speed range, and in minimizing thermal environment due to interference flow effects. Fuselage dimensions were largely fixed by payload size and packaging efficiency while aerodynamic and aerothermodynamic considerations established forebody shape and local contours. Integration of aerodynamic control requirements was of major importance in meeting flying quality goals in all

flight regimes, and minimizing vehicle weight as affected by control surface arrangement, size, and actuator requirements.

Prior to Shuttle Program "go-ahead" in August 1972, NASA funded extensive Shuttle System trade-off studies (Phase B contracts) to determine the following: (1) operational cost effectiveness; (2) desired configuration and geometry; (3) major subsystem definition; (4) configuration drivers consisting of landing speed, payload size and weight, and center of gravity envelope; (5) entry crossrange and aerodynamic heating; (6) stability and control requirements; and (7) flying qualities. From these studies emerged a baseline configuration at Shuttle Program ATP. Following ATP, further trade studies were conducted by JSC and the prime contractor to refine the baseline design.[5] Essentially four aerodynamic configurations were evaluated before the final baseline design was selected.

The phasing of the evolving configuration is illustrated in figure 10. The Rockwell blended delta configuration was baselined at ATP, with only "make-work" design changes permitted thereafter. The vehicle was sized for a dry weight of 170,000 lb, (77,110 kg) and landing payload of 40,000 lbs (18,144 kg). Initial wind tunnel tests indicated the ATP configuration did not meet the landing performance requirements. Wing optimization to meet these requirements led to baselining a configuration for the December 1972 Program Requirements Review (PRR).

The "make-work" philosophy was interrupted late in 1972 by a change in system requiremements prompted by NASA's desire to reduce the operational cost per flight. This requirement update reduced the vehicle dry weight to 150,000 lbs (60,039 kg) and landing payload to 32,000 lbs (14,515 kg).

In addition to this requirement change, Rockwell was directed by NASA to incorporate the double-delta wing design. A year of NASA in-house study indicated the double-delta wing had exceptional landing performance. In addition the aerodynamic stability and trim could be adjusted by modifying the lightly loaded forward delta (glove). This simple control of aerodynamic features allowed the design of the main delta wing box to be frozen. Any cg or aerodynamic stability problems which might surface during program development could then be corrected by glove modification thereby minimizing program impact.

During this period, the maximum utilization of uniform dimension tiles was baselined in an attempt to minimize the RSI production and installation costs. Incorporation of this "standard" tile design, led to a vehicle whose surface was composed of large flat areas, limiting curvature to smaller areas between the flat ones.

These changes in system requirements and design led to baselining a new configuration for the March 1974 PDR. Initial wind tunnel tests of this PDR configuration indicated the configuration was not workable. Aerodynamic tests showed difficulty in providing trim capability at the forward cg in the supersonic flight regime. Aeroheating tests indicated the blunt fuselage nose resulted in early transitional flow and high temperatures along the lower body surface. Also wing incidence, camber, and thickness distributions designed for maximum subsonic performance led to local fairings on the lower wing and fuselage surfaces which caused high local heating. These findings led to a configuration modification of the Orbiter to eliminate these deficiences.

Ensuing wind tunnel tests indicated the revision of the PDR configuration was an acceptable configuration. After minor changes, such as blunting the forward portion of the OMS pod to allow the aft payload bay to open 180°, this configuration was baselined as the CDR configuration at the OV-102 PDR in February 1975.

After a flurry of configuration development activity in the first 7 months of the Phase C & D contract, the aerodynamic configuration remained relatively stable allowing the aerodynamic effort to focus on the development and verification of the preflight aerodynamic predictions.

AERODYNAMIC DEFINITION APPROACH

Conventional flight test programs call for the incremental expansion of the flight envelope to demonstrate the design capability of the aircraft. This is not feasible with the Shuttle vehicle. Once the Shuttle is launched, it is committed for flight over the complete mission profile from ascent to orbital insertion, deorbit, re-entry, and landing. Predicted flight characteristics must be based on aerodynamic data derived from theory, ground testing, and analysis. Careful attention has been given to the interactions between flight control systems design and aerodynamic characteristics. Because of these considerations great care had to be exercised in the development

of the preflight aerodynamic estimates. This section of this paper addresses the management, development and verification of the preflight aerodynamic predictions.

TYPICAL ORBITER MISSION

At an altitude of approximately 600,000 ft, the Orbiter is designed to perform an unpowered, gliding re-entry at an angle of attack of approximately 40°. The angle of attack is modulated depending upon the crossrange requirements. Downrange modulation is achieved by periodically performing bank reversals across the prescribed ground track. Figure 11 presents a typical re-entry trajectory.

Although entry interface (EI) is defined as 400,000 ft altitude, a sensible atmosphere is not reached until Mach 27 at an altitude of approximately 300,000 ft, with a dynamic pressure of 2 psf. Early entry stability and control is provided primarily by the aft-mounted reaction control system (RCS) jets, (figure 12). The forward-mounted jets are reserved for on-orbit attitude control and ascent aborts. The roll and pitch jets are active until dynamic pressures of 10 and 20 psf, respectively, are obtained, at which point the elevons are sufficiently effective to provide pitch and roll control. The yaw jets provide stability augmentation until the vehicle has decelerated to Mach 1.

A gradual pitch down is initiated between Mach 14 and 12. By Mach 2 the vehicle is flying at more conventional angles of attack from 3° to 10°. Equilibirum subsonic gliding flight is achieved at an altitude of approximately 40,000 ft. The approach and landing interface occurs at 10,000 ft, and the vehicle subsequently reaches a glide slope of approximately -19°. Nominal touchdown velocity is 195 knots with a rollout of 7,000 to 9,000 ft.

ORBITER FUNCTIONAL CHARACTERISTICS

The functional characteristics of the Orbiter are presented in figure 13. The thick, double-delta wing is configured with full span elevons, comprised of two panels per side. Each elevon panel is independently actuated. All four panels are deflected together as an elevator for pitch control and left and right elevons are deflected differentially as an aileron for roll control.

The bodyflap, originally designed as a heat shield for the SSMEs, is now also used as the primary longitudinal trim device. The elevons are programmed to follow a set schedule during entry to provide the optimum aileron effectiveness.

The vertical tail consists of the fin and a split rudder. The rudder panels are deflected together for yaw control and are separated to act as a speedbrake to provide for subsonic energy modulation. The speedbrake, initially closed upon entry interface, opens fully just below Mach 10, and then follows a predetermined schedule until Mach 0.9 is reached. The rudder is not activated for yaw control until Mach 3.5.

PREFLIGHT PREDICTION REQUIREMENTS

The preceding discussion leads to the conclusion that prediction of the basic aerodynamic characteristics of the vehicle are required from Mach 0.2 through 27, and at an angle of attack range from near 0° to 40°. Figure 14, which delineates utilization of the vehicle control effectors, shows that predictions of aileron and elevon effectiveness would be needed over the same M, α range. Rudder power needs definition below Mach 3.5. The high dynamic pressure to be encountered forced consideration of structural deformation effects on aerodynamics. Also the effectiveness of the RCS would have to be determined from on-orbit conditions down to as low as 50,000 ft (Mach 1). The RCS effectiveness is a function of jet thrust, plume impingement and the vehicle flow field/plume interaction as shown in figure 15.

PREFLIGHT WIND TUNNEL PROGRAM

Key to the Space Shuttle development has been the acquisition of wind tunnel test data to support GN&C design and evaluation by providing a continuously maturing aerodynamic data base reflecting configuration and subsystem updates. By the first orbital flight (STS-1) in 1981, approximately 46,000 total wind tunnel test hours had been conducted for aerodynamics, heat transfer, and structural dynamics, consisting of approximately 24,900 for the Orbiter vehicle, 17,200 for the mated launch configuration, and 3,900 for the carrier aircraft program, as shown in figure 16. A total of 101 models have been built: 45 aerodynamic, 34 heat transfer, and 22

structural dynamics. All wind tunnel testing was coordinated with and approved by NASA management at JSC. A detailed review of the history and management of the wind tunnel program may be found in reference 1.

Orbiter aerodynamic test hours are summarized in figure 17. Approximately 38% of the Orbiter aerodynamic test hours were utilized in the subsonic regime, 44% in the transonic/supersonic regime, and 18% in the hypersonic regime. As may be seen from figures 16 and 17, the Space Shuttle wind tunnel program was by far the largest program ever undertaken by this country. Also seen in figure 17 is an additional 10,000 hours of testing performed by Langley for special investigations requested by Space Shuttle management.

SELECTION OF SCALING PARAMETERS

In order to accurately simulate flight conditions in a wind tunnel, the appropriate similarity parameters must be matched. Traditionally, Mach number and Reynolds number are the key parameters. Problems in flow simulation[6] occur when the geometric scaling of viscous flow is important, or when coupling between the viscous surface flow and the external flow field is strong. In the first case, the boundary layer can be considered separately from the inviscid flow field, and viscous effects can be scaled. This holds for Mach numbers up to approximately 10. It is well known, for example, that skin friction varies with Reynolds number in a predictable manner and can be scaled to flight conditions from suitable wind tunnel results.

For Mach numbers greater than approximately 10, a pressure interaction results from the outward streamline deflection induced by a thick boundary layer, and the viscous-inviscid interaction must be considered. For this case, there are two classical simulation parameters commonly considered:

(1) $\bar{\chi}'_\infty$, the viscous interaction parameter introduced by Hayes and Probstein[7]

$$\bar{\chi}' = \frac{M_\infty^3 \sqrt{C_\infty'}}{\sqrt{R_{e_{\infty_x}}}}$$

(2) $\bar{V}'_\infty$, the viscous parameter introduced by Whitfield and Griffith[8]

$$\bar{V}'_\infty = \frac{M_\infty \sqrt{C_\infty'}}{\sqrt{R_{e_{\infty_x}}}}$$

where M_∞ is the free-stream Mach number, C_∞' is the factor of proportionality in the linear viscosity-temperature relation,[9] and $R_{e_{\infty_x}}$ is the free-stream Reynolds number based on the appropriate characteristic length (x). The parameter $\bar{\chi}_\infty$ is the relevant parameter for the local effects (pressure coefficient, heat transfer, etc.) in both the strong and weak interaction cases; whereas $\bar{V}'_\infty$ is the relevant parameter in terms of overall integrated effect. For Shuttle, it has been observed that $\bar{V}'_\infty$ correlates total aerodynamic coefficients better than $\bar{\chi}_\infty$, and consequently, $\bar{V}'_\infty$ was selected as the hypersonic simulation parameter. A detailed discussion of the use of these scaling parameters for the Space Shuttle is presented in reference 10.

Figure 18 shows a comparison between flight $R_{e_{L_B}}$ and $\bar{V}'_\infty$ and the simulation capability of typical wind tunnels used to develop the Orbiter aerodynamic data base. It can be seen that the tunnel capabilities reasonably match flight conditions above Mach 3. It should be noted that although flight Reynolds number and Mach number were not simulated above Mach 15, if $\bar{V}'_\infty$ is the correct similarity parameter, the tunnel prediction of aerodynamic characteristics should be good.

One inadequacy worth noting is that at the time of the Shuttle aerodynamic development (prior to STS-1) neither experimental facilities nor theory could accurately predict real gas effects.

SIMULATION OF REACTION CONTROL JET INTERACTION

Early entry aerodynamic characteristics are highly influenced by interactions between the reaction control system (RCS) jet plumes and the local flow field over the Orbiter as shown in figure 15. The total jet effects are comprised of three factors: (1) jet thrust, (2) surface impingement, and (3) jet interaction with the flow field. Impingement and interaction effects are interrelated. Jet interaction was obtained from wind tunnel testing while surface impingement was estimated from vacuum chamber tests and theory. Coupling is present between the plume effects and aerodynamic surfaces, and between the jets themselves.

A series of scaled model RCS nozzles with different expansion ratios were employed during the wind tunnel test program. General Dynamics/Convair, under contract to the NASA (NAS9-14095),[11] developed a method whereby the experimentally-measured induced plume effect (surface impingement plus flow field interaction) could be separated into two component parts and the impingement term extrapolated to flight conditions. To obtain a correct modeling of the reaction control system plume effects in the wind tunnel, it was necessary to observe certain scaling criteria. The primary factors for consideration, aside from dimensional scaling, are plume shape, jet-to-free-stream momentum ratio (ϕ_j/ϕ_∞) and mass flow rate ratio $(\dot{m}_j/\dot{m}_\infty)$. The RCS pitch jets (up and down firing jets) correlated better with momentum ratio whereas the yaw jets (side firing jets) correlated better with mass flow rate ratio.

These scaling parameters are defined as:

$$\frac{\phi_j}{\phi_\infty} = \frac{\dot{m}_j \, V_j}{2 \bar{q} \, S} \, n_j = 7.3879 \, \frac{n_j}{\bar{q}}$$

and

$$\frac{\dot{m}_j}{\dot{m}_\infty} = \frac{\phi_j}{\phi_\infty} \frac{V_\infty}{V_j} \frac{1}{n_j} (\sin \theta_j)^{1/2} = 1.300 \times 10^{-3} (\frac{V_\infty}{\bar{q}})$$

A detailed discussion of the selection of these scaling parameters is presented in reference 11.

THE WIND TUNNEL PROGRAM

The wind tunnel program can be divided into three phases. These phases are related to the development schedule as illustrated in figure 10.

The first of these phases (Phase I) was the configuration development phase. This phase, which covered the time period of ATP to SRR, addressed ATP configuration refinement, evaluation of the PDR configuration, and definition of the CDR configuration.

The prime contractor devoted the majority of their Phase II efforts to developing and verifying the aerodynamic characteristics for the ALT/carrier program although initial development testing for the OFT program was also performed. These latter development tests were directed toward establishing the basic stability and control characteristics across the Mach range; establishing control surface effectiveness and hinge moments; initial RCS testing; and viscous interaction testing. The FCS was converging on a detail design during the Phase II time period and concerns surfaced regarding the sensitivity of the FCS to nonlinear aerodynamics. In order to investigate potential nonlinearities, JSC management requested the LaRC to supplement the contractor's test program. These tests investigated the following areas: (1) non-linear aerodynamic characteristics of the basic vehicle and its control surfaces; (2) aerodynamic damping characteristics; (3) control surface interactions; and (4) high Mach/altitude simulations. In addition, the possibility of high altitude snap roll caused by asymmetric separation of the wing's leeside flow field was explored.

The final phase (Phase III) of the wind tunnel program was initiated in early 1978 to verify the predicted aerodynamic characteristics of the final vehicle configuration prior to the first orbital flight (STS-1). The objectives of this phase were to:

a. Verify and/or update the aerodynamic characteristics of the final, "as built" configuration across the Mach range of 0.2 to 15.
b. Test fine-cut (small increments) in Mach number, angle of attack, angle of sideslip, and control surface position along the nominal flight trajectory.
c. Minimize model-to-model and tunnel-to-tunnel discrepancies.

The final, preflight Aerodynamic Design Data Book (ADDB)[12] is primarily based on these verification tests. The verification phase consisted of three parts:

a. Seven initially planned verification tests.
b. Five anomaly resolution tests.
c. Five supersonic/hypersonic lateral-directional nonlinearity tests.

The complete verification phase is shown in figure 19.

Two high-fidelity wind tunnel models, of 2% and 5% scale, were designed and constructed based on the March 1976 OV-102 configuration drawings to ensure accurate modeling of all aerodynamic surfaces and simulation of all revelant cavities and protuberances as shown in figure 20. Although some minor changes to the TPS thicknesses were made after March 1976, these changes were closely monitored to ensure that there were no aerodynamicly significant differences between the wind tunnel models and the actual flight vehicle OV-102.

Part 1 of the verification phase consisted of the wind tunnel tests required for verification as it was originally conceived. These tests covered the Mach range of 0.2 to 15 using the two high-fidelity models without planned duplication of test conditions with different combinations of models and facilities. Several additional tests and considerable analyses were required to actually complete the preflight verification process. In order to acquire the highest quality data possible within time and fiscal constraints, a test team was established for each test consisting of the prime contractor, JSC, and facility engineers, co-chaired by the JSC and the prime contractor lead engineers. This team followed the test from initiation through model design and construction, test plan development, conduct of tests, and analysis of results.

The design of the verification tests drew heavily on the experience and results of a series of wind tunnel tests conducted by LaRC. These tests utilized a 1.5-scale model (OV-101/140C configuration) with remotely controlled elevons. They were conducted to investigate transonic and low supersonic lateral-directional nonlinearities and showed the importance of obtaining wind tunnel data in small increments and of utilizing remotely controlled aerodynamic surfaces.[13] Two of the major benefits of testing with remotely controlled surfaces are: (1) permits efficient acquisition of small increments of the primary variable of interest, i.e., the control surface position; and (2) permits the acquisition of more accurate data by "sweeping" the control surface position while other test variables are held constant.

The verification phase relied heavily on the NASA-Ames Research Center (ARC) wind tunnel facilities, as had the development test phase. Table 2 shows the utilization of facilities for Phase III.

Although Part 1 of the verification tests were largely successful, initial analysis of the data from these tests indicated additional wind tunnel tests were required to resolve the following test anomalies:

a. Transonic - resolve blockage and shock reflection effects.
b. Supersonic - verify relatively large facility (AEDC) flow tare corrections.

The tests shown under Part 2 in figure 19 were conducted as part of the verification tests phase to address the transonic blockage/shock reflection and supersonic tare correction problems.

The quick-look analysis of these tests still did not provide any clear-cut solutions to the original problems. Therefore, in July 1978, the Technical Panel for Orbiter Aerodynamics was formed at the request of the JSC Center Director to address these problems. The objective of the Panel was to expedite the analysis of the Orbiter aerodynamic design data to produce a mature data base that would support the launch of the first manned orbital flight planned for March 1980. This Panel was

comprised of working-level aerodynamicists representing expertise from ARC, DFRC, LaRC, JSC, AFFTC, and the prime contractor. The major functions of the Panel were:

a. Recommend and conduct wind tunnel tests.
b. Evaluate and recommend the most valid test data for use in establishing the ADDB preflight predictions.
c. Perform an independent, detailed analysis of critical areas.
d. Perform a thorough review of the proposed ADDB prior to publication and make recommendations for accceptance or change.
e. Obtain Panel consensus that the ADDB is the "best" representation of the Orbiter aerodynamics.
f. Give technical approval of the official ADDB.

The results of a wind tunnel test conducted by LaRC to assess the OV-102 configuration showed that there were no significant aerodynamic differences between OV-101 and OV-102. As a result, the large number of wind tunnel tests LaRC had conducted using the 1.5% model (OV-101 configuration) were used in developing the final fairings for the preflight ADDB. The high fidelity OV-102 model data was still considered prime and weighed the heaviest of all the data. The LaRC tests contributed significantly to filling in gaps of the OV-102 data base and to establishing model-to-model and tunnel-to-tunnel repeatability. The product of the Panel was the official Space Shuttle Orbiter ADDB published in October 1978 and revised in April 1979.[14]

Prior to the formation of the Panel, the technique of reviewing the "correctness" of the ADDB published by the prime contractor was to conduct a formal review after publication. Unless major discrepancies were identified and agreed to, no changes were usually made as a result of the formal review. Because the Panel worked closely with the prime contractor, making recommendations and changes during the development of the ADDB, a much more detailed review and refinement than by previous means of review was made possible. Almost all of the changes recommended by the Panel were accepted and implemented with minimum schedule impact. A significant amount of work by individual members was published directly in the ADDB.

After the Panel's work was complete, a minor update to the April '79 ADDB was made and the official aerodynamic data base was frozen in May 1980 to conduct final GN&C verification for STS-1. This data, the official preflight Orbiter aerodynamic data base, was published as a NASA Contractor Report in November 1980,[15] and was designated as the "STS-1 ADDB."

In January 1980, while conducting an in-house research test on high angle of attack aerodynamics, LaRC found a large difference in directional stability at Mach 6 from what the STS-1 ADDB predicted. This gave rise to some potential FCS concerns about performing a bank reversal in flight near Mach 6. An investigation of this potential problem led to Part 3 of the verification test phase: Supersonic/hypersonic lateral-directional nonlinearity tests.

It turned out that the lateral-directional characteristics are highly nonlinear with sideslip angle (β) at certain angles of attack. Further, this phenomena is not limited to Mach 6, but occurs over a Mach range of 2 to 8, at various α's. Also, nonlinearities of the sideslip derivatives with Mach, α, and speedbrake were identified that had not been observed previously. The basic problem was that the sideslip derivatives are linear only over a range of $1/2^{\circ}$ beat in some cases. The smallest tested previously was 1° and most data was at 2°. The cause of these nonlinearities is thought to be a complex vortex interaction with the vertical tail/speedbrake.

Discovery of a problem of this magnitude so late in the Shuttle program development (projected launch date of STS-1 was just over 1 year from discovery of problem) presented a schedule problem of how to acquire the necessary wind tunnel data, analyze the results, and put the data fairings in a form that was acceptable for input to the simulators so that a safety assessment could be performed prior to the STS-1.

In order to resolve the aerodynamic/FCS anomaly in time to support STS-1, a team was formed consisting of JSC, the prime contractor, LaRC, and wind tunnel facility engineers. This included aerodynamicists, flight control engineers, and simulation engineers at JSC. The wind tunnel tests conducted are shown under Part 3 in figure 19.

Detailed analysis of the test data was performed on-site during each wind tunnel test such that by the end of the test, final fairings were complete and the data had been converted into a form ready for the flight simulators. The data was then evaluated on an engineering simulator at JSC.

The results showed that the large nonlinearities with β could cause loss of control during a bank reversal when combined with certain FCS uncertainties such as winds and errors. As a result, the trajectory of the first flight (STS-1) was changed to avoid a bank reversal near Mach 6.

These new wind tunnel data were then used to produce a major update in the STS-1 ADDB, published in April 1982 as the Pre-Operational ADDB.[12] The Pre-Operational (Pre-Op) ADDB, although published after STS-1, contains no flight data (except for limited ALT results) and represents the true best estimate of preflight aerodynamics of the Space Shuttle Orbiter. Ultimately, the Pre-Op ADDB will be updated based on orbital flight test results to produce the Operational Aerodynamic Data Book (OADB) for the Orbiter. This will be the aerodynamic data base used for Shuttle operational planning such as mission planning, trajectory design, and crew training.

<div align="center">WIND TUNNEL DATA BASE ANALYSIS</div>

It was a major undertaking just to collect the wind tunnel data base. The fruits of this undertaking would be meaningless unless the results of these tests could be presented to the aerodynamic analysts in a digestable form. The Space Shuttle Program management turned to the computer to facilitate this analysis. Chrysler Corporation's Space Division devised and operated a system of computer programs called "DATAMAN" to document and present test results to the aerodynamic analysts in a variety of plotted forms. The analyst could have at his disposal the data in the desired form allowing an efficient analysis to be performed. Chrysler received data tapes from the various facilities, transformed the various tapes to a common format, and used the computer program system to correlate, document, and produce data upon request to the aerodynamic analysts. A detailed review of this unique capability is presented in reference 16.

<div align="center">ORBITER AERODYNAMIC CHARACTERISTICS</div>

Preflight predicted aerodynamic characteristics of the final Orbiter vehicle are summarized in this section. These characteristics derived from an extensive wind tunnel test data base adjusted for those effects which could not be simulated in the wind tunnel. Before discussing the corrections made to this data base and the actual aerodynamic characteristics, the management, control, and verification of the aerodynamic data base will be reviewed.

The challenge of the management of the aerodynamic data base falls into two areas: 1) creating and controlling a common data base for the multitude of users within NASA, and the contractors across the nation; and 2) verifying that data base. Late in Phase B, a common Orbiter aerodynamic configuration was selected as a focus for all in-house and contractor efforts. The aerodynamics for this configuration were compiled into an ADDB to be used for all computer simulations. The use of a central controlled ADDB continued into the Phase C & D time period. (An ADDB of estimated aerodynamic characteristics for the ATP configuration was submited with the Rockwell proposal.) As the configuration evolved a data book consisting of the estimated aerodynamic characteristics for each configuration was produced and subsequently verified experimentally. To further standardize the data base the process of centrally digitizing and producing computer tapes of each data book was initiated early in Phase C & D. Thus, the aerodynamic data base evolved into an ADDB and its corresponding digital computer tape, under configuration control of one of the major program panels.

ADDB verification was accomplished by a detailed technical review by NASA experts prior to each programmatic milestone until approximately 1-year before the first manned orbital flight. (The procedure used in this time frame was addressed previously in Phase III of the Wind Tunnel Section.)

<div align="center">WIND TUNNEL DATA BASE ADJUSTMENTS</div>

The traditional free-stream Reynolds number was selected for the flow field scaling parameter below Mach 15, while a viscous interaction parameter ($\bar{V}'_\infty$) was utilized at higher Mach numbers. Since the test facilities were able to provide near-flight Reynolds number simulations over a large Mach number range, as shown in figure 18, no corrections to the wind tunnel results were required. At lower Mach numbers, the traditional adjustments were applied for Reynolds number effect on friction drag. Additional adjustments were applied to the profile drag to account for the added roughness of the thermal protection system tiles, and for minor protuberances, which could not be simulated on the wind tunnel test models.

In general, no attempt was made to obtain a wind tunnel measurement of the effects of structural deformation on the longitudinal aerodynamics through testing of conventional aeroelastic or deformed models. Since at higher $\bar{q}$'s these effects can be significant, some adjustment to the wind tunnel data must be made to provide adequate estimates of the flight aerodynamics. The approach used in the Shuttle Program to estimate the aeroelastic effects is thought to be unique.

First, a sensitivity analysis was performed with the aid of a structural/aerodynamic analysis computer program.[17,18] The geometry model used is shown in figure 21. This program was used to systematicly stiffen various portions of the vehicle structure to analytically evaluate the effect of the stiffness changes on the aerodynamics. The results indicated that the major longitudinal aeroelastic effects were produced by deformation of the wing back-up structure where the elevon actuator is attached, resulting in a change of the elevon position not measured by the vehicle position sensors. The effect was modeled by combining a rotary spring constant, as determined from vehicle loading tests, with wind tunnel derived aerodynamic hinge moment characteristics to determine a correction (usually less than 1°) to the rigid elevon deflection angle. The "elastic" elevon angle is used to look-up the rigid aerodynamic characteristics in determining the vehicle longitudinal aeroelastic characteristics.

The computer program indicated the major aerodynamic effect in the directional axis was the deformation of the vertical tail and the aft fuselage. Of particular concern was the predicted 40% reduction in rudder power due twisting of the vertical tail around its elastic axis. It was felt that this large effect could not be left to theoretical prediction techniques alone. After establishing the structural characteristics of the vertical tail and aft fuselage from the structural test article, an aeroelastically scaled vertical tail was constructed which simulated the root spring constant and tail stiffness distribution. It was then tested on a standard force model across the high $\bar{q}$ Mach range. The results from these wind tunnel tests were then analytically adjusted to "free" the orbiter from the sting mounting constraint necessary in the wind tunnel. The adjusted wind tunnel data are compared with the computer program predictions in figure 22 for a $\bar{q}$ of 300 psf (14,364 N/m^2). As can be seen, the correction is significant. A detailed development of this unique approach for evaluating aeroelastic effects is presented in reference 26.

AERODYNAMIC CHARACTERISTICS

The key aerodynamic parameters which have a significant influence on the Orbiter performance, and stability and control are shown in table 3. Lift, drag, and pitching moment are the primary aerodynamic parameters governing the entry trajectory and range capability. Pitching moment determines the bodyflap setting required for trim. Design areas sensitive to trim setting are elevon and bodyflap heating during initial entry, and control surface actuator stall limits at transonic speeds. In addition, there is an interaction between elevon setting and lateral-directional control capability because of the change of aileron effectiveness with elevon position. Lateral-directional trim and control capability is governed by the aileron, rudder, and sideslip derivatives. Above Mach 3.5 the aileron is used for both roll and yaw trim before the rudder becomes effective.

In the spacecraft mode of operation, bank maneuvers are initiated by the yaw jets and the aileron is used to coordinate the maneuver. Between Mach 3.5 and 1.5 the flight control system gains are scheduled to provide a transition to a conventional aircraft mode where the bank maneuvers are initiated by the ailerons about the roll axis and the rudder is used to coordinate the maneuver. Both the aileron and rudder are used for trim below Mach 3.5. The derivatives C_{n_β}, C_{ℓ_β}, $C_{n_{\delta_a}}$, $C_{\ell_{\delta_a}}$, $C_{n_{\delta_r}}$, $C_{\ell_{\delta_r}}$ were key parameters in establishing control capability, reaction control system propellant usage, and the switch-over point from spacecraft to aircraft control modes.

HIGH ALTITUDE AERODYNAMICS

Entry interface for the Shuttle has been defined as 400,000 ft (120,000 meters) altitude. In this high altitude region, rarefied gas flows are encountered by the Orbiter as it enters the atmosphere. Aerodynamic design issues in this region involve determining the effectiveness of the RCS control jets and their influence on the Orbiter flow field, in addition to defining viscous interaction effects associated with low Reynolds number/high Mach number flows.

223

Initial entry aerodynamic characteristics are strongly influenced by interactions between the RCS jet plumes and the local flow field over the Orbiter (figure 15). The application of the RCS data to a typical entry flight condition of $\bar{q} = 1.0$ lb/ft^2 (47.9 N/m^2) at an altitude of 260,000 ft (79,250 meters) are presented in figure 23 for three left downfiring RCS jets. The RCS impingement and flow interaction results have an adverse effect on pitch and roll control while increasing yaw control.

Viscous interaction primarily affects the shear forces with essentially no affect on normal force. Variation of $\bar{V}'_\infty$ along the nominal entry trajectory is illustrated in figure 24. High values of $\bar{V}'_\infty$ correspond to low values of Reynolds number which is associated with the thickening of the hypersonic laminar boundary layer causing increased shear on the lower surface of the Orbiter. Evidence of this is seen in figure 25 as an increase in axial force coefficient with increasing $\bar{V}'_\infty$ yields no change in normal force. There is insignificant effect of $\bar{V}'_\infty$ on pitching moment for 0° bodyflap as shown at the top of figure 26. At negative (trailing edge-up) bodyflap deflections, the movement of the bodyflap has little effect on the boundary layer on the lower surface of the Orbiter, and consequently, the effect of $\bar{V}'_\infty$ on pitching moment is similar to the 0° deflection case. However, for positive (trailing edge-down) deflections, the bodyflap control effectiveness decreases with increasing $\bar{V}'_\infty$, (figure 26). At large values of $\bar{V}'_\infty$, the correspondingly low Reynolds number results in a thickening of the boundary layer which causes the separation point to move forward with increasing control deflection. This causes the center of pressure to move forward, resulting in reduced pitching moment effectiveness with increasing $\bar{V}'_\infty$. Effects of $\bar{V}'_\infty$ on aerodynamic performance characteristics are indicated in figures 27 and 28 for a nominal entry trajectory. The decrease in L/D ratio caused by the increase in axial force is accounted for in design of the entry trajectory.

LONGITUDINAL CHARACTERISTICS

Longitudinal stability and control characteristics for low speed to hypersonic Mach numbers are illustrated in figures 29 and 30. These data are based on an extensive series of wind tunnel tests. Representative wind tunnel data are shown on the curves. The low-speed longitudinal characteristics shown in figure 29 demonstrate stall-free characteristics over operating flight conditions. The predicted characteristics are compared with test data obtained with a 0.36-scale model in the ARC 40x80-ft (12.19x24.38 m) wind tunnel. The changes in low-speed stability shown by the large changes in pitching moment at high α's are due to leeside separation on the Orbiter wing induced by vortices from the wing/fuselage junction. The leeside flow separation influences the supersonic stability characteristics also. It can be seen in figure 30 that for Mach 10 and 5, the variation of pitching moment with normal force coefficient for zero and positive elevon deflection follows the typical hypersonic pitch characteristics. This relationship between pitching moment and normal force coefficient does not follow the "sine square" variation for negative elevon deflections. The change in characteristics is due to the change in flow pattern on the leeside of the Orbiter wing as influenced by negative elevon deflections.

The surface flow patterns on the leeside of the Orbiter wing at supersonic speeds consist of three distinct flows. At low α's, the flow, which is initially perpendicular to the leading edge, is turned parallel to the free-stream by the presence of the fuselage (figure 31a). When the angle of attack is great enough to cause the wing leading edge shock to detach, the trailing edge shock will become strong enough to separate the boundary layer (figure 31b). This separation is the result of subsonic flow aft of the detached shock expanding around the leading edge and reattaching at supersonic speeds. The flow must still be turned into the free-stream direction as before. The turning is accomplished by a strong shock that causes the boundary layer to separate. The wake begins to affect the flow pattern at high angle of attack causing a secondary type of separation (figure 31c). Leeside flow boundaries at Mach 6.0 are shown in figure 32. The relationship between spanwise location of the shock induced separation, $\dfrac{b_s}{b}$, and Mach number was obtained from a correlation of delta wing data. The shock detached boundary was obtained from oil flow photographs.

The effect of leeside separation on wing pitching moment is shown in figure 33. The subsonic leading edge suction that occurs when the bow shock detaches results in a more stable pitching

224

moment slope. The change to a more stable slope is the result of leading edge suction when the wing bow wave detaches and a reduction of lift over the wing area aft of separation line. The center of pressure is more aft for the lift gain (due to leading edge suction) than for the lift loss due to shock-induced pressure aft of the separation line. The wing pitching moment becomes more stable, thus accounting for the increased stability shown in figure 30 for $+10^{\circ}$ elevon deflection.

Elevon effectiveness is also influenced by leeside separation. Loss in elevon effectiveness at high negative (trailing edge up) deflection can be attributed to the effect of back-pressure on the leeside flow field. Flap type controls will often cause boundary layer separation, especially in hypersonic low-density flows. Such back-pressure effects are of practical concern since it is desirable to control the Orbiter with leeward control deflection (trailing edge up) in order to minimize control surface heating. Figure 34 shows elevon effectiveness data obtained from the AEDC tunnel A at Mach 5 for an elevon deflection of -35°. The measured elevon effectiveness is seen to be less than shown by shock expansion theory. This is probably due to shock-induced separation. The extent of separation increases with α. After the α for shock detachment is reached, the back-pressure effect from the elevon will affect the wing flow. At high α's, the positive lift produced by the wing vortices outweighs the negative lift generated by the elevon-induced flow separation over the inner wing surface. The result is a loss of elevon effectiveness below the shock expansion value. Adjusting the theory for leeside separation results in reasonable agreement between theory and experiment.

Static trim capability for the elevon and bodyflap mentioned for trim to the forward and aft cg positions is shown in figure 35. The control schedules presented on the figure are for determining maximum obtainable cg trim limits. A reserve for maneuvering, trimming Ycg offset, manufacturing misalignments, and aerodynamic uncertainties has been added to the limits of the elevon effectiveness data to establish the limits shown on the figure. The aft cg limits are based on a positive elevon deflection of 15° for Mach numbers less than or equal to 10. A positive elevon deflection of 10° was used for Mach numbers greater than 10 due to thermal protection system design limits during maximum heating conditions. Forward cg trim limits are based on an incremental pitching moment coefficient reserve of 0.015 for Mach numbers less than or equal to 10 and 0.02 for Mach numbers greater than 10. Figure 35 indicates a slightly reduced forward cg trim margin at Mach 5.0 in the α range from 20° to 45°. This is attributed to the loss in elevon effectiveness due to leeside separation. Center of gravity trim limits for the entry α schedule are shown in figure 36. Both figures 35 and 36 indicate that a wide trim margin exists across the Mach number range.

Elevon control power, in conjunction with the bodyflap and speedbrake, provide trim capability between the design cg limits. The elevon schedule, shown in figure 37, illustrates the nominal and the most positive and negative settings for trim at forward and aft cg positions. The extreme settings account for control margin and uncertainties in aerodynamic characteristics.

LATERAL DIRECTIONAL CHARACTERISTICS

Lateral-directional stability and control characteristics for a mid cg along the nominal entry trajectory are illustrated in figures 38, 39, and 40. The Orbiter exhibits a stable dihedral effect (negative C_{ℓ_β}) across the complete Mach range during both the spacecraft and aircraft control modes (figure 38). During the spacecraft mode, and during transition to the aircraft mode, the vehicle is directionally unstable. C_{n_β} becomes positive indicating static stability in yaw between Mach 2 and 1, and remains directionally stable throughout the aircraft mode (Mach numbers below approximately 1.5). Aileron and rudder control effectiveness characteristics are illustrated in figures 39 and 40.

Early analytical studies predicted an effect of elevon deflection on the lateral-directional characteristics. Studies showed that the relatively large sized elevon in the presence of the deep, flat-sided fuselage could induce a change in the pressure distribution in the aft region of the fuselage. The change in the pressure distribution resulted in an incremental change in side force, yaw, and rolling moment when the vehicle was yawed. The effect of elevon on lateral-directional stability is illustrated in figures 41 and 42. The aileron control derivatives $C_{\ell_{\delta_a}}$ and $C_{n_{\delta_a}}$ are also affected by elevon position as shown in figures 43 and 44. The sensitivity of these derivatives to elevon position influences vehicle control boundaries.

Low-speed directional stability characteristics exhibit a strong combined Reynolds number and α effect as shown in figure 45. The figure illustrates the importance of full-scale Reynolds number testing on high α aerodynamics. Test data obtained from models tested at low Reynolds number (below 5×10^6 based on MAC) show essentially no change of directional stability with α. The early work of Polhamus[19] and Jorgensen and Brownson[20] indicated that Reynolds number and body corner radius could have a significant effect on the high α characteristics of the Orbiter. These predictions were borne out when the Orbiter model was tested at near full-scale Reynolds number in the ARC 40x80-foot (12.2x24.4 m) wind tunnel. It can be seen in figure 45 that the high Reynolds number test data show a decrease in directional stability with angle of attack which is in contrast to the low Reynolds number data which show essentially no change in stability with α.

AERODYNAMIC UNCERTAINTIES

The two program management decisions given in the Background section (to freeze the Orbiter systems configuration at ATP and to fly a manual Orbital flight on the initial mission) had a significant influence on the approach selected for the aerodynamic design and verification of the Orbiter, particularly with regard to aerodynamic uncertainties. These decisions led to the development of two types of aerodynamic uncertainties: (1) Wind tunnel uncertainties, and (2) Wind tunnel-to-flight uncertainties.

WIND TUNNEL UNCERTAINTIES

The first decision baselined both the FCS and the aerodynamic configuration (as well as other systems and subsystems) in August 1972 at the ATP milestone. Thereafter, the only aerodynamic and FCS changes that were permitted were those which were required to fix critical system design problems. As evaluations of the baseline systems were conducted, it became clear that some significant changes to both the FCS and aerodynamic design would be required. This resulted in the final FCS and the aerodynamic design being conducted in parallel. This presented a problem of how to design a FCS "tuned" to the vehicle aerodynamics while the baseline aerodynamic data base was still evolving. Somehow, the FCS had to be designed to be insensitive to "reasonable" changes in the aerodynamic characteristics. This led to the requirement for a set of aerodynamic "design-to" uncertainties that would be used along with the baseline nominal aerodynamics in FCS design. These "design-to" uncertainties, designated "tolerances", were defined as the minimum error that is expected in the preflight aerodynamic predictions.

With the wind tunnel data base as the foundation for the preflight predictions, it was assumed that the minimum error that could be expected would be the ability to reproduce experimental results between various wind tunnel tests. Therefore, repeat tests were performed using various wind tunnel facilities, different models, and on occasion, different test organizations. Although the individual causes for any differences were not specifically identified, it is felt the total difference is representative of what may be expected for wind tunnel test repeatability.

As an illustration of the mechanics of this procedure, consider pitching moment coefficient, where repeat tests are presented along with ADDB estimates in figure 46. It can be seen from this figure that a 0.05 scale model (model 39-0) was tested in both ARC 11x11 foot facility, and in the LaRC 16-foot transonic facility. Similarly, a 0.015 scale model, model 44-0, was tested by LaRC in three facilities: 1) the Ling-Temco-Vought High Speed Wind Tunnel (LTV 4 x 4); 2) the LaRC 8-foot tunnel; and 3) the ARC 11x11 foot facility. In addition, the 0.02 scale model, model 105-0 was tested in the LaRC 16T tunnel. With all these potential sources of differences, a peak-to-peak repeatability in pitching moment coefficient (C_m) of approximately 0.006 was observed. This repeatability represents the combined error sources of the following: 1) the same model in several tunnels (tunnel-to-tunnel repeatability); 2) different models in the same tunnel (model-to-model repeatability); and 3) different test organizations (testing technique differences).

Based on this correlation, the difference between the wind tunnel results and the ADDB at various angles of attack were correlated with Mach number (figure 47). Tolerances (wind tunnel uncertainties) were obtained by fairing a curve through these data points using engineering judgement. The nominal flight angle of attack was given a high weighting in the fairing process. A similar process was used to develop tolerances for lift and drag coefficients, the sideslip derivatives, aileron derivatives, and rudder derivatives. Reference 21 provides a more detailed report on the development of the Orbiter wind tunnel uncertainties.

The second program management decision, to fly a manned vehicle on the initial orbital flight test of the Space Shuttle, raised the question of how to maximize mission safety without the benefit of conducting a graduated flight test program as is traditionally done in most aircraft development programs. This decision led to the requirement to provide a reasonable estimate of the maximum possible errors in the preflight aerodynamic predictions that might occur on the first Space Shuttle flight. These aerodynamic uncertainties were designated "variations".

In order to certify that the Space Shuttle system was ready for the first flight, a multitude of flight simulations were conducted using the aerodynamic variations, along with other system uncertainties, to "stress" test the FCS. Based on the results of these simulations, a cg, elevon schedule, and the FCS gains were selected for STS-1 which maximized the stability and control margins, thereby maximizing mission safety.

However, these "worst case" uncertainties must not be so conservative as to completely invalidate the FCS design. Since the preflight predictions were primarily based on wind tunnel tests, variations would represent the possible errors between wind tunnel and flight aerodynamics. It was felt that the most reasonable approach for the development of variations would be to analyze the wind tunnel to flight test differences of previous aircraft programs. Unfortunately, the verification of preflight predicted aerodynamics was not a major objective of most of the earlier flight test programs. This severely limited the amount of data available for conducting flight test to wind tunnel comparisons. The flight data base was further limited by restricting the comparison to those vehicles which were geometrically similar to the Orbiter.

Variations were established by fairing the differences between the flight and predicted aerodynamics as a function of Mach number. Because the selections of the configurations and the fairing process are very subjective in nature, a team of aerodynamicists from NASA Dryden Flight Research Center, NASA Johnson Space Center, Air Force Flight Test Center, and the prime contractor was formed to conduct the analysis and reach a consensus on variations.

The team's flight-to-predicted pitching moment correlation and their recommended variation fairings are presented as a function of Mach number in figure 48. As can be seen from this figure, the flight data is limited to below Mach 3. In Mach regimes where flight data was unavailable and the ideal gas assumption was justified, variations were obtained by multiplying the wind tunnel-derived tolerances by a safety factor, usually 1.5. A similar process was used to develop variations for the other aerodynamic parameters. A more detailed development of variations is given in reference 22.

A detailed investigation of the effect of real gas effects[10] was conducted in 1974 using state of the art theoretical techniques. Geometric limitation of the computer codes at that time did not lend sufficient confidence to use these results in adjusting the ideal gas wind tunnel data. Instead, a conservative estimate of the real gas effect was added to the pitching moment tolerances to estimate variation in the high altitude flight region. Presented in figure 49 is pitching moment variation as a function of the viscous interaction parameter in this flight region. The predicted real gas effects gave a more nose moment up to the basic vehicle pitching moment than ideal gas predictions. Therefore, the real gas increments were added to the positive pitching moment tolerances resulting in the unsymmetrical variations illustrated in this figure. A procedure for statistically combining these uncertainties is delineated in reference 23.

It is believed that the Space Shuttle Orbiter is the first winged aircraft/spacecraft to be designed using a systematic development and application of aerodynamic uncertainties.

THE ACCOMPLISHMENTS

The success of the first orbital flight of the Space Shuttle in April 1981 demonstrated the successful aerodynamic design and development of a vehicle configuration capable of flying both as a spacecraft and as an aircraft, and that the preflight predictions were of sufficient accuracy for a safe, manned re-entry. The question now becomes how well did the aerodynamicist do in the predictions? These preflight aerodynamic predictions[12] represent the culmination of the most intense aerodynamic development effort ever undertaken. The foundation of these predictions was an extensive wind tunnel program of more than 27,000 occupancy hours. This wind tunnel data base has been extensively analyzed by a team of aerodynamicists representing expertise from NASA, the prime contractor, and the Department of Defense. State of the art computer codes supplemented the wind

tunnel analysis. The success in predicting the flight aerodynamics represented a test of the nation's state of the art aerodynamic capability in the 1970's. For the first time in aircraft development history, the aerodynamicist was required to establish uncertainty levels (bounds) for preflight predictions. An assessment of how well the aerodynamic community performed is indicated by the ability to predict flight data within the wind-tunnel-to-flight-uncertainties (i.e. variations).

CORRELATION OF FLIGHT WITH PREDICTED

FLIGHT TEST PROGRAM

One of the major objectives of the Orbiter flight test program is the accurate determination of the aerodynamic characteristics where placards in the operational flight envelope have been identified due to possible uncertainties (variations) in the aerodynamics. For the first orbital flight (STS-1), flight test maneuvers were not conducted in order to minimize safety risks. During the second and subsequent flights, specially designed flight test maneuvers were conducted to permit aerodynamic data extraction.

Since during entry the Orbiter is in gliding flight with a relatively steep glide path slope, correlation of Orbiter flight data with predicted was somewhat more difficult than with more conventional powered aircraft. The aerodynamic analyst was faced with the dilemma of having all flight conditions varying simultaneously from entry to touchdown. Accordingly, the correlation of cause and effect was considerably more difficult.

Although a number of parameters have a significant effect on the aerodynamics, Mach number was selected as the prime correlating parameter in order to provide an overview of the entire flight. Therefore, an analysis technique must be selected to minimize the effect of the other parameters.

In order to make a meaningful correlation of data from several flights, the effect of flight-to-flight differences in the independent variables needed to be minimized. Since the same basic trajectories were flown for STS-1 thru -4, $\bar{V}_\infty'$, and speedbrake setting (δ_{SB}) vary only slightly (for a given Mach number) from flight-to-flight. The most significant independent variable was elevon position (δ_e), which was progressively more positive (trailing edge down) on each successive flight. The elevon position varied from -3.5° on STS-2 to 5.8° on STS-4.

In order to correlate data over several flights, the flight minus predicted was correlated with Mach number. The predicted variations (uncertainties) are shown to gage the significance of any differences.

LONGITUDINAL PERFORMANCE FLIGHT RESULTS

In wind tunnel testing, the independent parameters are known precisely, while the accuracy of the aerodynamics is not so well known. In full scale flight testing the aerodynamics are, by definition, fully simulated and the aerodynamic forces and moments may be extracted without accurate knowledge of the flight conditions. For the Orbiter, determination of the flight independent variables particularly $\bar{q}$, with sufficient accuracy for aerodynamic correlations is very difficult. Significant correlation errors can occur when using the independent variables to non-dimensionalize the flight forces and moments and to "look-up" the corresponding predicted aerodynamic coefficients. Therefore, in correlation of flight results with predictions, analysis techniques must be selected to minimize the effect of possible errors in the independent variables.

L/D was selected for comparisons of predicted and flight aerodynamics since it is only sensitive to errors in flight accelerations and is independent of dynamic pressure. As seen in figure 50, flight results show the predicted L/D to be within variations down to near Mach 1. Subsonic L/D was underpredicted by approximately 5-10%.

The longitudinal aerodynamic center of pressure (X_{CP}/L_B), which is also independent of $\bar{q}$, was selected for trim comparisons. For a trimmed vehicle, the longitudinal center of pressure coincides with the flight cg. Figure 51 presents a comparison of the flight and predicted centers of pressure. As can be seen in this figure at Mach numbers above 10, the predicted X_{cp}/L_B is more aft than the flight value by as much as 0.7% of the reference body length (1.9% of the MAC), which is

well outside variations. As shown from Mach 3 to 10, flight results indicate that longitudinal trim was accurately predicted even though unusually high α's between 15° and 30° were flown. Although the flight results agreed with the predicted data within the variation (uncertainty) bounds, the agreement is less than satisfactory.

LATERAL-DIRECTIONAL STABILITY AND CONTROL CORRELATIONS

In order to permit the accurate extraction of stability and control characteristics, specially designed maneuvers were designed and conducted starting with STS-2.[24] The two primary types of stability and control maneuvers are: (1) Programmed Test Inputs (PTI) and (2) Aero Stick Inputs (ASI). Although both types of maneuvers are designed preflight to yield the optimum vehicle motion for data extraction, the PTIs generally result in better quality data because they are precisely executed, as designed, by the on-board computer. The ASIs are manually executed by the crew. More detailed descriptions of the flight test maneuvers, instrumentation, and data extraction techniques may be found in references 24 through 27.

Correlations of flight with predicted data are shown in figures 52 through 55 for lateral-directional stability, aileron effectiveness, and rudder effectiveness. Over the majority of the entry flight regime, flight results show good agreement with predicted data. However, at a few points during entry, both the lateral-directional stability and aileron effectiveness show differences between flight and predicted data approaching the variations level. Based on results extracted from the PTIs, rudder effectiveness appears to be well predicted throughout the flight regime.

As might be expected, the two regimes which show the largest differences between flight and predicted data are the transonic and hypersonic real gas regimes. The transonic wind tunnels have an inherent problem area of blockage and shock reflection due to tunnel walls, while at the same time having an order of magnitude lower Reynolds number than flight. And no tunnel today has the capability to truly simulate the real gas environment. In the hypersonic regime above Mach 10, the lateral stability, C_{ℓ_β}, appears to be less stable than was predicted while the directional stability, C_{n_β}, does not show any discernable trends. Flight results shown in figure 54 indicate that the elevon has a stronger effect on aileron effectiveness than was predicted.

In the transonic speed regime, the vehicle appears to be laterally more stable than predicted. However, there is considerable scatter in the flight directional stability data. Below Mach 3, the flight results indicate that the aileron is less effective in roll than predicted.

Recalling that the aerodynamic variations were derived from wind tunnel-to-flight differences experienced by previous aircraft,[22] it appears that, based on four flights, the Space Shuttle Orbiter stability and control aerodynamics were generally better predicted than most other aircraft.

RCS JET INTERACTION

The interference between the RCS jet plumes and the flow field at high altitudes is one of the more significant differences observed between flight and predicted data. The term "jet interference" is used to indicate combined jet interaction and plume impingement effects. During the first flight of the Space Shuttle (STS-1), the execution of the first bank maneuver during entry resulted in damped oscillations in sideslip angle and roll rate that were significantly larger than were predicted by preflight simulations. As shown in figure 56, oscillations up to 4° in sideslip occurred in flight whereas only 1° was predicted. Analysis of flight data indicates this was due to an overprediction of the rolling moment due to side-firing jets ($RM_{JI_{SFJ}}$) in the high Mach number, high altitude regime. As shown in figure 57, flight results obtained from PTIs conducted on STS-2, -3, and -4 not only confirm this overprediction, but also indicate that the jet interference is a function of the number of jets firing.[28] Because the $RM_{JI_{SFJ}}$ is of opposite sign and greater than the rolling moment due to direct thrust, it causes a reversal in the total rolling moment due a jet firing.

Flight results have also shown that the yawing moment jet interference ($YM_{JI_{SFJ}}$) and side force jet interference ($SF_{JI_{SFJ}}$) due a side-firing jet were underpredicted. Analysis of flight results

have also indicated that the pitching moment ($PM_{JI_{DFJ}}$) and rolling moment ($RM_{JI_{DFJ}}$) jet interference due to down-firing jets is less than predicted, as shown in figure 58. (A more comprehensive analysis may be found in reference 28.)

The flight test results obtained to-date indicate that both the side-firing jets and the down-firing jets are in general more effective than predicted.

POSTFLIGHT ANALYSIS

Several papers at the Langley "Shuttle Performance: Lessons Learned" conference[29] held in March of 1983, addressed the aerodynamic prediction deficiencies identified in a previous section.

An analysis is presented in reference 30 concludes that the underprediction of the subsonic L/D was due primarily to the over-prediction of profile drag. An over-estimate of the drag increment added for nonsimulation of the thermal protection system (TPS) steps and gaps led to this profile prediction deficiency.

Reference 30 presents an analysis of the longitudinal trim characteristics. The hypersonic pitching moment prediction deficiency is attributed to an error in prediction of the center of pressure. This is further substantiated by the good agreement between flight and predicted bodyflap and elevon effectiveness.

A possible explanation of the basic vehicle center of pressure prediction deficiency is addressed in reference 31. In this analysis, Mach, real gas, and viscous effects are incremented to Mach 8 wind tunnel data. Mach and real gas increments were obtained from computational fluid dynamic codes that were not available in the Shuttle development time frame. An estimate of pitching moment increments due to an increase in viscous shear acting on the bottom surface of the vehicle is obtained by semi-empirical means. This buildup process is presented in figure 59. Figure 60 shows a good prediction of trim bodyflap when these corrections are applied.

Finally, reference 32 concludes that the proper wind tunnel simulation parameter for RCS jet interaction still has not been identified.

CONCLUDING REMARKS

This paper has reviewed the aerodynamicists' success in conquering the challenges that were present in the Space Shuttle Program.

Apparently, the current state of the art real gas prediction techniques would properly account for the hypersonic center of pressure change encountered during re-entry of the Space Shuttle, although the quest for the proper RCS wind tunnel simulation parameter continues.

Although the flight tests for the majority of the Shuttle systems are completed, the aerodynamic flight test program is scheduled to continue through flight 17 in order to certify flight over the design cg range of $0.65 \, L_B$ to $0.675 \, L_B$. This extended program will allow the program not only to refine the ability to predict the aerodynamics of the Orbiter, but also to provide the researcher with an extensive flight data base which should be used to improve future testing and prediction techniques.

The challenge of the future rests in the hands of the researcher and the future program analysts. That challenge is to fully exploit the methods, the information, and the experience gained from the most extensive, complicated, aerodynamic development program ever accomplished: America's Space Shuttle.

REFERENCES

1. Whitnah, A. M.; and Hillje, E. R.: Space Shuttle Wind Tunnel Testing Summary, NASA RP-TBD, 1983.
2. Rockwell International Space Division, "Aerodynamic design Data Book, Volume 1, Orbiter Vehicle," November 1977, Report No. SD72-SH-0060-1K.

3. Smith, E. P.: "Space Shuttle Orbiter and Subsystem," Rockwell International Space Division Report No. SD72-SH-0144, June 1973.

4. Hooks, I.; Homan, D.; Romere, P. O.;: Aerodynamic Challenges of ALT, NASA JSC Space Shuttle Conference, NASA CP-TBD, June 1983.

5. Surber, T. E. and Olsen, D. C.: "Space Shuttle Orbiter Aerodynamic Development," Journal of Spacecraft and Rockets, Vol. 15, No. 1, January-February 1978, pp 40-47.

6. NASA LaRC, "High Reynolds Number Research," October 1976, NASA CP-2009, pp 2-17.

7. Hayes, Wallace D. and Probstein, Ronald F.: "Hypersonic Flow Theory," New York and London, Academic Press, 1959, pp 333-345.

8. Whitfield, Jack D. and Griffith, B. J.: "Hypersonic Viscous Drag Effects on Blunt Slender Cones," AIAA Journal, Vol. 2, No. 10, October 1964, pp 1714-1722.

9. Bertram, Mitchell H.: "Hypersonic Laminar Viscous Interaction Effects on the Aerodynamics of Two-Dimensional Wedge and Triangular Planform Wings," NASA TN-D3523, August 1966.

10. Woods, W. C.; Arrington, J. P.; and Hamilton II, H. H.: A Review of pre-flight Estimates of Real-Gas Effects on Space Shuttle Aerodynamic Characteristics, NASA CP-2283, March 1983.

11. Rausch, J. R., General Dynamics Convair Division, "Space Shuttle Orbiter Rear Mounted Reaction Control Systems Jet Interaction Study," May 1977, Report No. CASD-NSC-77-003.

12. Rockwell International Space Division; Pre-Operational Aerodynamic Design Data Book, Vol. 1, Orbiter Vehicle, SD72-SH-0060-1L-7, April 1982.

13. Ware, G. M. and Spencer, Jr., B.: "Remotely Driven Model Control Surfaces for Efficient Wind-Tunnel Operations, AIAA 21st Aerospace Science Meeting, AIAA 83-0148, January 1983.

14. Rockwell International Space Division: Aerodynamic Design Data Book, Vol. 1, Orbiter Vehicle, SD72-SH-0060-1L-2, April 1979.

15. Rockwell International Space Division: Aerodynamic Design Data Book, Orbiter Vehicle, STS-1, Final Report, NASA CR-160903, Nov. 1980.

16. Kemp, N. D.: Compiling the Space Shuttle Win Tunnel Data Base: An Exercise in Technical and Managerial Innovations, NASA CP-2283, March 1983.

17. "Aerodynamic Preliminary Analysis System, Part I-Theory, "NASA CR-145284, April 1978.

18. "Aerodynamic Preliminary Analysis System, Part II-User's Manual and Program Description," NASA CR-145300, April 1978.

19. Polhamus, E. C.: "Effect of Flow Incidence and Reynolds number on Low Speed Aerodynamic Characteristics of Several Noncircular Cylinders with Application to Directional Stability and Spinning," NASA Technical Report R-29, 1959.

20. Jorgenson, Leland H. and Brownson, Jack J.: "Effect of Reynolds Number and Body Corner Radius on Aerodynamic Characteristics for Space Shuttle-Type Vehicle at Subsonic Mach Numbers," NASA TN D-6615, January 1972.

21. Young, James C.; and Underwood, Jimmy M.: The Development of Aerodynamic Uncertainties for the Space Shuttle Orbiter. AIAA Paper 82-0563, March 1982.

22. Weil, Joseph; and Powers, Bruce G.: Correlation of Predicted and Flight Derived Stability and Control Derivatives - With Particular Application to Tailless Delta Wing Configurations. NASA TM-81361, July 1981.

23. Gamble, J. D.; and Young, J. C.: The Development and Application of Aerodynamic uncertainties in the Design of the Entry Trajectory and Flight Systems of the Space Shuttle Orbiter, AIAA 9th Atmospheric Flight Mechanics Coneference, AIAA-82-1335, August 1982.

24. Underwood, J. M.; and Cooke, D. R.: Correlation of Flight with Wind Tunnel Stability and Control Aerodynamics of the Space Shuttle Orbiter, 13th Congress of the International Council of the Aeronautical Sciences, ICAS-82-3.3.2, August 1982.

25. Cooke, D. R.: Space Shuttle Stability and Control Test Plan. AIAA Paper 82-1315, August 1982.

26. Maine, Richard E.; and Iliff, Kenneth W.: User's Manual for MMLE3, A General FORTRAN Program for Maximum Likelihood Parameter Estimation. NASA TP-1563, 1980.

27. Maine, Richard E.; and Iliff, Kenneth W.: The Theory and Practice of Estimating the Accuracy of Dynamic Flight-Determined Coefficients. NASA RP-1077, July 1981.

28. Stone, J. S., and Baumbach, J. J.: Space Shuttle Orbiter Reaction and Control Subsystem Flight Data Anomalies, NASA CP-2283, March 1983.

29. Arrington, James P.; and Jones, Jim J.: Shuttle Performance: Lessons Learned, NASA CP-2283, March 1983.

30. Romere, P. O., and Whitnah, A. M.: Space Shuttle Entry Longitudinal Aerodynamic Comparisons of Flights 1-4 with Preflight Predictions, NASA CP-2283, March 1983.

31. Griffith, B. J.; Maus, J. R.; and Best, J. T.: Explanation of the Hypersonic Longitudinal Stability Problem - Lessons Learned, NASA CP-2283, March 1983.

32. Roberts, B. B.; Wallace, R. O.; and Kanipe, D. B.: "Rocket Exhaust Plume Induced Flowfield Interaction Experiences with the Space Shuttle," AIAA-82-1549, AIAA 18th Thermophysics Conference, June 1983.

TABLE 1.- AERODYNAMIC DESIGN CRITERIA

PARAMETER	VALUE
ANGLE OF ATTACK	
HYPERSONIC	25 TO 50 DEG
TRANSONIC	0 TO 15 DEG
SUBSONIC	-5 TO 20 DEG
CENTER-OF-GRAVITY RANGE	
MINIMUM TRAVEL	2% BODY LENGTH
DESIGN RANGE	$0.65\ L_B - 0.675\ L_B$
LANDING PERFORMANCE	
PAYLOAD	(14,515 Kg) 32,000 LB
LANDING WEIGHT (WITH PAYLOAD)	(85,230 Kg) 187,900 LB
MINIMUM DESIGN TOUCHDOWN SPEED, V_D	(88 m/s) 171 KNOTS
LONGITUDINAL STABILITY	
MINIMUM HYPERSONIC STATIC MARGIN	POSITIVE
MINIMUM SUBSONIC STATIC MARGIN	
(AFT CENTER OF GRAVITY)	$-2\%\ L_B$ (-5.45% MAC)
LIFT/DRAG MODULATION	
PEAK SUBSONIC VALUE (GEAR UP, δ_{SB} = 0)	NOT LESS THAN 4.4
PEAK SUBSONIC VALUE (GEAR UP, δ_{SB} = 85 DEG)	NOT LESS THAN 2.5

TABLE 2.- SPACE SHUTTLE ORBITER WIND TUNNEL UTILIZATION SUMMARY

TEST IDENTIFICATION	FACILITY	MODEL SCALE
TRANSONIC		
OA145A	ARC 11 x 11 FT	-.05
OA270A	LaRC 16T	.05
OA270B	LaRC 16T	.02
LA70	CALSPAN 8 FT	.015
LA76	LTV 4 x 4 HSWT	.015
LA77	ARC 11 x 11 FT	.015
LA111	LaRC 8 FT TWT	.015
LA115	LaRC 8 FT TWT	.015
SUPERSONIC		
OA145B	ARC 9 x 7 FT	.05
OA145C	ARC 8 x 7 FT	.05
OA209	AEDC "A"	.02
LA63A	LaRC UPWT-1	.015
LA63B	LaRC UPWT-2	.015
LA75	LaRC UPWT-2	.015
LA76	LTV 4 x 4 HSWT	.015
LA101	LaRC UPWT-1	.015
LA110	LaRC UPWT-1	.015
LA114	LaRC UPWT-2	.02
LA125	LaRC UPWT-2	.02
LA131	LaRC UPWT-2	.02
LA144	LTV 4 x 4 FT	.02
HYPERSONIC		
OA113	CALSPAN HST (48 IN.)	.01
OA171	NSWC TUNNEL 9	.02
OA208	AEDC "B"	.02
OA257	LaRC 20 IN.	.01
OA258	AEDC "B"	.02
OA259	AEDC "B"	.01

TABLE 3.- KEY AERODYNAMIC PARAMETERS

AERODYNAMIC PARAMETER	FLIGHT REGIME	WHY PARAMETERS ARE SIGNIFICANT	AERO CONCERN IN DEFINITION OF PARAMETERS
L/D, C_m, $C_{m_{\delta e}}$	ALL	• CROSSRANGE • TERMINAL AREA ENERGY MANAGEMENT • ELEVON REQUIRED TO TRIM • RCS FUEL USAGE	• VISCOUS INTERACTION EFFECTS • FLOW SEPARATION • REAL GAS EFFECTS NOT SIMULATED IN WIND TUNNEL
HINGE MOMENTS	TRANSONIC	• ACTUATOR DESIGN • DEFINES CONTROL SURFACE STALL AND RATE LIMITING CONDITIONS	• WIND TUNNEL WALL, BLOCKAGE, AND SHOCK REFLECTION EFFECTS
$C_{n_{\delta a}}$, $C_{l_{\delta a}}$	HIGH SUPERSONIC	• AILERON IS USED FOR BOTH ROLL AND YAW TRIM ABOVE MACH 3.5 BEFORE RUDDER IS ACTIVATED • RCS FUEL USAGE	• CONTROL SURFACE INTERACTION • EFFECT OF ELEVON ON AILERON EFFECTIVENESS
$C_{n_{\delta a}}$, $C_{l_{\delta a}}$, $C_{n_{\delta r}}$, $C_{l_{\delta r}}$	TRANSONIC/ SUPERSONIC	• RUDDER IS USED FOR BOTH YAW AND ROLL TRIM FOR $1.5 < M < 3.5$ • AILERON COORDINATES TURN • RCS YAW JET IS NEEDED UNTIL RUDDER IS EFFECTIVE • DEFINES SWITCH-OVER POINT FROM SPACECRAFT TO AIRCRAFT FCS MODE	• CONTROL SURFACE INTERACTION • RUDDER EFFECTIVENESS AT HIGH α AND MACH • AEROELASTIC EFFECTS • TRANSONIC WIND TUNNEL ACCURACIES

Booster

Orbiter

Launch configuration
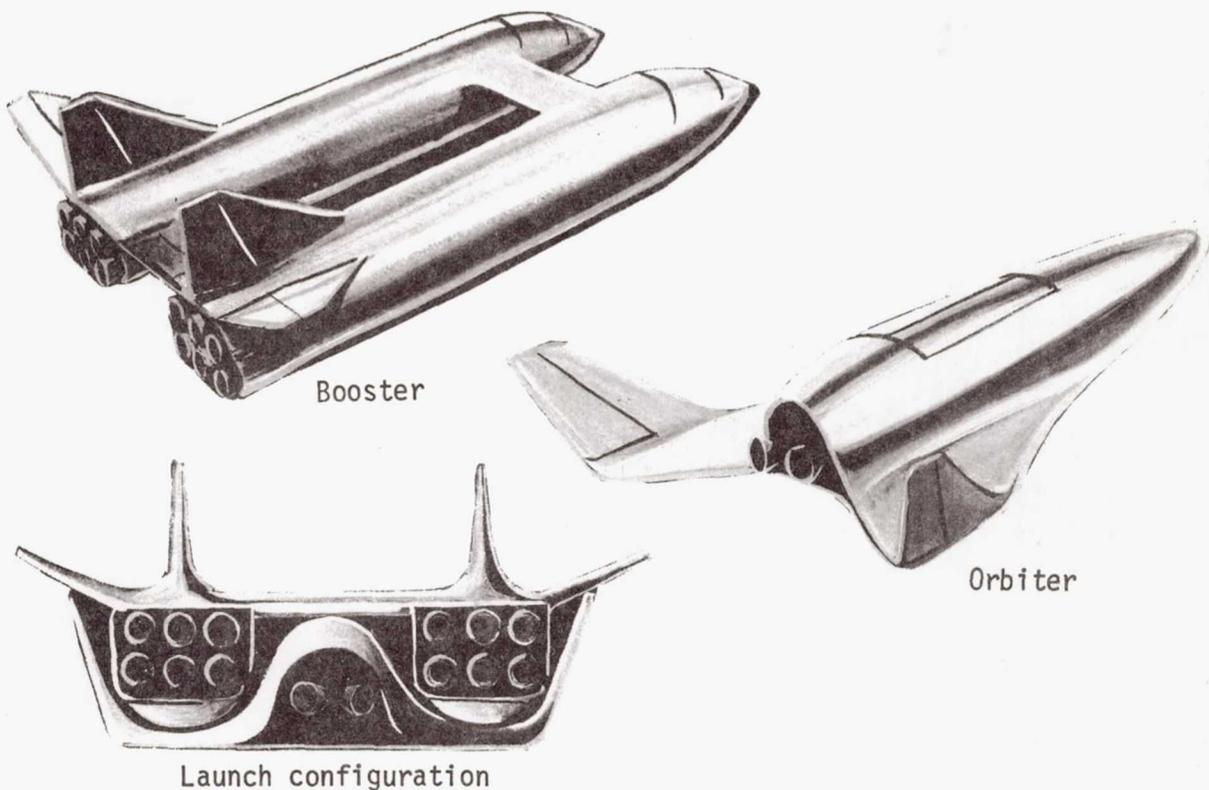
FIGURE 1.- TYPICAL PHASE A CONFIGURATION CONCEPT.
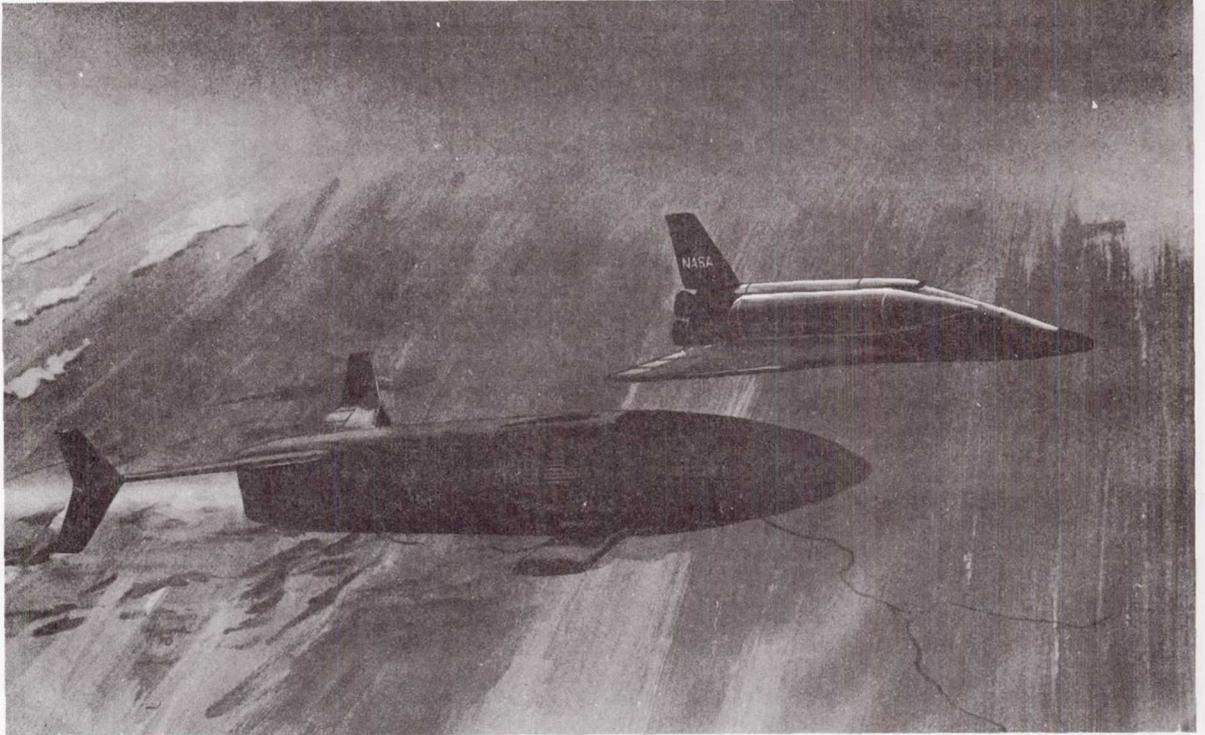
FIGURE 2.- TYPICAL PHASE B CONFIGURATION CONCEPT.
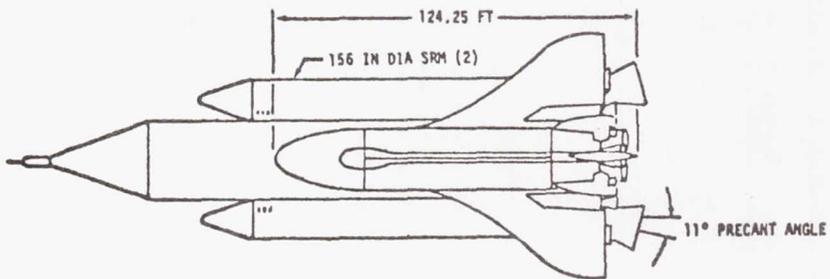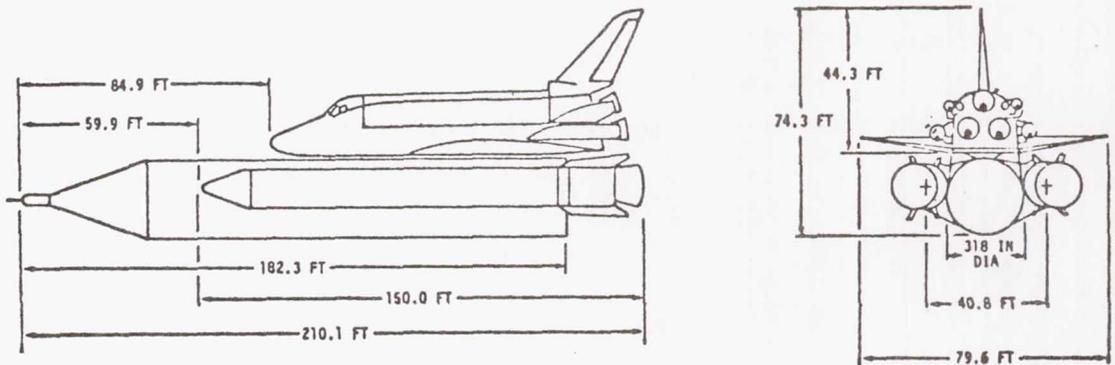
FIGURE 3.- TYPICAL PARALLEL BURN CONFIGURATION.

234

EXTERNAL
TANK (ET)
333.0 IN. DIA
(845.8 cm)

SOLID ROCKET BOOSTER
(SRB) 146.0 IN. DIA
(370.8 cm)

78.1 FT
(23.80 m)

1.57 FT
(0.48 m)

54.5 FT
(16.61 m)

0° NULL ± 8° GIMBAL

122.2 FT (37.25 m)
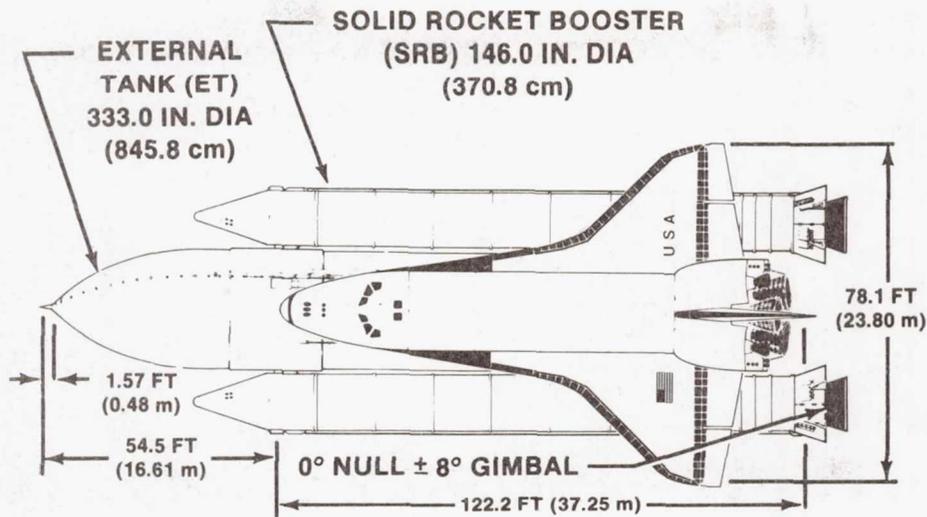
GROSS LIFT-OFF WEIGHT-2022.6 x 10^6g (4459K LB)
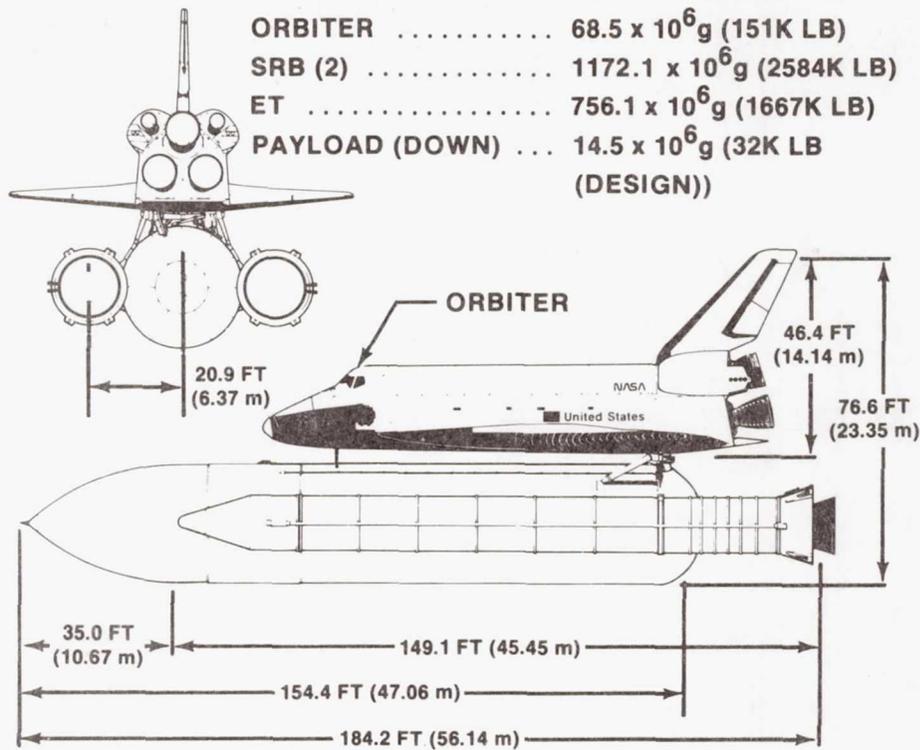
ORBITER . . . . 68.5 x 10^6g (151K LB)
SRB (2) . . . . 1172.1 x 10^6g (2584K LB)
ET . . . . 756.1 x 10^6g (1667K LB)
PAYLOAD (DOWN) . . . 14.5 x 10^6g (32K LB
(DESIGN))

ORBITER

46.4 FT
(14.14 m)

76.6 FT
(23.35 m)

20.9 FT
(6.37 m)

NASA

United States

35.0 FT
(10.67 m)

149.1 FT (45.45 m)

154.4 FT (47.06 m)

184.2 FT (56.14 m)

FIGURE 4.- SPACE SHUTTLE INTEGRATED VEHICLE FINAL CONFIGURATION.
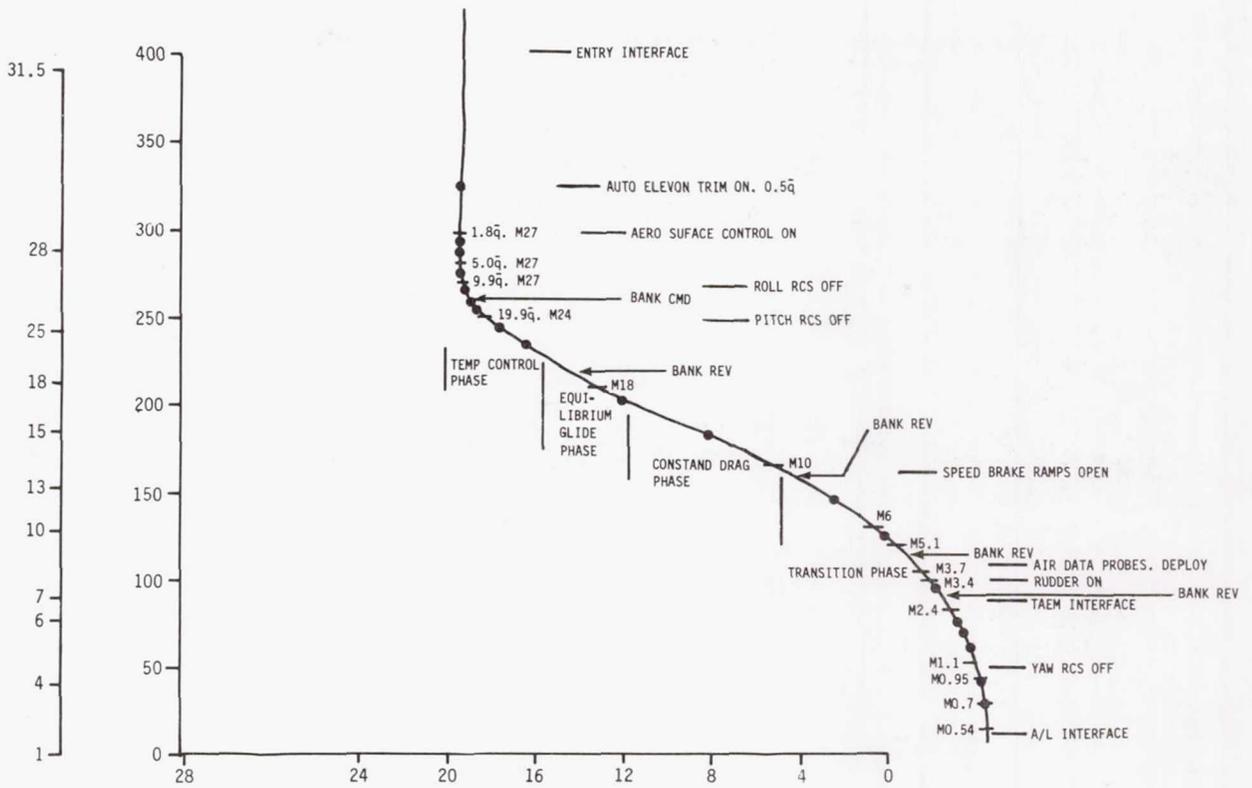
FIGURE 5.- ORBITER ENTRY PHASES.

GEOMETRY	COMPONENT			
	WING		VERTICAL TAIL	
AREA	2690	FT^2	413.25	FT^2
SPAN	936.68	IN.	315.72	IN.
ASPECT RATIO	2.265		1.675	
TAPER RATIO	0.2		0.404	
SWEEP (LE)	81/45	DEG	45	DEG
DIHEDRAL	3.5		– –	
INCIDENCE	0.5	DEG	– –	
MAC	474.81	IN.	199.81	IN.

CONTROL SURFACE	AREA (FT^2)	MAX DEFLECTIONS (DEG)
ELEVON (1 SIDE)	206.57	–35 TO +20
BODY FLAP	135.75	–11.7 TO +22.5
SPEEDBRAKE	97.148	0 TO 87.2
RUDDER	97.148	–22.8 TO +22.8
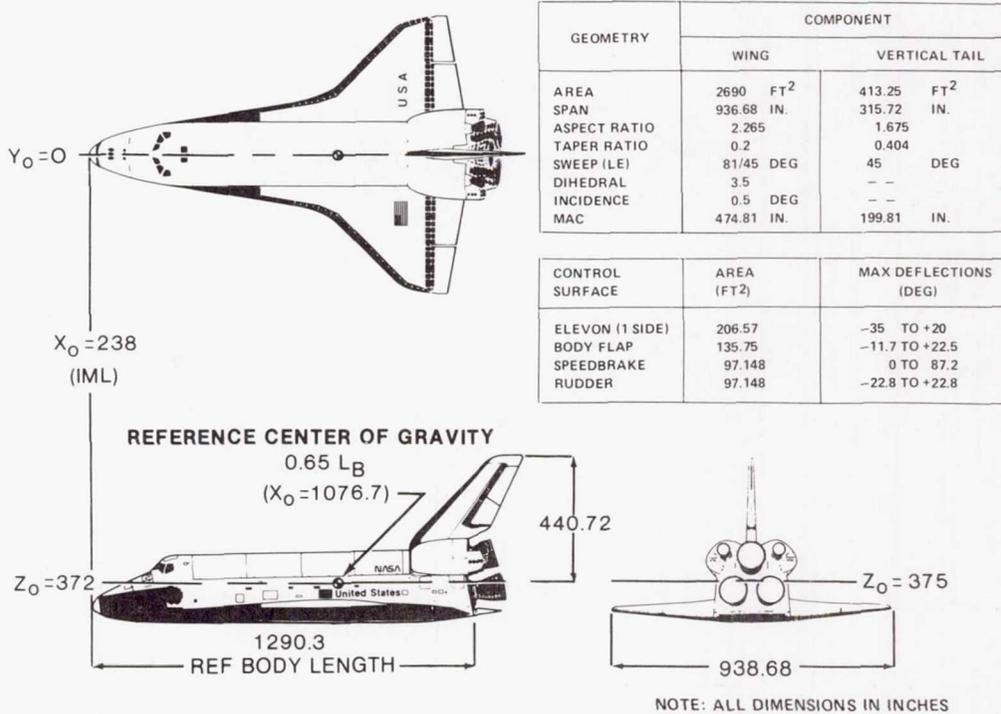
FIGURE 6.- SPACE SHUTTLE ORBITER FINAL CONFIGURATION.

236
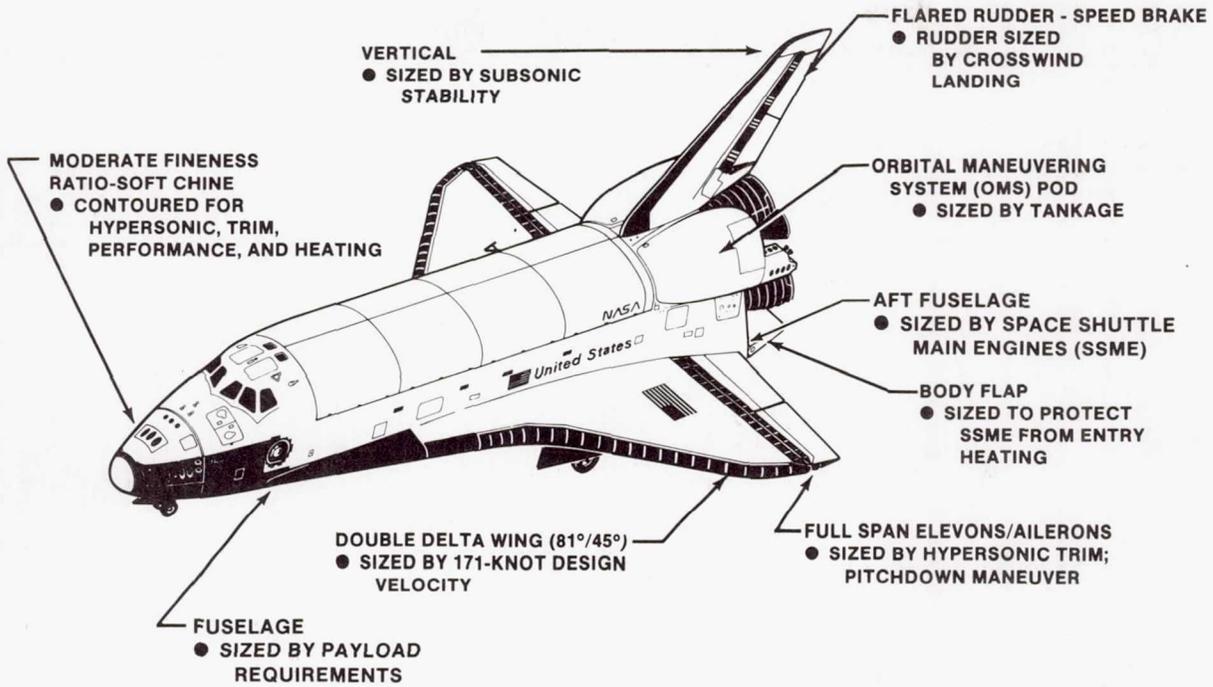
FIGURE 7.- ORBITER SIZING CRITERIA.
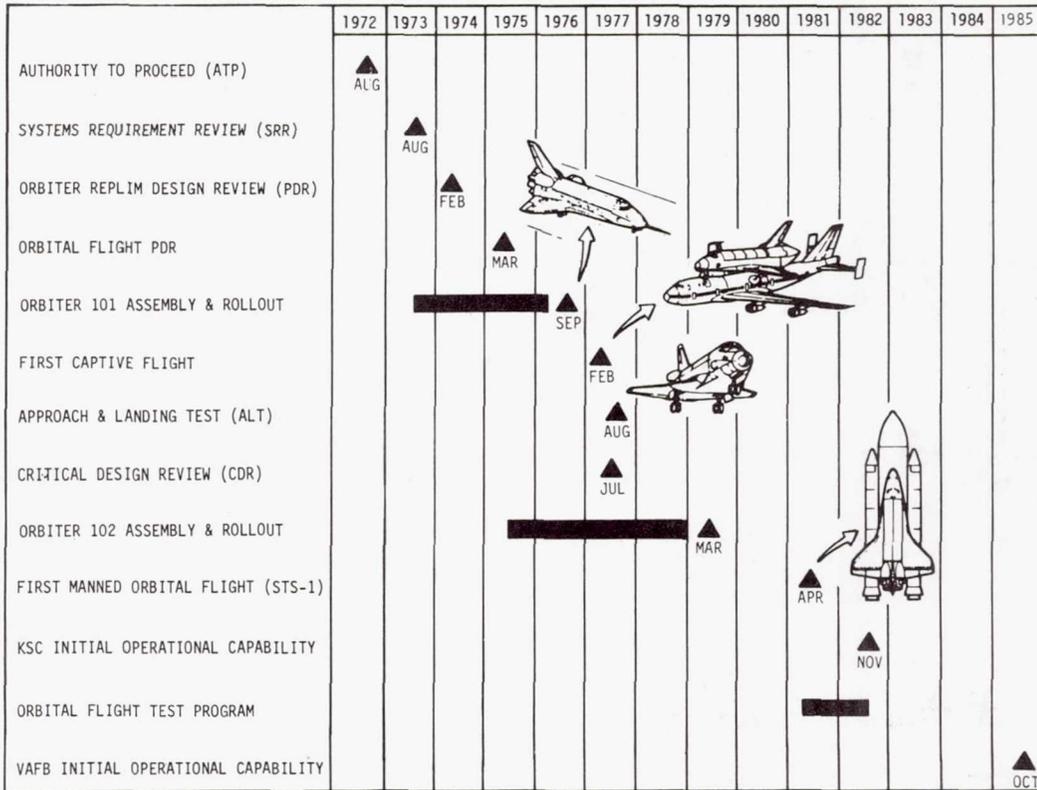
FIGURE 8.- SPACE SHUTTLE PROGRAM MILESTONES.

CONFIGURATION DESIGNATION	ATP	PRR	PDR	CDR
CONFIGURATION CONTROL DRAWING NUMBER	VL70 - 000001	VL70 - 000040A	VL70 - 000089B	VL70 - 000140C, VC70 - 000002
WING DESIGN	50° BLENDED DELTA	50° BLENDED DATA	45°/79° DOUBLE DELTA	45°/81° DOUBLE DELTA
WING AREA, FT^2 (m^2)	3220 (299.14)	3220 (299.14)	2690 (249.90)	2690 (249.90)
WING SPAN, FT (m)	84.0 (25.60)	84.0 (25.60)	78.1 (23.80)	78.1 (23.80)
OVERALL LENGTH, FT (m)	125.8 (38.34)	125.8 (38.34)	125.2 (38.18)	122.2 (37.25)
PLAN VIEW				
DRY WEIGHT, LB (kg)	170,000 (77,110)	170,000 (77,110)	150,000 (68,039)	150,000 (68,039)
LANDING PAYLOAD, LB (kg)	40,000 (18,144)	40,000 (18,144)	25,000 (11,340)	32,000 (14,515)
CG RANGE (% REFERENCE LENGTH)	65.0 - 68.0	65.0 - 68.0	66.0 - 68.0	65.0 - 67.5
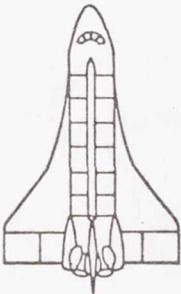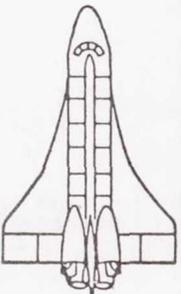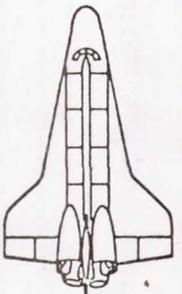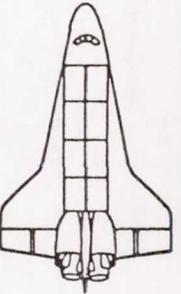
FIGURE 9.- ORBITER CONFIGURATION EVOLUTION.
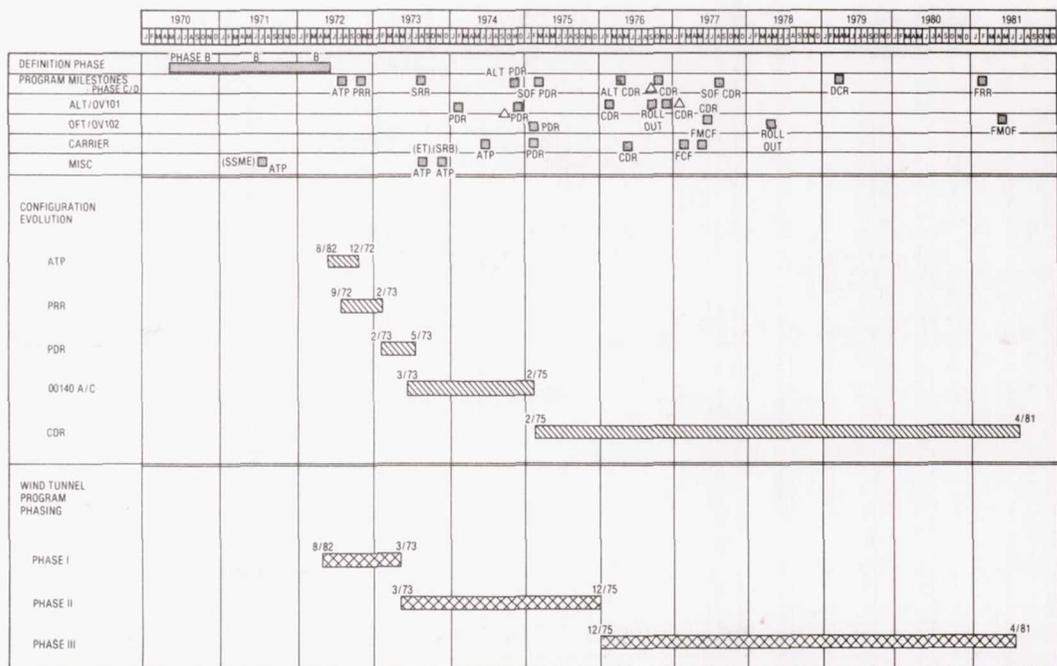
FIGURE 10.- SPACE SHUTTLE PROGRAMMATIC PHASING.
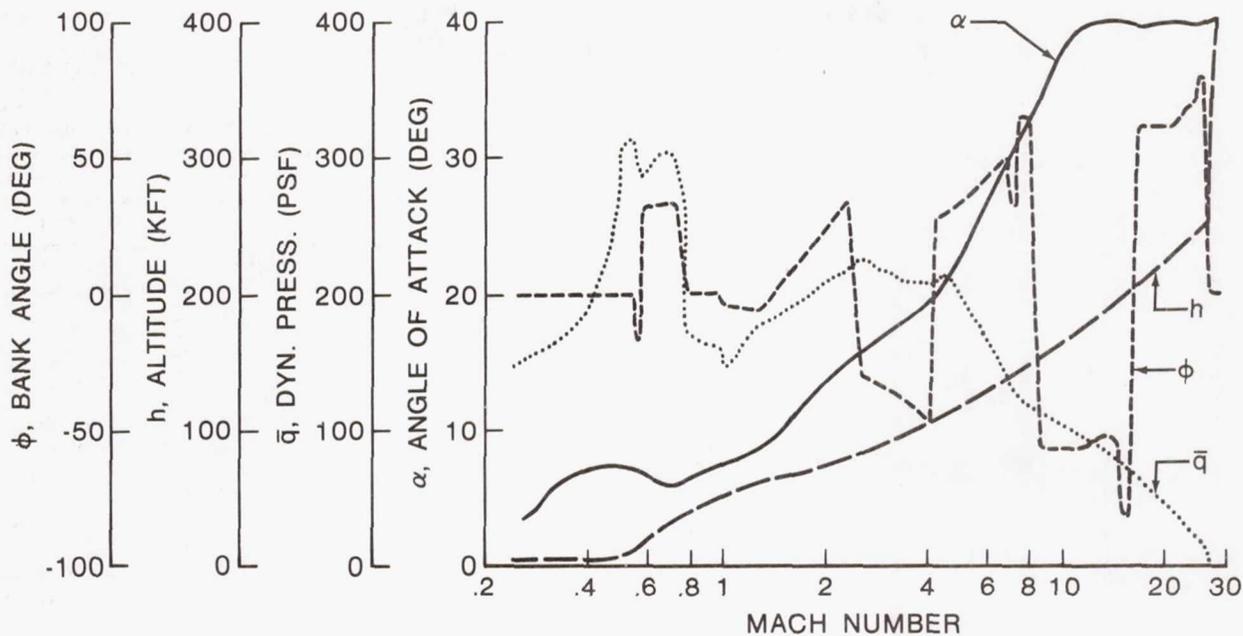
FIGURE 11.- TYPICAL ORBITER ENTRY TRAJECTORY.

PITCH-DOWN THRUSTERS

1 FWD RCS MODULE, 2 AFT RCS SUBSYSTEMS IN PODS
38 MAIN THRUSTERS (14 FWD, 12 PER AFT POD)

YAW THRUSTERS

OMS ENGINE

FIXED PITCH-UP/ROLL THRUSTERS

VERNIER THRUSTERS
FORWARD RCS MODULE

PITCH-UP/ROLL THRUSTERS

YAW THRUSTERS

PITCH-DOWN/ROLL THRUSTERS

AFT PROPULSION SUBSYSTEM (OMS/RCS POD)
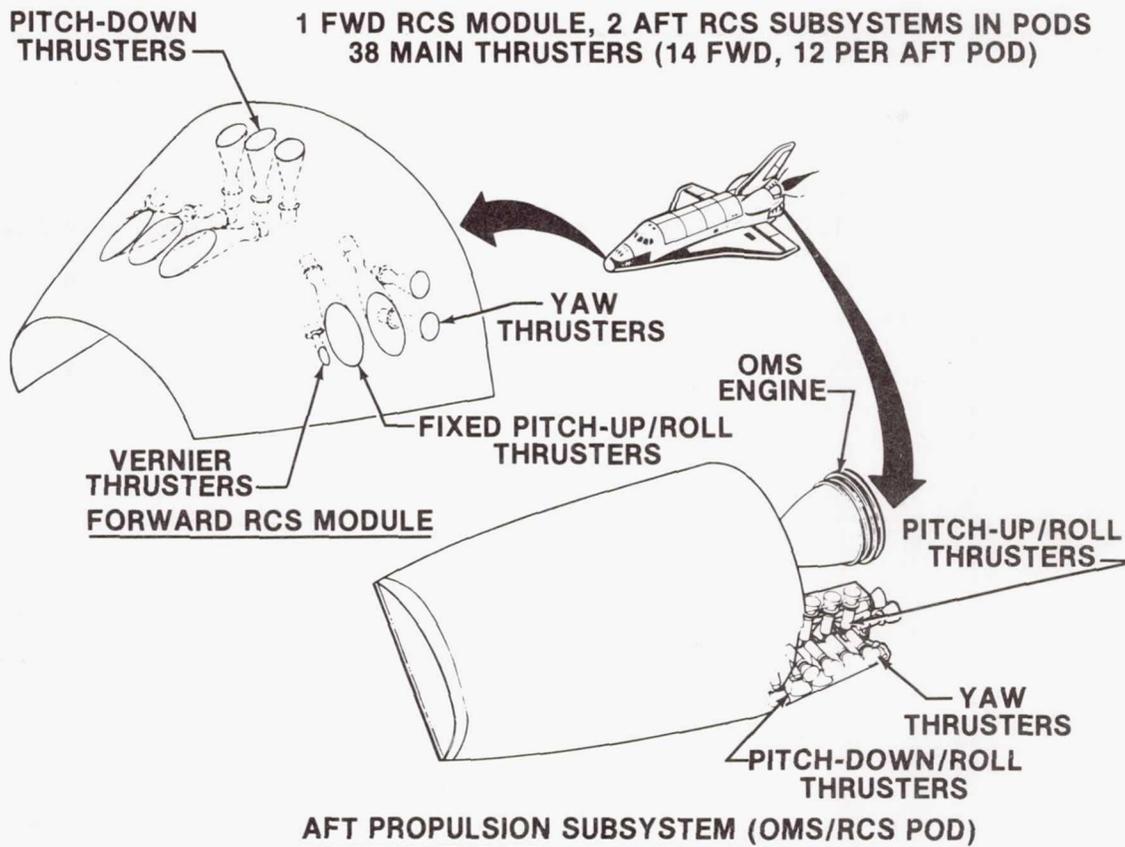
FIGURE 12.- REACTION CONTROL SYSTEM (RCS).

VERTICAL
- DIRECTIONAL STABILITY
- CONTROL EFFECTIVENESS

FLARED RUDDER-SPEED BRAKE
- L/D MODULATION AT LOW MACHS
- SUPPLEMENTS SUPERSONIC YAW STABILITY
- YAW CONTROL BELOW MACH 3.5

MODERATE FINENESS RATIO-SOFT CHINE
- HYPERSONIC L/D
- WING/BODY MATCHING

AFT REACTION CONTROL JETS
- SIDE FIRING JETS SUPPLEMENTS YAW STABILITY ABOVE SONIC SPEEDS

BODY FLAP
- PRIMARY LONGITUDINAL TRIM DEVICE
- SHIELD NOZZLES

DOUBLE DELTA WING (81°/45°)
- HIGH LIFT EFFICIENCY
- MINIMIZE WING AREA
- INCREASE CROSS RANGE

FULL SPAN ELEVONS/AILERONS
- CONTROLLER FOR LONGITUDINAL STABILITY AUGMENTATION
- SHORT PERIOD LONGITUDINAL TRIM
- ROLL CONTROL AND TRIM

FORWARD REACTION CONTROL JETS

FIGURE 13.- ORBITER FUNCTIONAL CHARACTERISTICS.

MACH

| 30 | | 25 | | 20 | | 15 | | 10 | | 5 | | 1 |

q PSF

| 02 | 10 | 20 | 30 | 40 | 50 | 60 | 70 | 80 | 90 | 100 | 110 | 120 | 150 | 200 | 190 | 160 |

| ALPHA | $40 < \alpha < 43$ | | $30 < \alpha < 40$ | | $10 < \alpha < 30$ |

| PITCH | ···RCS··· |
| | ·················ELEVONS················· |

| ROLL | ·RCS· |
| | ·················AILERONS················· |

| YAW | ·················RCS················· |
| | * RUDDER * |
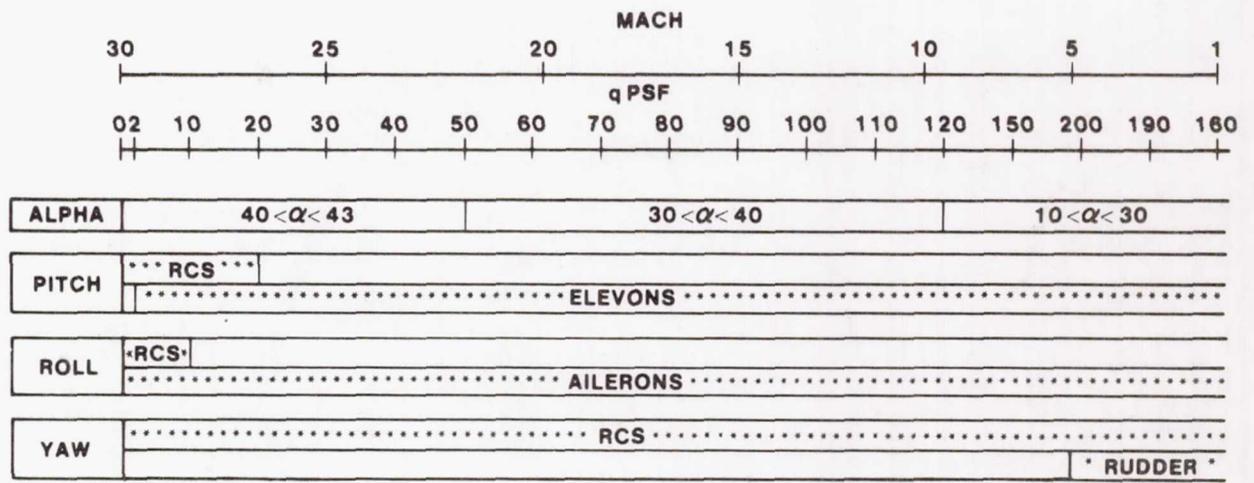
FIGURE 14.- USE OF RCS AND AEROSURFACES BY FCS.

RCS EFFECTIVENESS COMPONENTS
- **JET THRUST**
- **PLUME IMPINGEMENT**
- **FLOW FIELD INTERACTION**
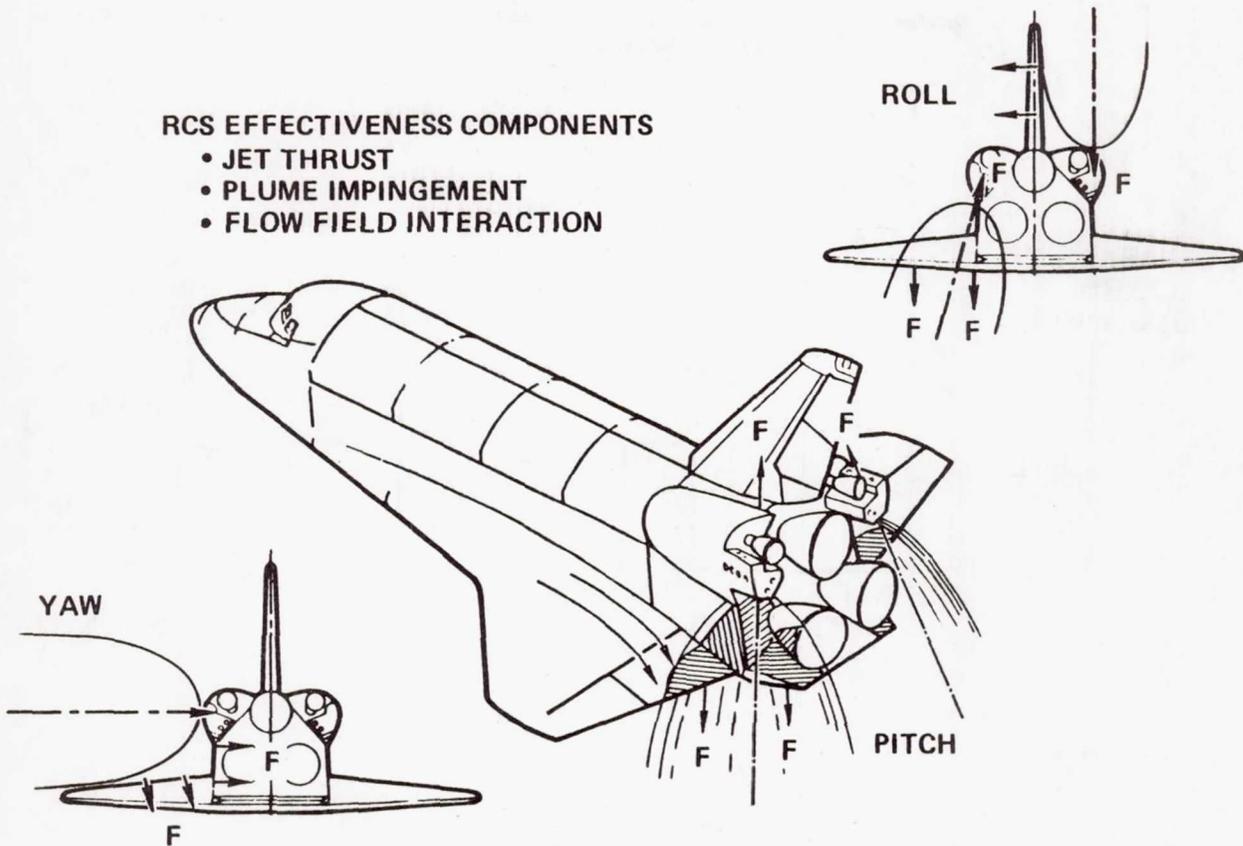
FIGURE 15.- INTERACTION OF RCS JETS WITH VEHICLE AND FLOWFIELD.
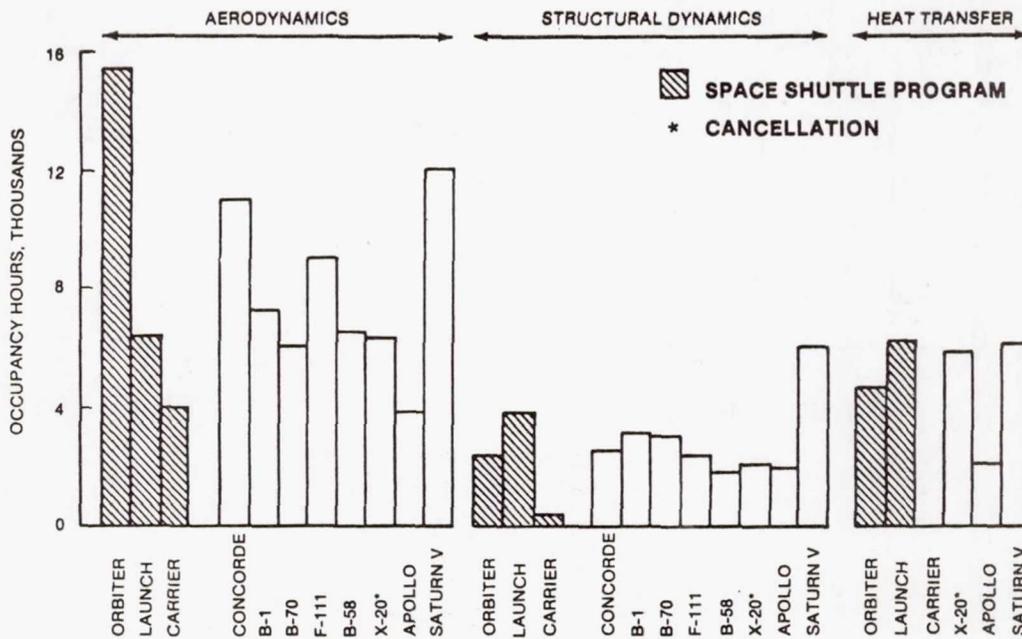
FIGURE 16.- SPACE SHUTTLE WIND TUNNEL PROGRAM.

241
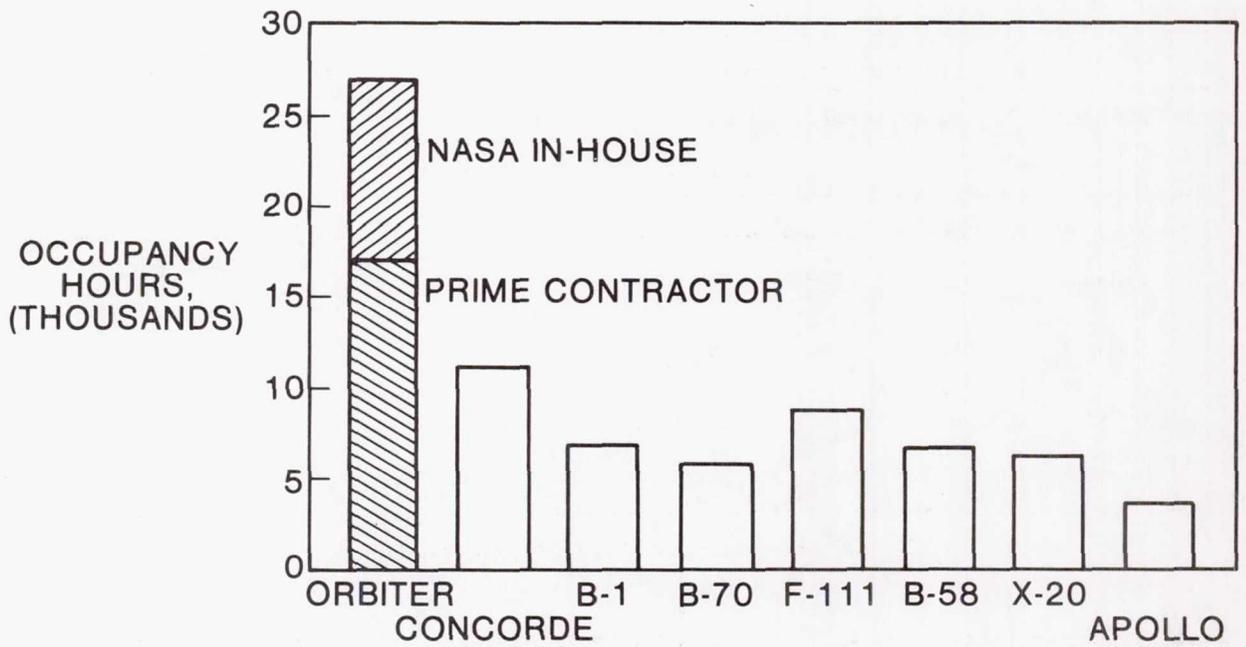
FIGURE 17.- ORBITER WIND TUNNEL PROGRAM.
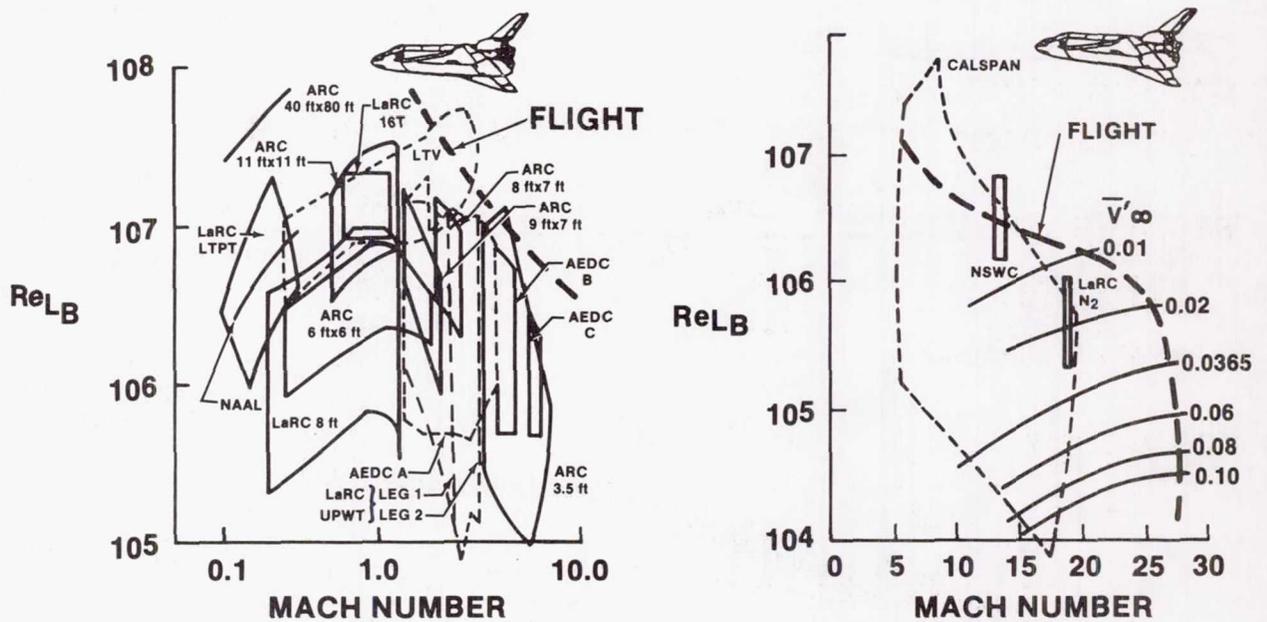
FIGURE 18.- FACILITY SIMULATION CAPABILITY.

	1977	1978	1979	1980	1981
	M A M J J A S O N D	J F M A M J J A S O N D	J F M A M J J A S O N D	J F M A M J J A S O N D	J F M A M
SHUTTLE PROGRAM MILESTONES	▨▨▨▨▨▨ ALT △ CDR	△ OV-102 ROLL OUT	△ STS-1 ADDB		△ STS-1 △ FRR
VERIFICATION TEST PROGRAM	◄— PART I —►	◄— PART II —►		◄————————— PART III —————————►	
• SUBSONIC	160 ▨ OA101				
• TRANSONIC	480 ▨ OA145A	45 ▨ LA115 312 ▨ OA270A/B/C		120 ▨ OA400	
• SUPERSONIC	448 ▨ OA145B/C	69 ▨ OA209 48 ▨ LA125		138 ▨ LA144	
• HYPERSONIC		47 ▨ OA208 180 ▨ OA171		148 ▨ LA141A 200 ▨ LA141B	128 ▨ OA258 40 ▨ OA259 324 ▨ OA257

FIGURE 19.- WIND TUNNEL VERIFICATION TEST PROGRAM.

OML DUPLICATED TO 0.1-IN. FULL SCALE
- RCC LEADING EDGE
- SRSI AND FRSI ON WING AND FUSELAGE

VERTICAL TAIL
- SPANWISE GAPS
- AERO SEALS

MAIN PROPULSION AND OMS NOZZLES (TRIMMED TO ACCOMODATE STING MOUNT)

CARGO BAY DOORS
- GAPS
- HINGE COVERS

AFT RCS POD

T-O UMBILICAL

RECESSED THERMAL GLASS
- WINDSHIELD
- OBSERVATION WINDOWS
- HATCH WINDOWS

BODY FLAP
- SPANWISE GAPS
- AERO SEALS

RCS NOZZLE CAVITIES

FLIPPER DOORS

VENT CAVITIES
- CARGO BAY
- FORWARD RCS
- CABIN
- OMS RCS
- AFT FUSELAGE

AIR DATA PROBES

STAR TRACKER PORT CAVITIES

ELEVONS
- SPANWISE GAPS
- 6-IN. GAP

FIGURE 20.- WIND TUNNEL MODEL FIDELITY.

(WING = 96 PANELS)

ELEVON

$Y_O = 0$

(TAIL = 48 PANELS)

(FUSELAGE = 30 PANELS)

RUDDER

TAIL

FUSELAGE

WING
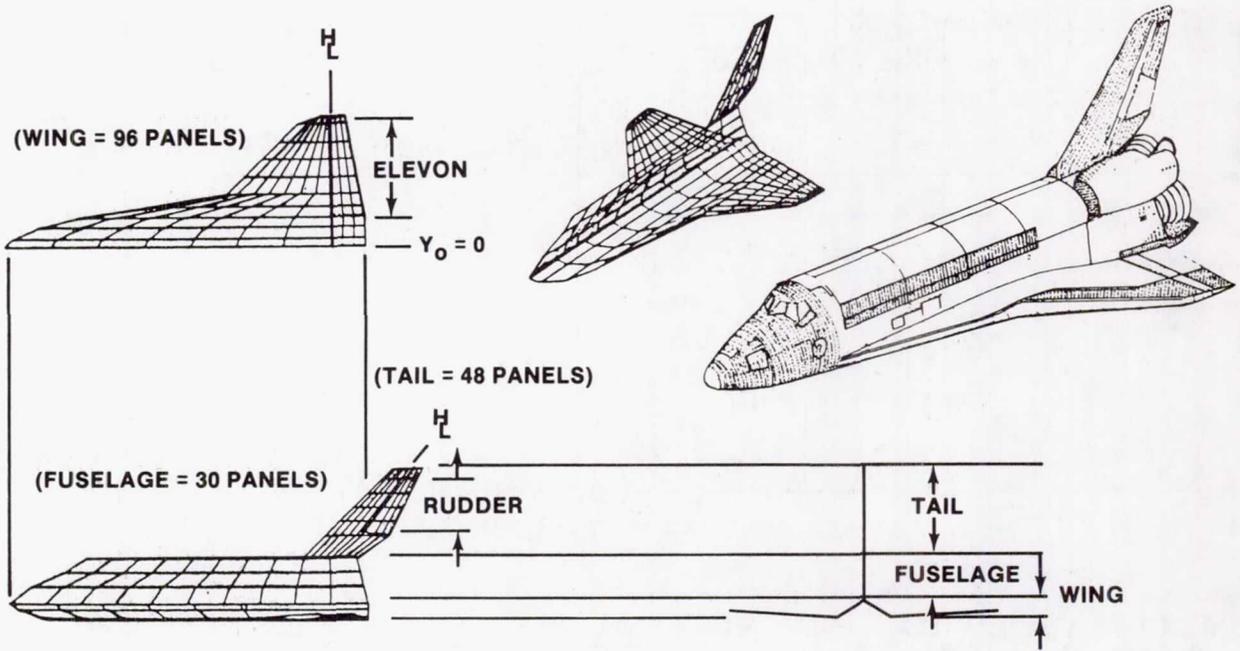
FIGURE 21.- ORBITER AERODYNAMIC PANELING.

$\dfrac{\overset{FLEX}{C_{Y_{\delta_R}}}}{\underset{C_{Y_{\delta_R}}}{RIGID}} \quad \eta_{\dot{Y}_R}$

$\dfrac{\overset{FLEX}{C_{n_{\delta_R}}}}{\underset{C_{n_{\delta_R}}}{RIGID}} \quad \eta_{n_R}$

$\dfrac{\overset{FLEX}{C_{\ell_{\delta_R}}}}{\underset{C_{\ell_{\delta_R}}}{RIGID}} \quad \eta_{\ell_R}$

DYNAMIC PRESSURE

300 psf (14,364 n/m²)

$\bar{q}$ = 300 psf
————— WIND TUNNEL
- - - - THEORY
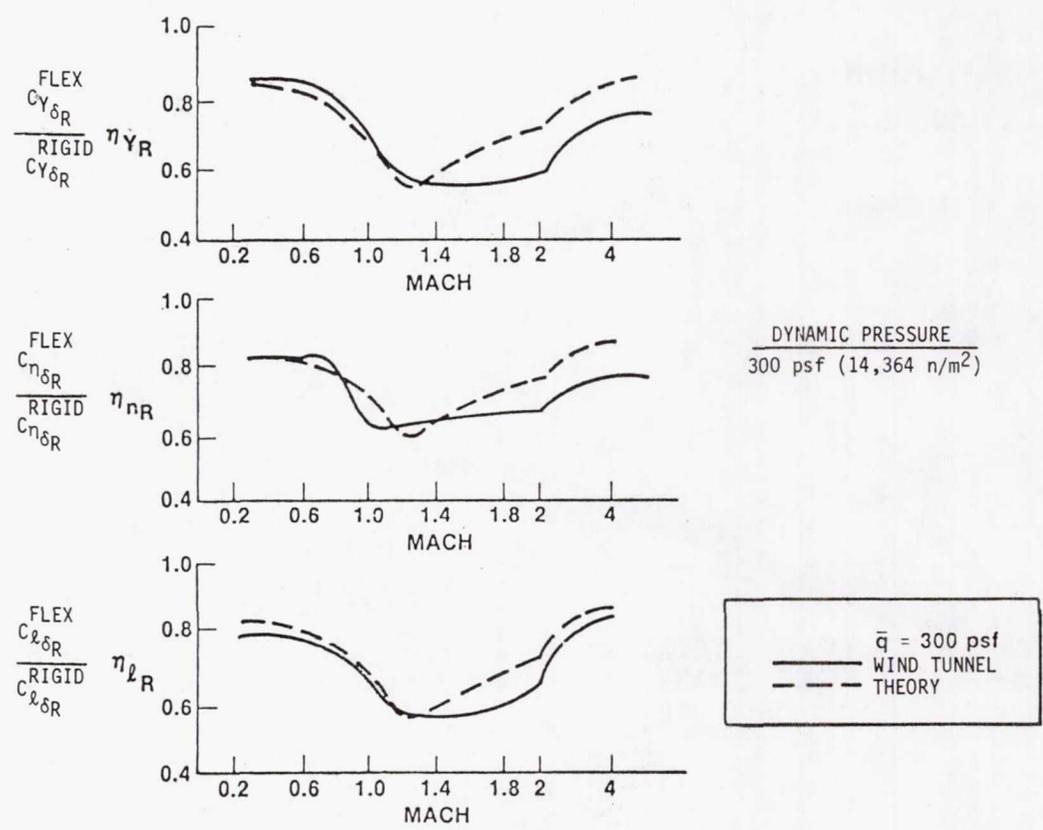
FIGURE 22.- COMPARISON OF WIND TUNNEL WITH THEORETICAL PREDICTION OF THE
AEROELASTIC EFFECTS ON RUDDER DERIVATIVES.

244

$\alpha = 20° \quad \beta = 0° \quad \delta_E = \delta_{BF} = 0° \quad \bar{q}_\infty = 1.0 \ psf \ (47.9 \ N/m^2)$

CONTROL AXIS	3-JET MOMENT (N-m)	IMPINGEMENT MOMENT (N-m)	INTERACTION MOMENT (N-m)	NET MOMENT (N-m)
ROLL	+36,590	-8,030	-27,040	+1,520
PITCH	-126,600	+8,690	+43,775	-74,135
YAW	-38,300	-7,860	-4,860	-51,020

VACUUM THRUST FOR
ONE JET (N)

$T = 3870$
$N_j = 3570$
$A_j = -756$
$Y_j = 1298$
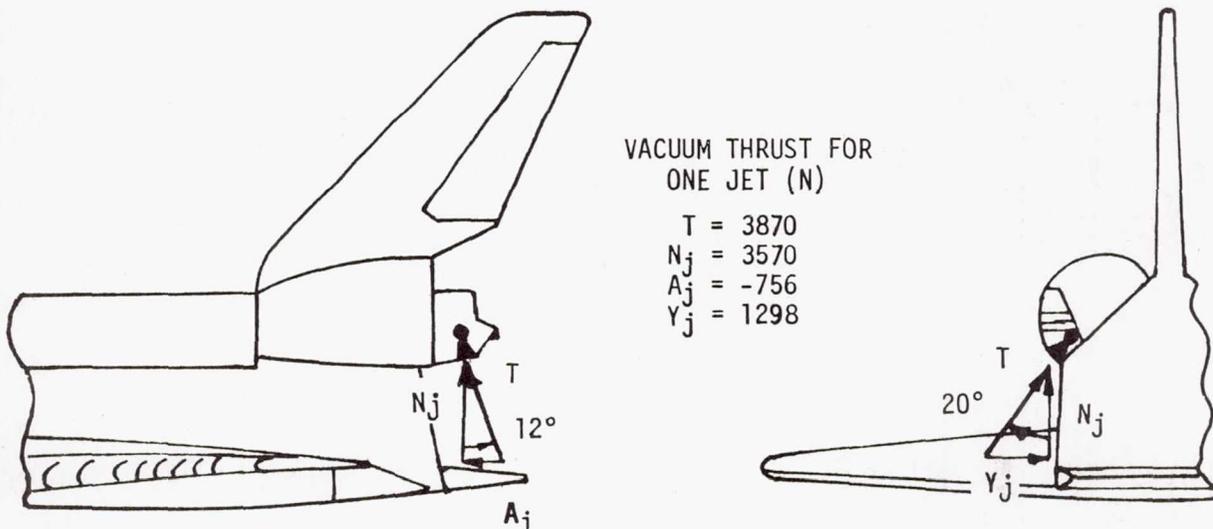
FIGURE 23.- REACTION CONTROL JET MOMENTS.
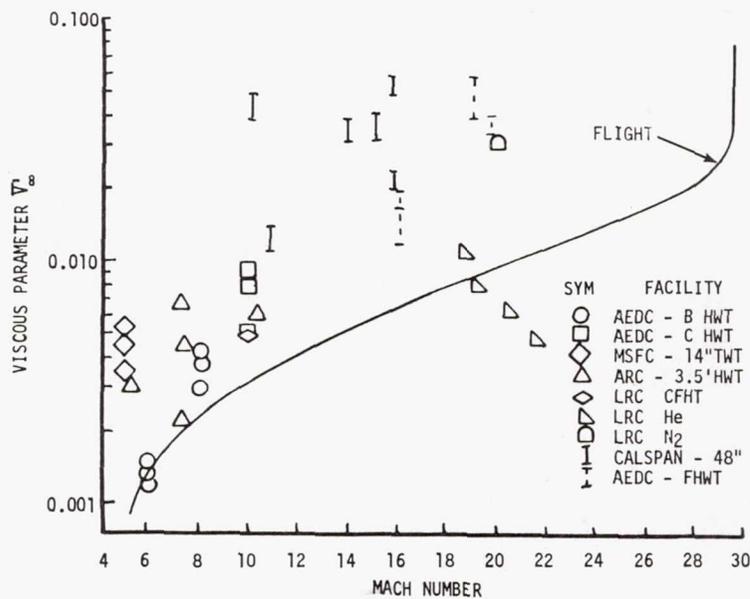
FIGURE 24.- VARIATION OF VISCOUS PARAMETER ALONG NOMINAL ENTRY TRAJECTORY.
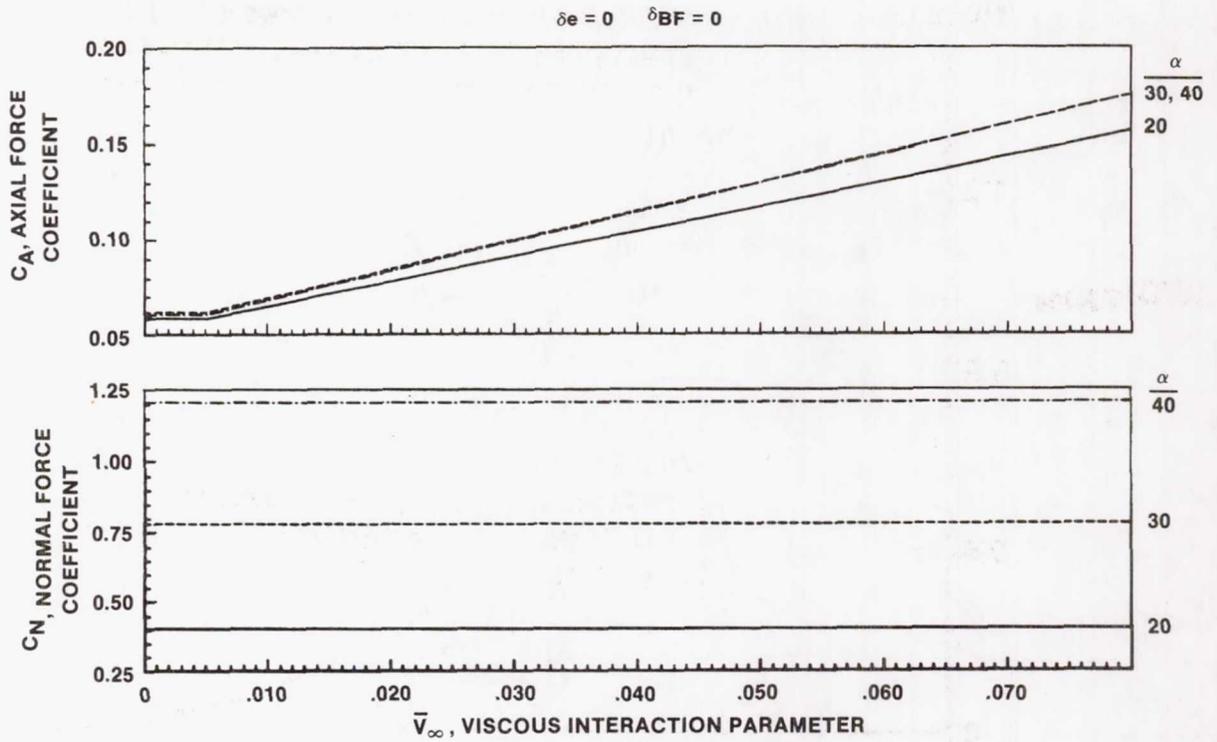
FIGURE 25.- EFFECT OF VISCOUS INTERACTION ON NORMAL AND AXIAL FORCE.
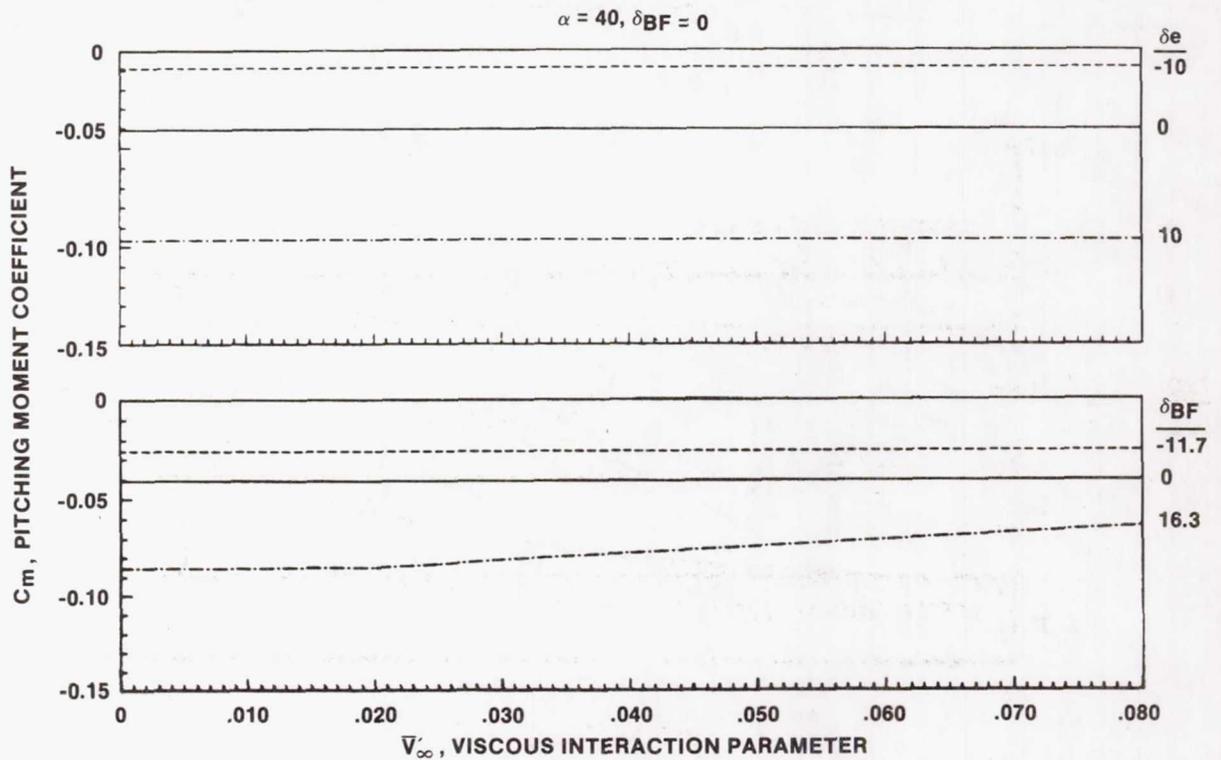
FIGURE 26.- EFFECT OF VISCOUS INTERACTION ON PITCHING MOMENT.

246
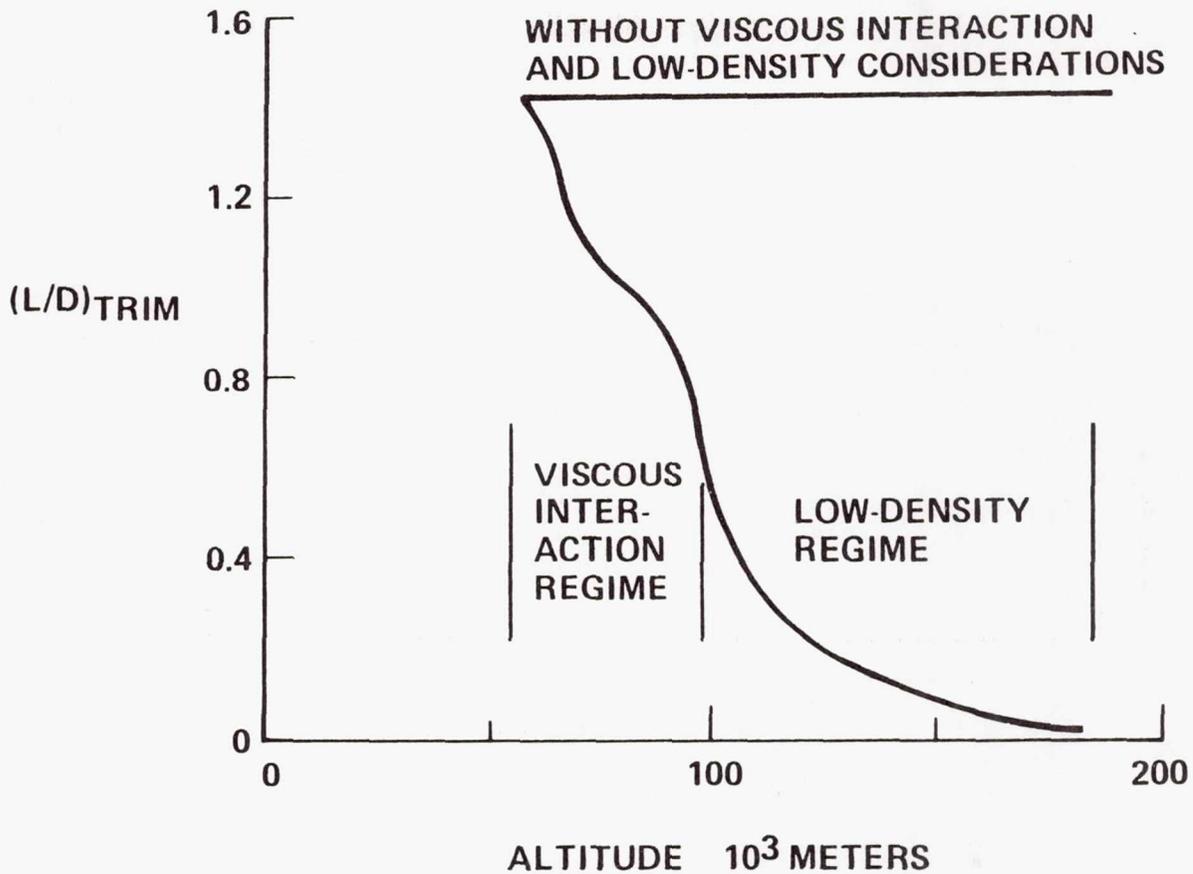
FIGURE 27.- VISCOUS INTERACTION EFFECT ON L/D.
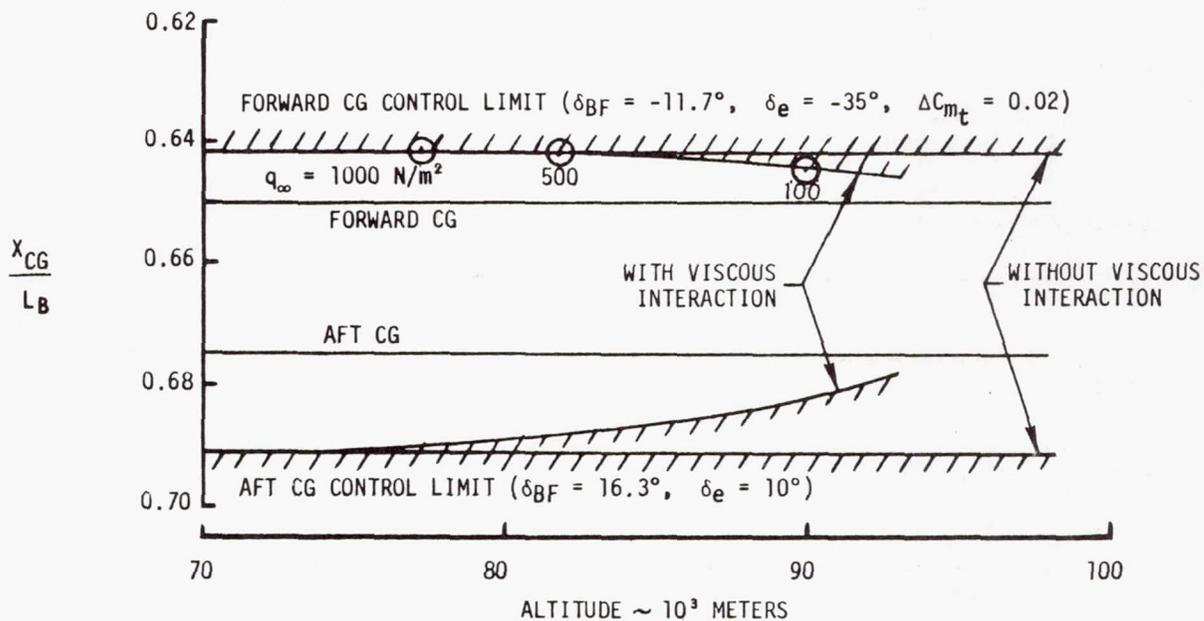
FIGURE 28.- EFFECT OF VISCOUS INTERACTION ON c.g. TRIM CAPABILITY.

MACH 0.25
ARC 40 X 80 DATA

LIFT COEFFICIENT, C_L

$\delta_e = +10^o$

0°

-10°

$a \sim$ DEG

ANGLE OF ATTACK (DEG)

C_L

$\delta_e = -10^o$

-5°

0°

$+5^o$

$+10^o$

PITCHING MOMENT, $C_{m_{0.65\,L_B}}$
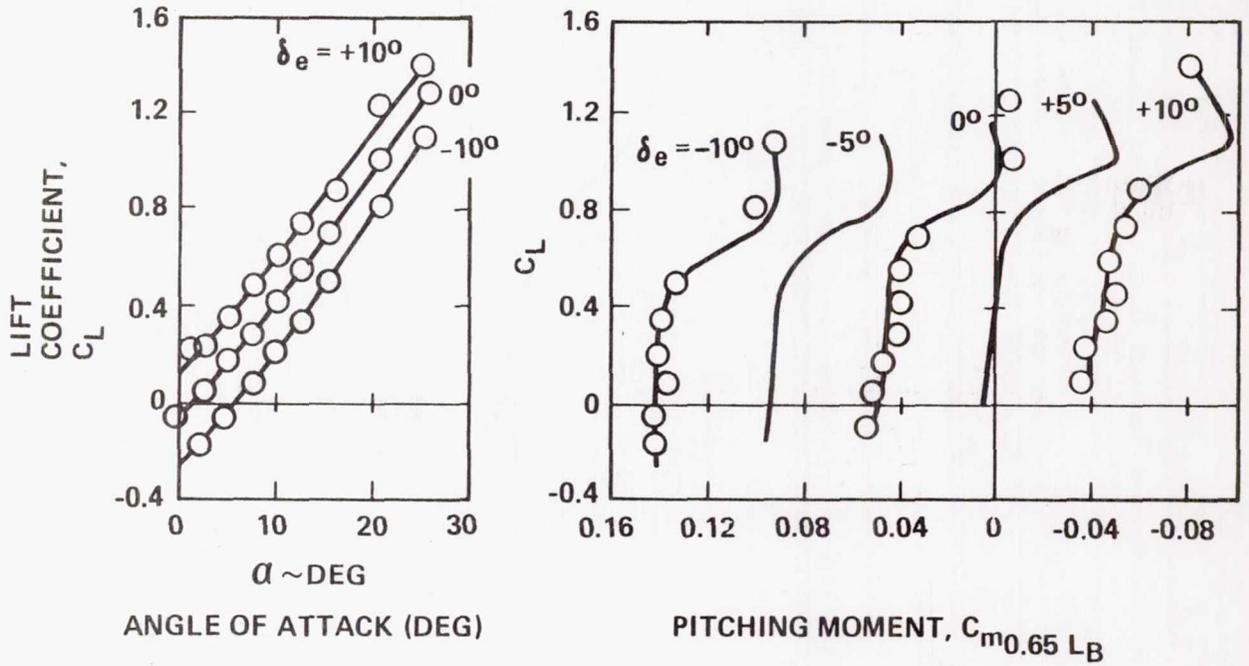
FIGURE 29.- LOW-SPEED LONGITUDINAL CHARACTERISTICS.

MACH 10

◁ AEDC AND CALSPAN

NORMAL FORCE, C_N

$\delta_e = -35^o$

0°

10°

PITCHING MOMENT, C_m

MACH 5

◇ LaRC UPWT
□ AEDC A
☆ MSFC 14 TWT

$\delta_e = -35^o$

0°

10°

PITCHING MOMENT, C_m
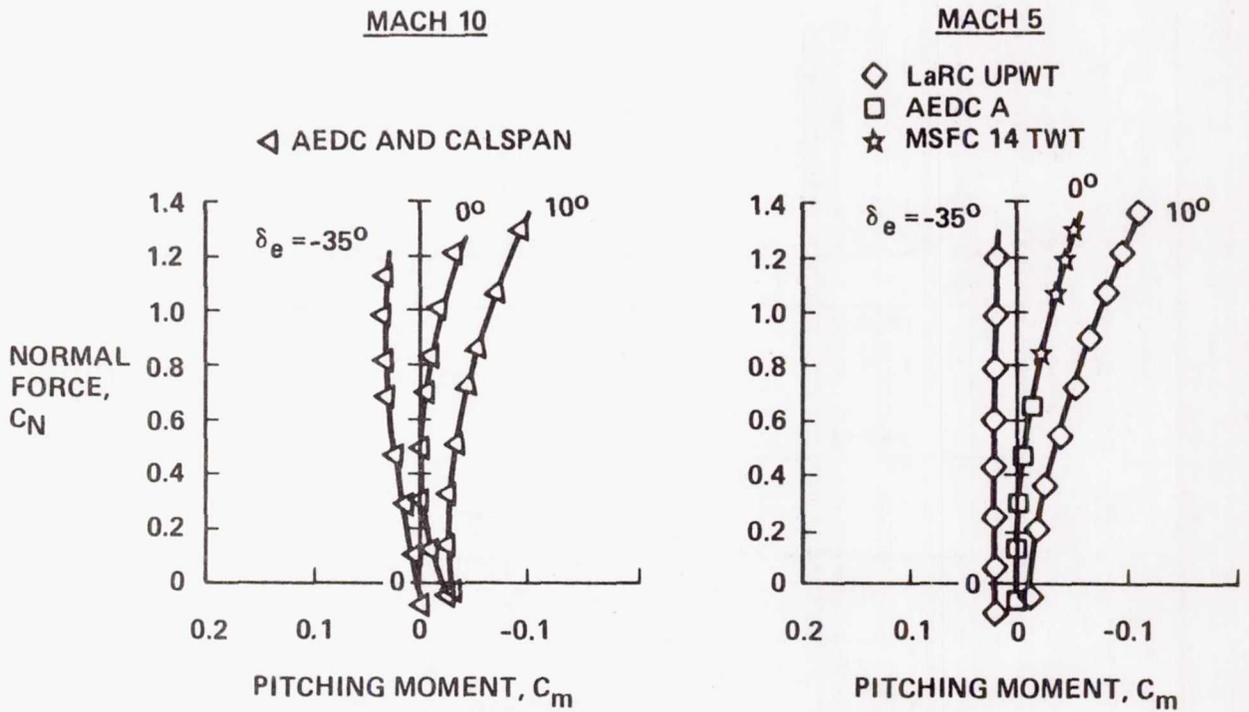
FIGURE 30.- LONGITUDINAL CHARACTERISTICS SUMMARY.

MACH 1.2   **MACH 0.6**

ARC 11 X 11 DATA

NORMAL FORCE, C_N (vertical axis)

$\delta_e = -10°$, $0°$, $10°$

$\delta_e = 0°$, $5°$, $10°$

PITCHING MOMENT, C_m PITCHING MOMENT, C_m
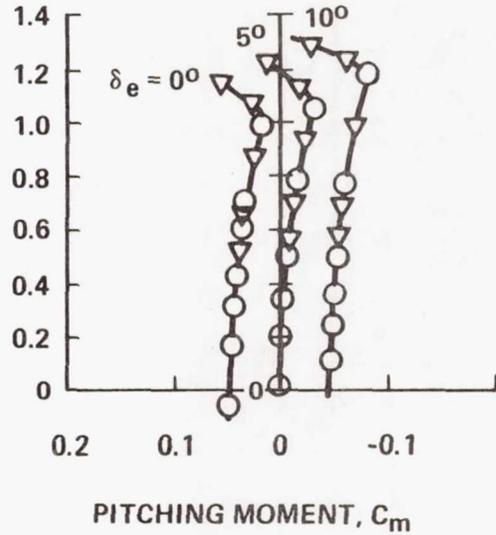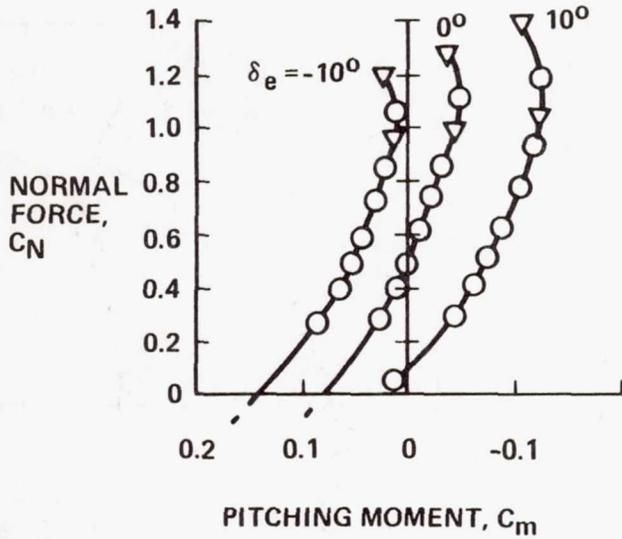
(b) SUBSONIC/SUPERSONIC.

FIGURE 30.- CONCLUDED.

$V \cos \alpha$

SHOCK-INDUCED SEPARATION

SHOCK-INDUCED SEPARATION

$\alpha < 15°$

$15° < \alpha < 30°$

$\alpha > 30°$

OBLIQUE SHOCK

SEPARATION SHOCK

(A)   (B)   (C)
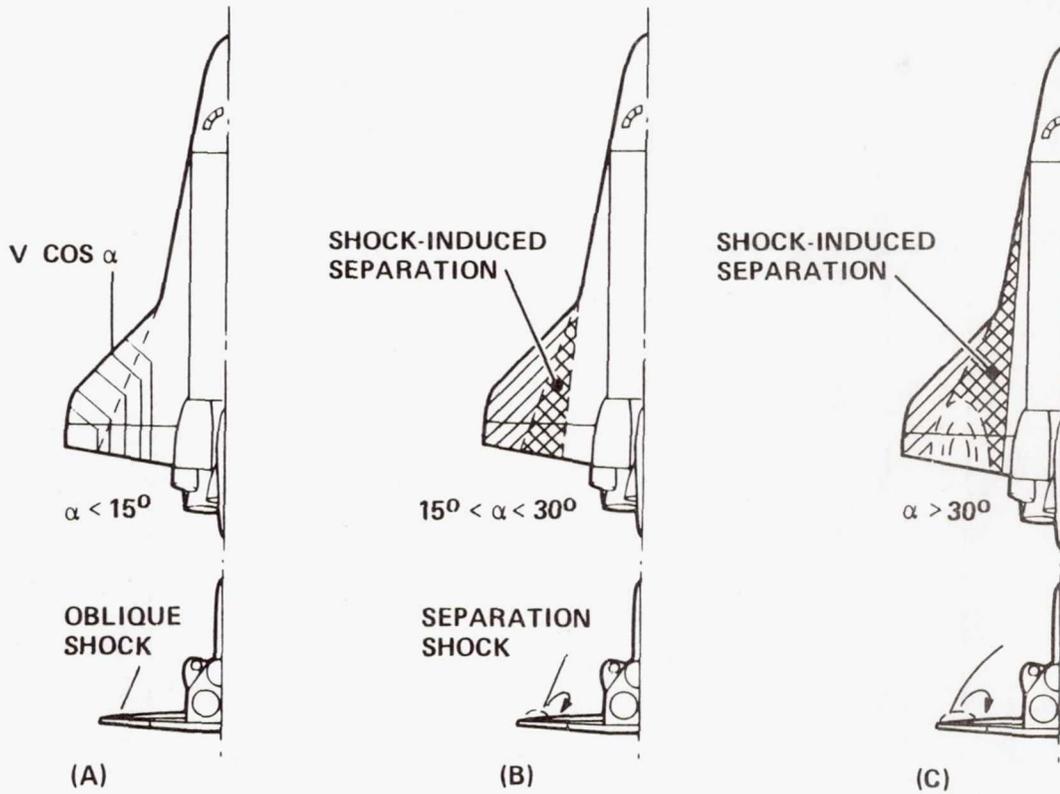
FIGURE 31.- LEESIDE FLOW PATTERNS.

ATTACHED FLOW   SHOCK INDUCED SEPARATION   LEADING EDGE SEPARATION

SHOCK
ATTACHED

SHOCK
DETACHED

$$\frac{b_s}{b} = \frac{TAN \frac{1}{M}}{TAN(\frac{\pi}{2}-\Lambda)}$$

FROM OIL FLOW
PHOTOGRAPHS

$\frac{b_s}{b}$

ANGLE OF ATTACK, DEG
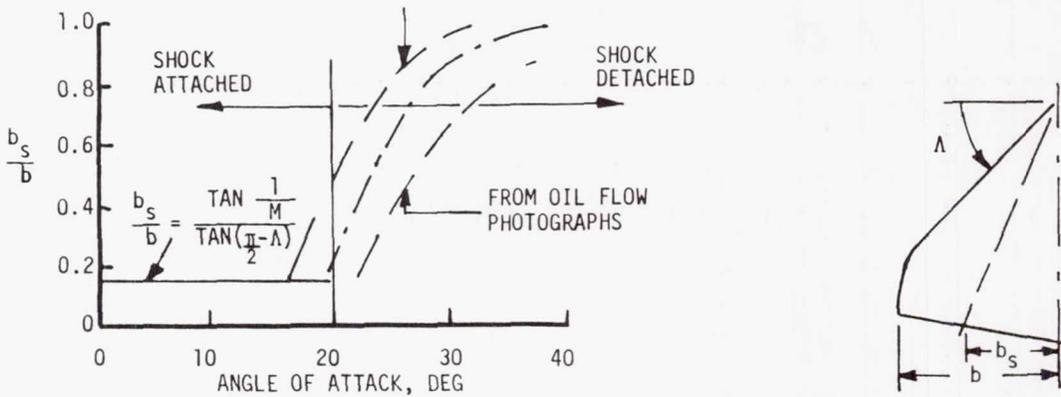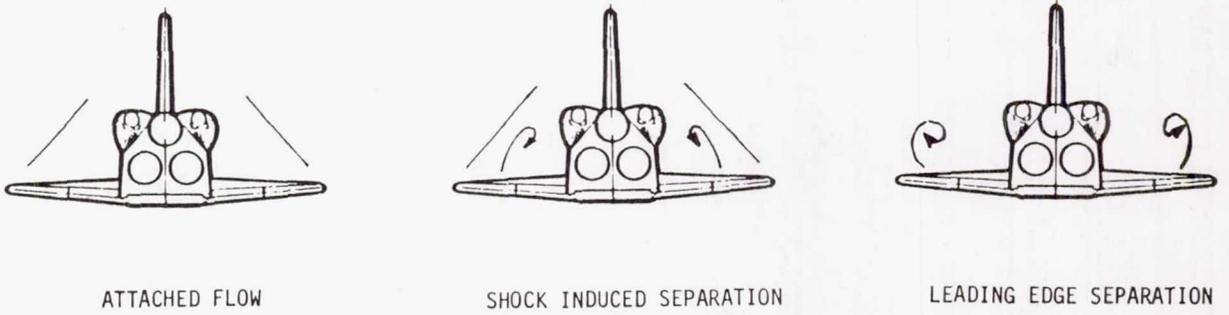
FIGURE 32.- LEESIDE FLOW BOUNDARIES.

ANGLE OF ATTACK (DEG)

SHOCK DETACHED
MACH 5.0

SHOCK DETACHED
MACH 8.0

SHOCK
DETACHED
MACH 2.5

ΔC_m
WING

CENTER OF PRESSURE (CP)
LEADING EDGE SUCTION -
LIFT GAIN

CP SHOCK-INDUCED
SEPARATION - LIFT LOSS

MOMENT CENTER

SYM	MACH	FACILITY
△	2.5	AEDC A
◇	5.0	AEDC A
◯	8.0	AEDC B
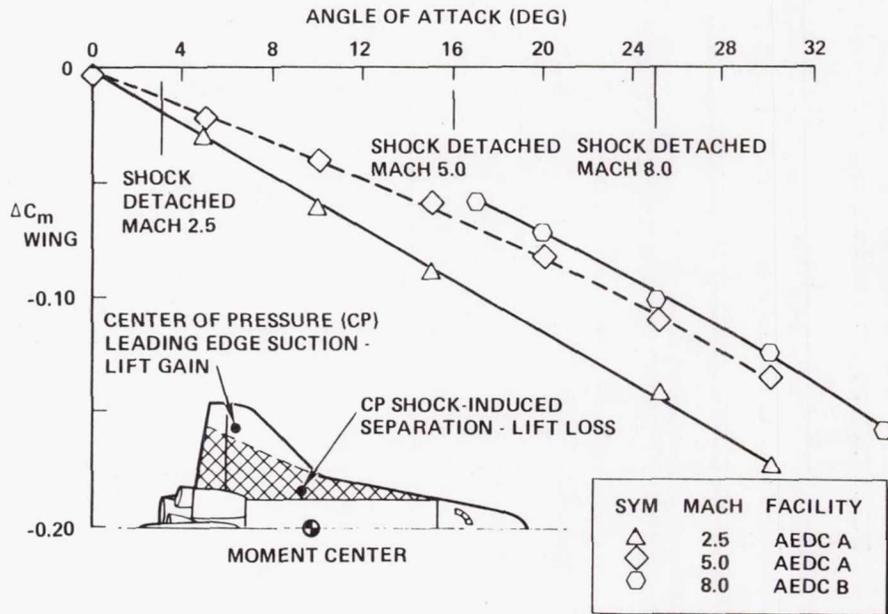
FIGURE 33.- LEESIDE FLOW SEPARATION EFFECT ON PITCH STABILITY.
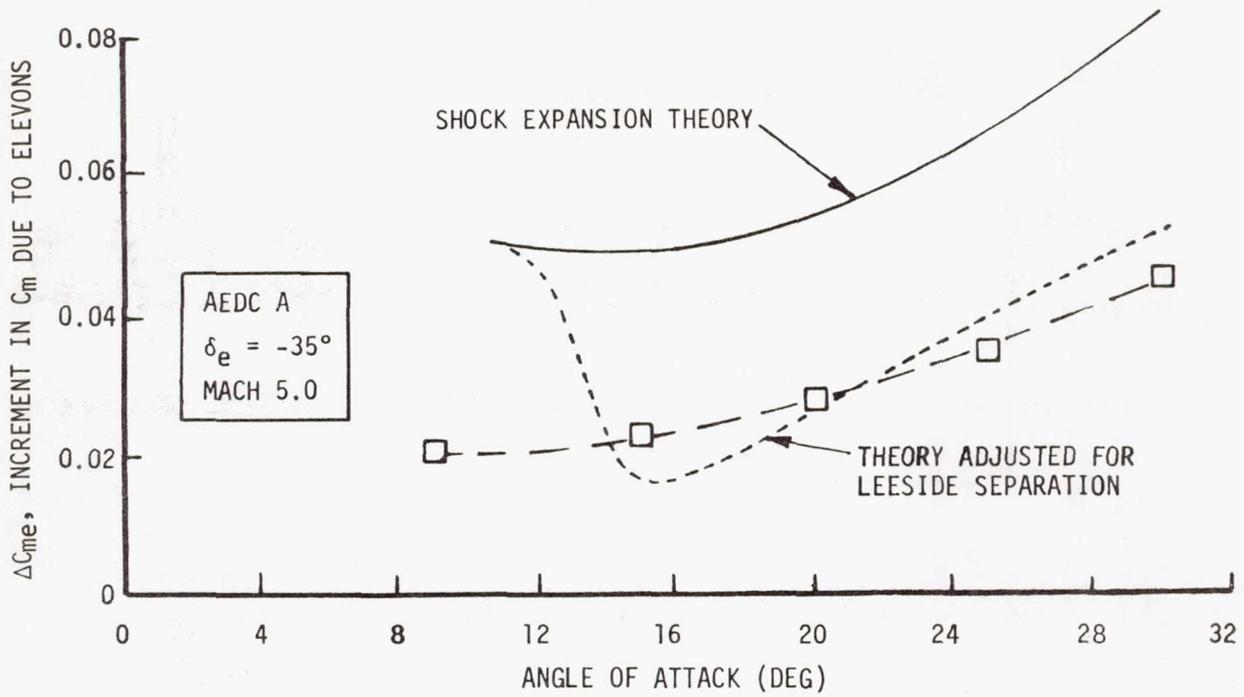
FIGURE 34.- HYPERSONIC ELEVON EFFECTIVENESS.

MACH NO.	NOM α
10.0	30
5.0	22
1.2	10
0.6	10
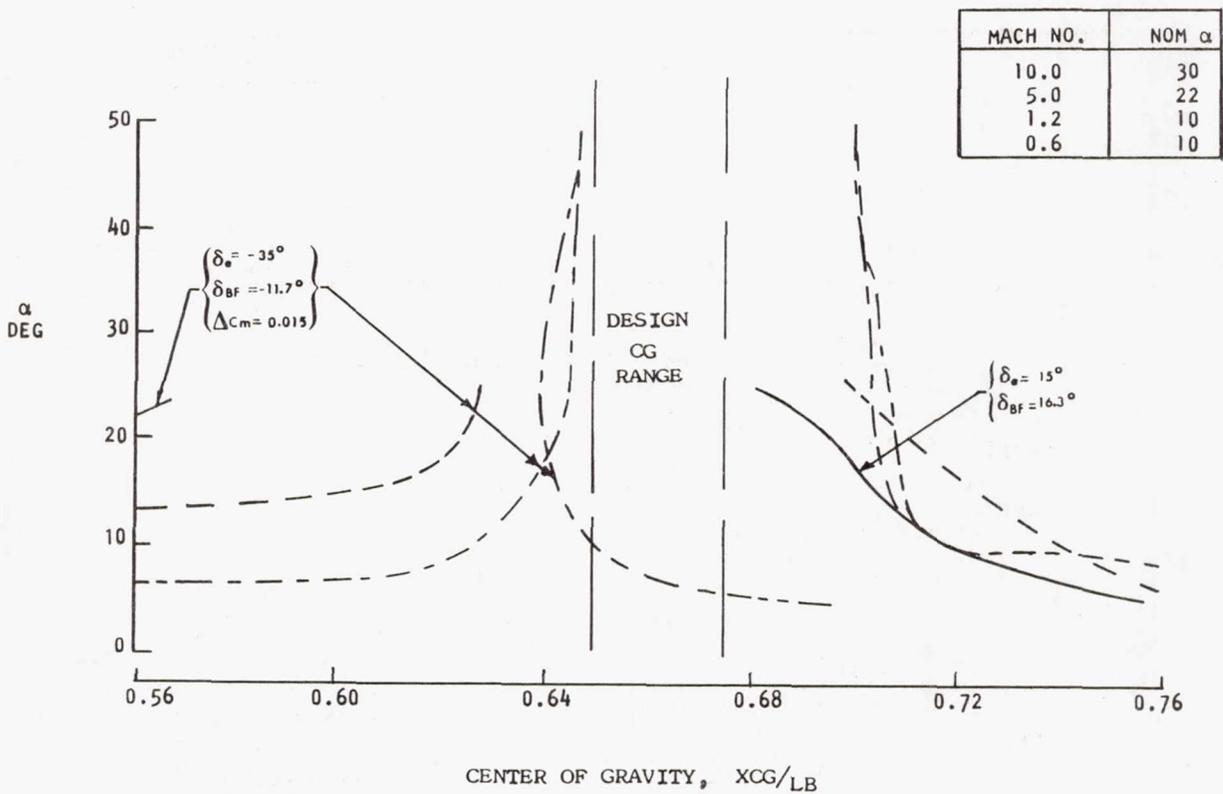
FIGURE 35.- TRIM CAPABILITY.
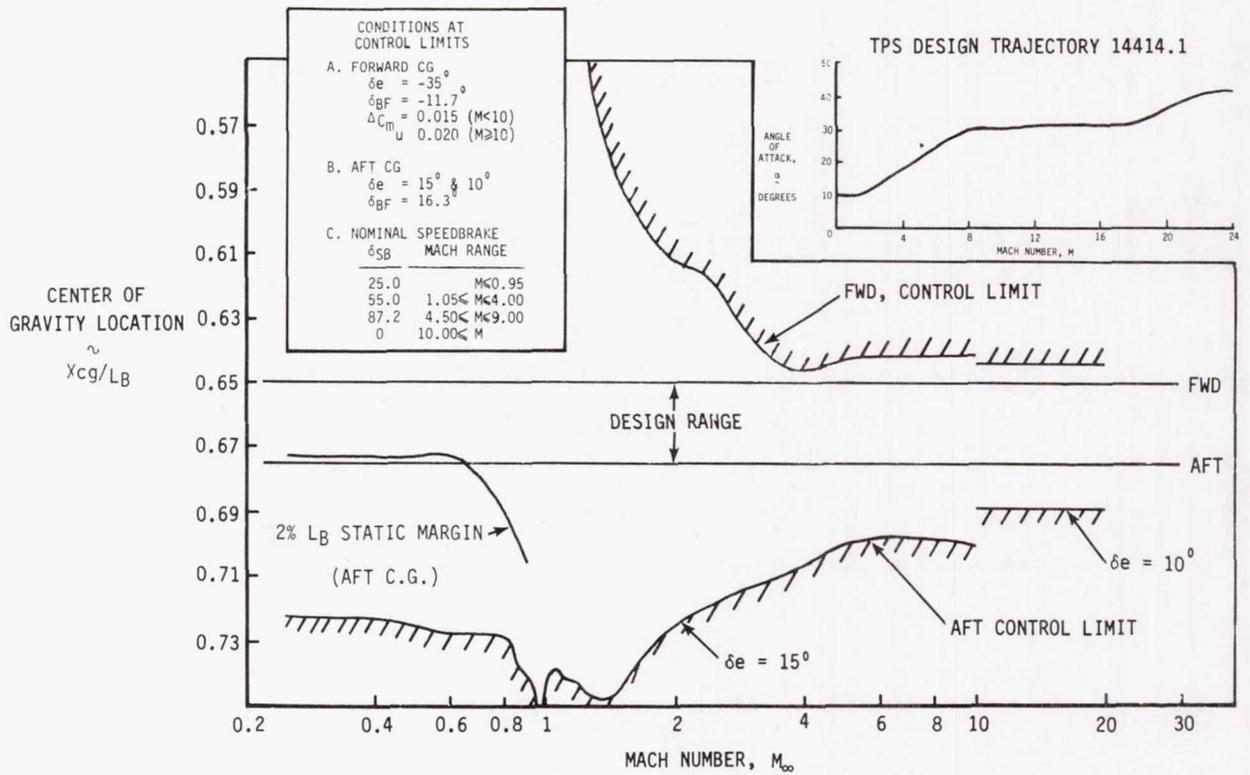
FIGURE 36.- ORBITER TRIM LIMITS.
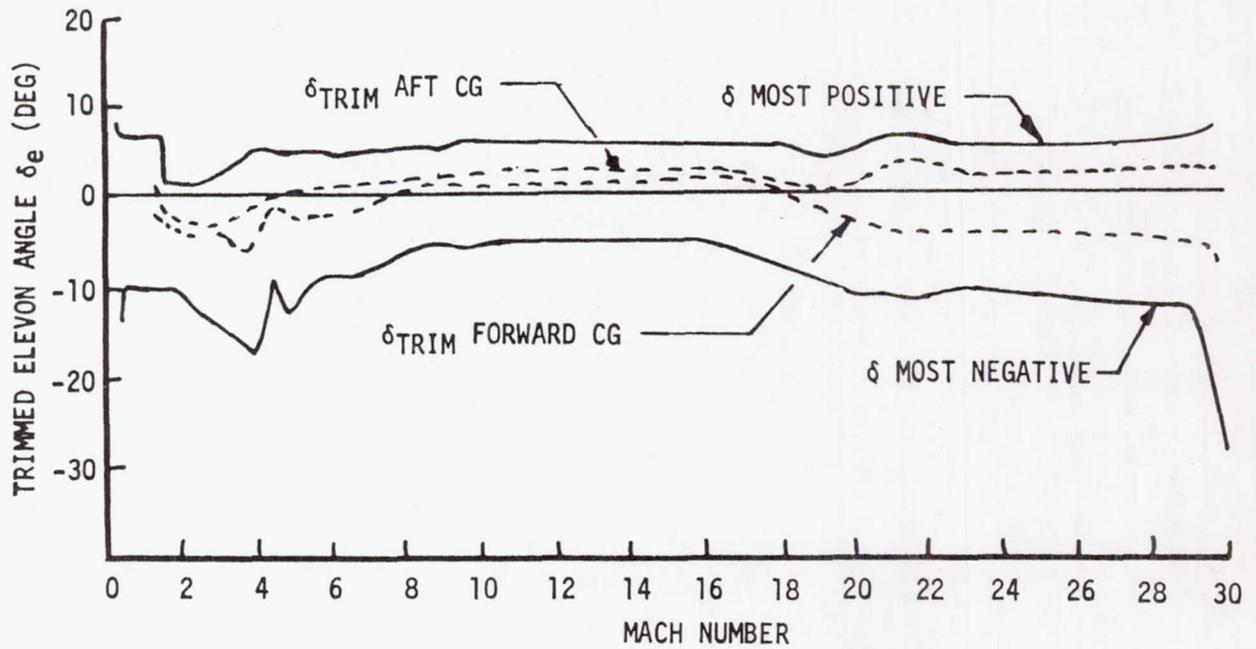
FIGURE 37.- ELEVON DEFLECTION SCHEDULE.
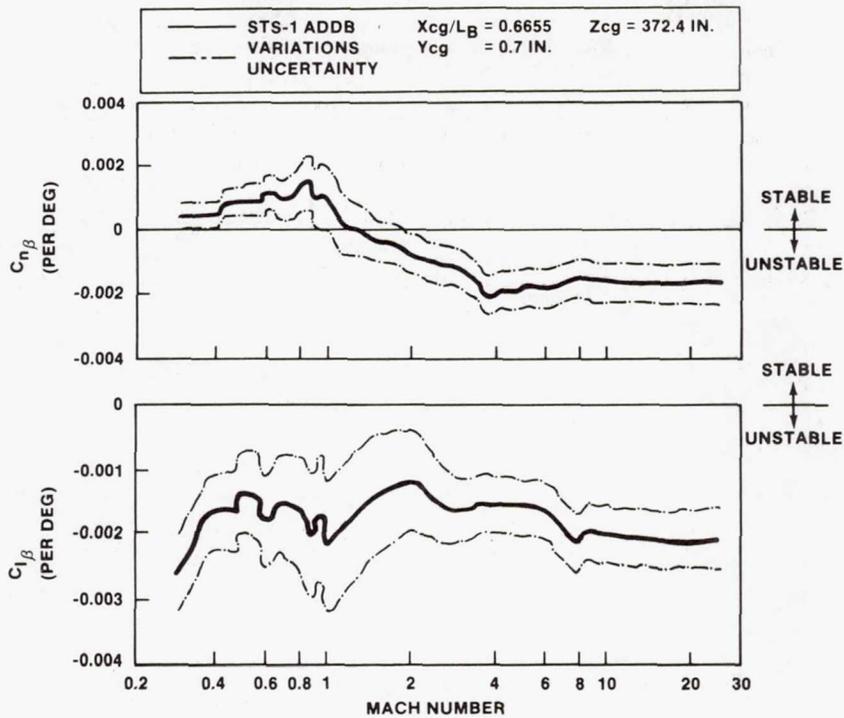
FIGURE 38.- PREDICTED LATERAL-DIRECTIONAL STABILITY.
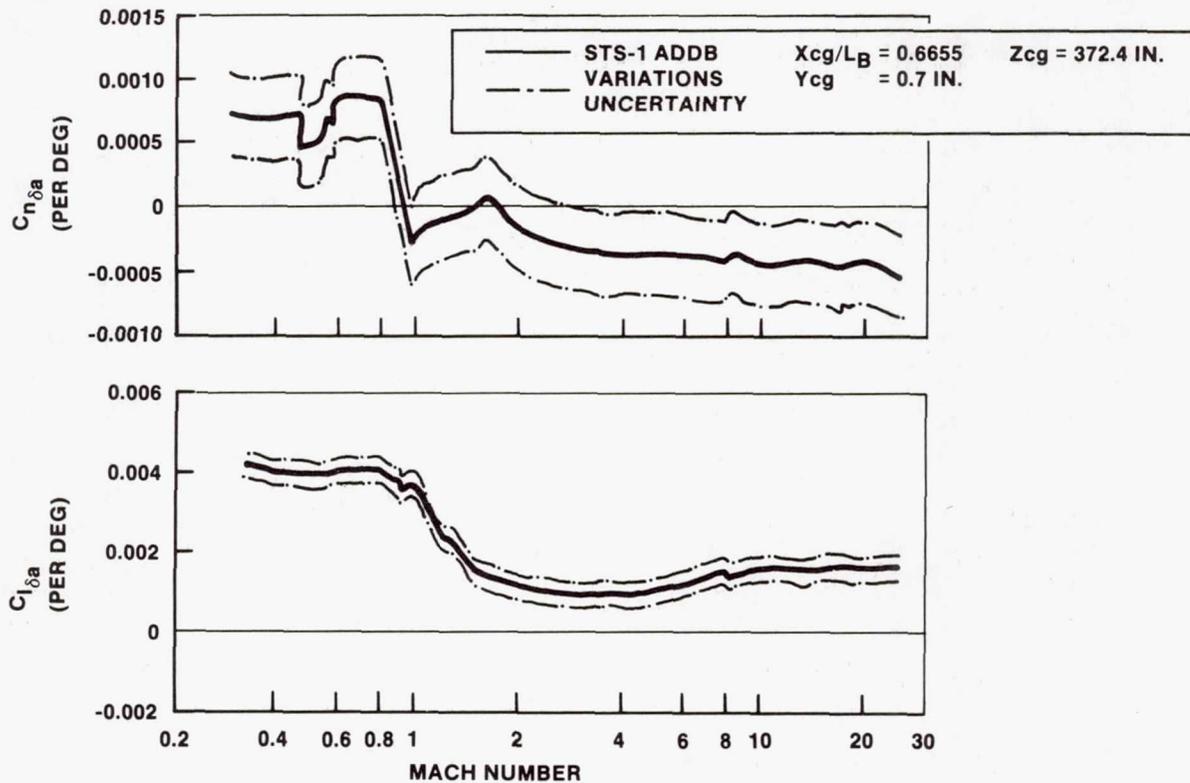
FIGURE 39.- PREDICTED AILERON EFFECTIVENESS.
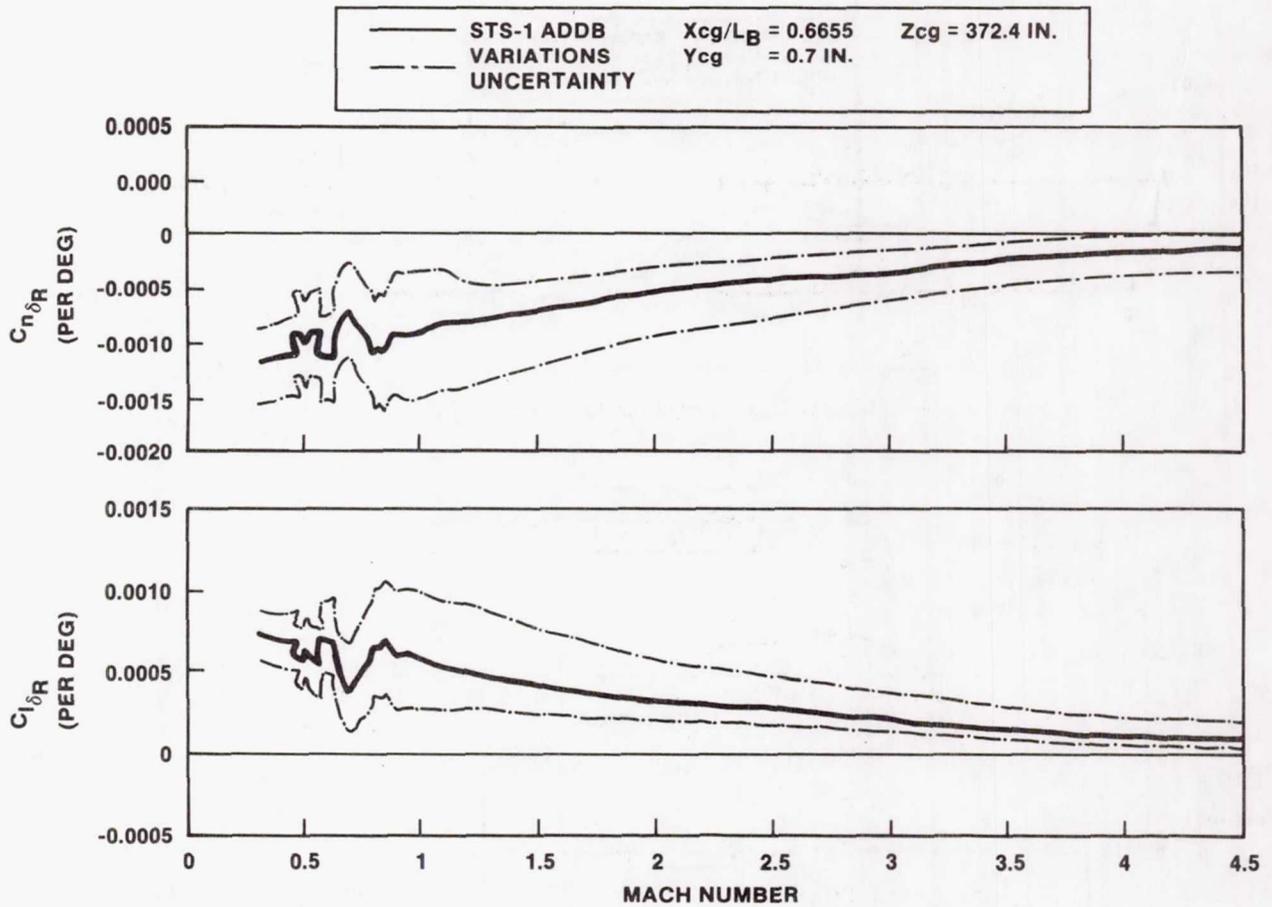
FIGURE 40.- PREDICTED RUDDER EFFECTIVENESS.
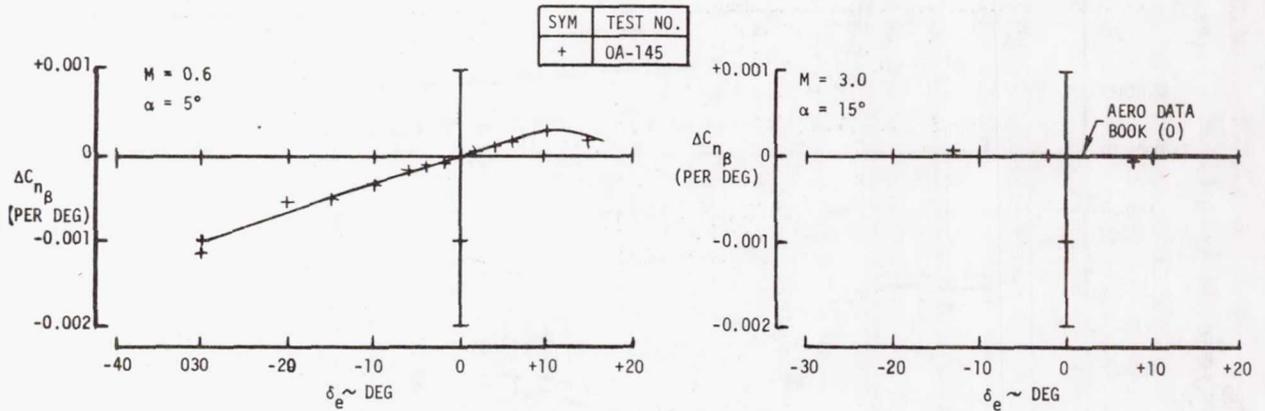
FIGURE 41.- EFFECT OF ELEVON ON DIRECTIONAL STABILITY.
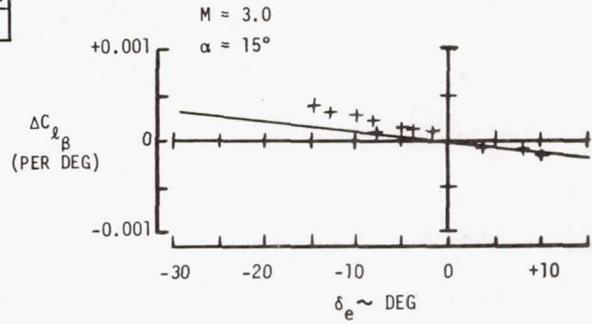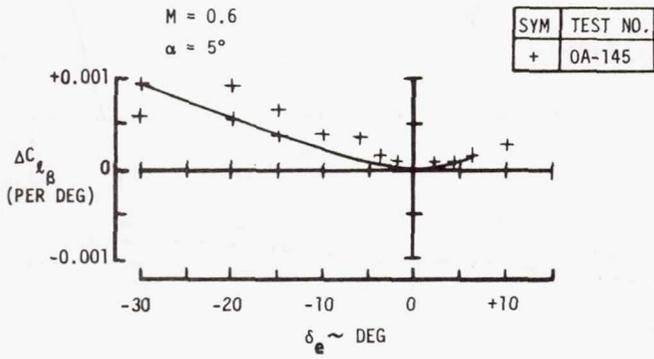
FIGURE 42.- EFFECT OF ELEVON ON DIHEDRAL STABILITY.
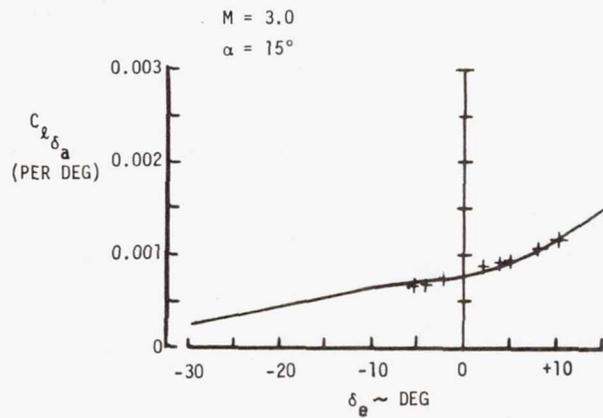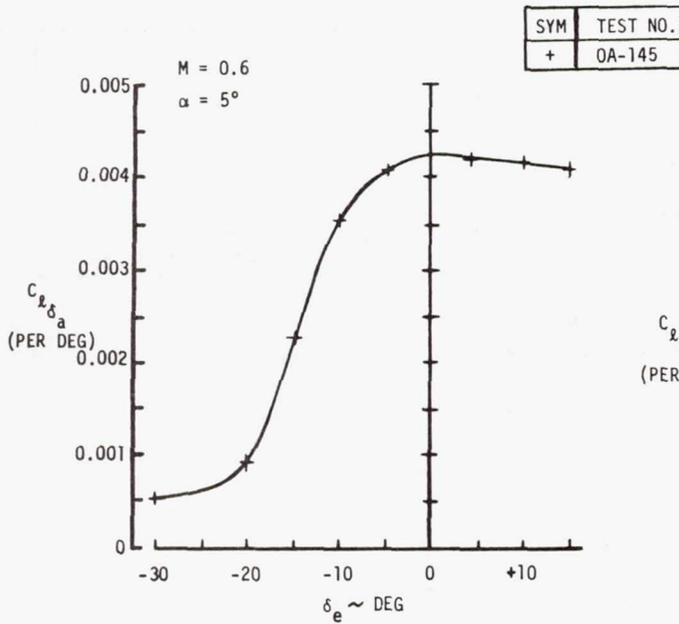
FIGURE 43.- EFFECT OF ELEVON ON AILERON ROLL DERIVATIVES.
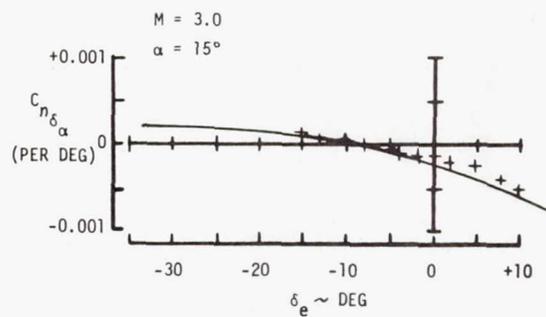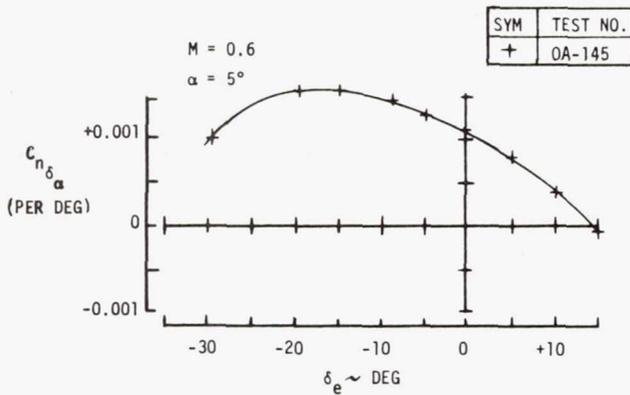
FIGURE 44.- EFFECT OF ELEVON ON AILERON YAW DERIVATIVES.
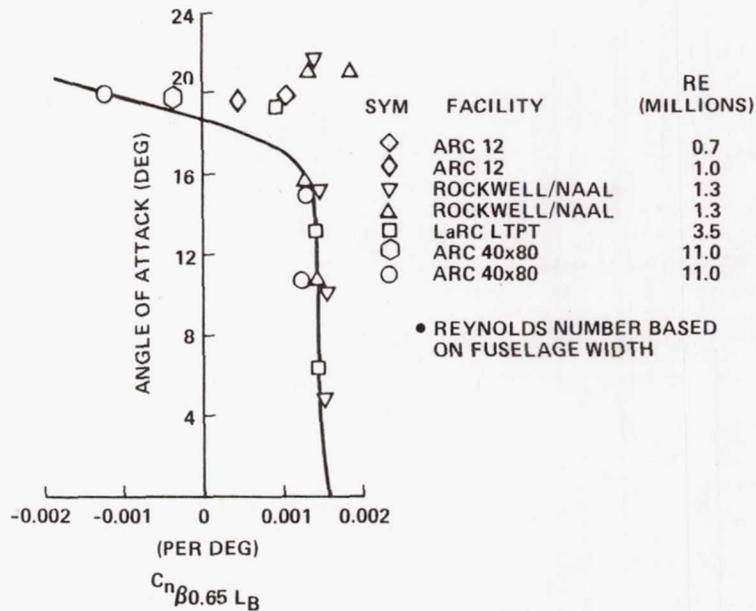
FIGURE 45.- COMBINED EFFECT OF REYNOLDS NUMBER AND ANGLE OF ATTACK ON
LOW-SPEED DIRECTIONAL STABILITY.

SYM	DATA SOURCE	FACILITY	MODEL	SCALE	ORGANIZATION
○	OA145A	ARC 11 x 11	39-0	0.050	RI
□	LA76	LTV 4 x 4	44-0	0.015	LaRC
◇	OA270A	LaRC 16T	39-0	0.050	RI
△	OA270B	LaRC 16T	105-0	0.020	RI
▽	LA77	ARC 11 x 11	44-0	0.015	LaRC
★	LA115	LaRC 8 TWT	44-0	0.015	LaRC
——	AERODYNAMIC DATA BOOK				
- - -	DATA SCATTER BOUNDARIES				
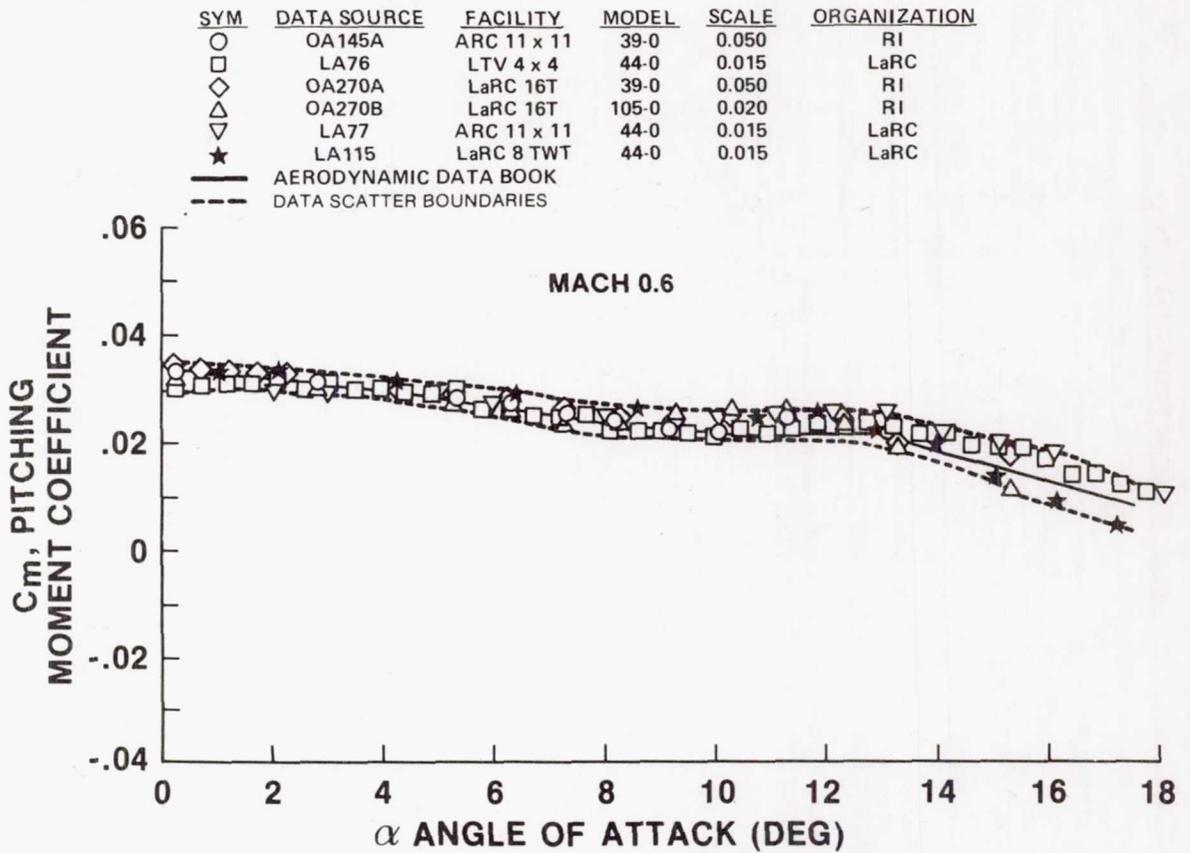
FIGURE 46.- PITCHING MOMENT DATA FOR TOLERANCES.
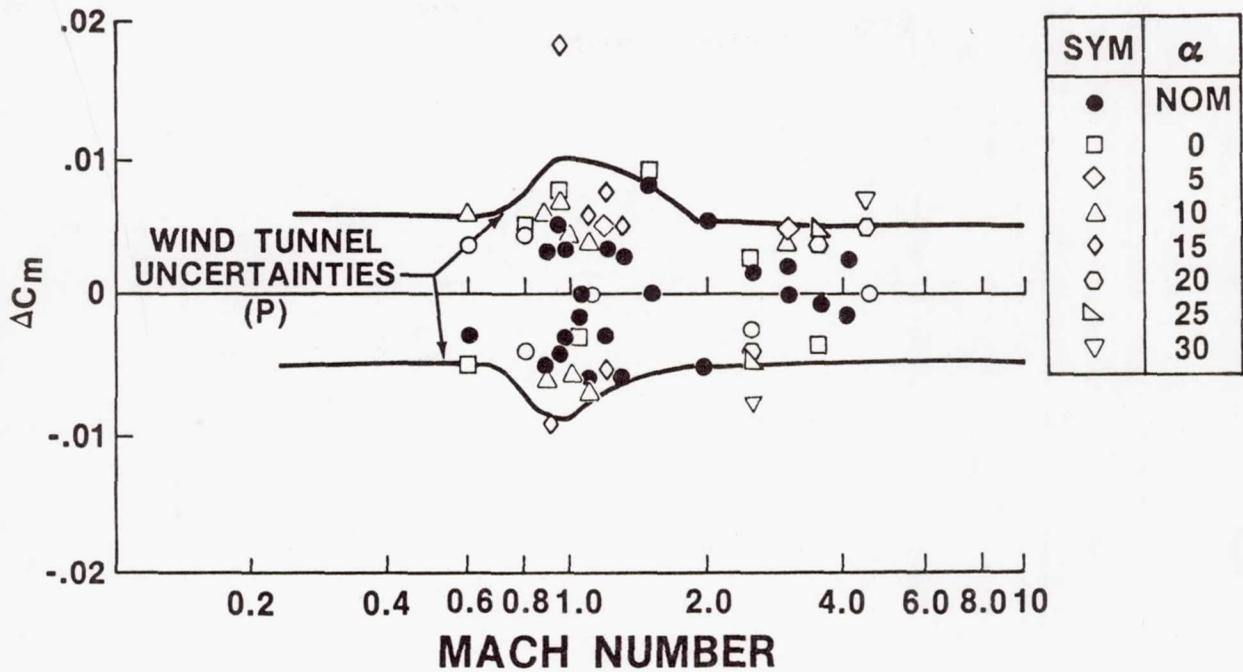
FIGURE 47.- CORRELATION OF UNCERTAINTY IN WIND TUNNEL PITCHING MOMENT
WITH MACH NUMBER.
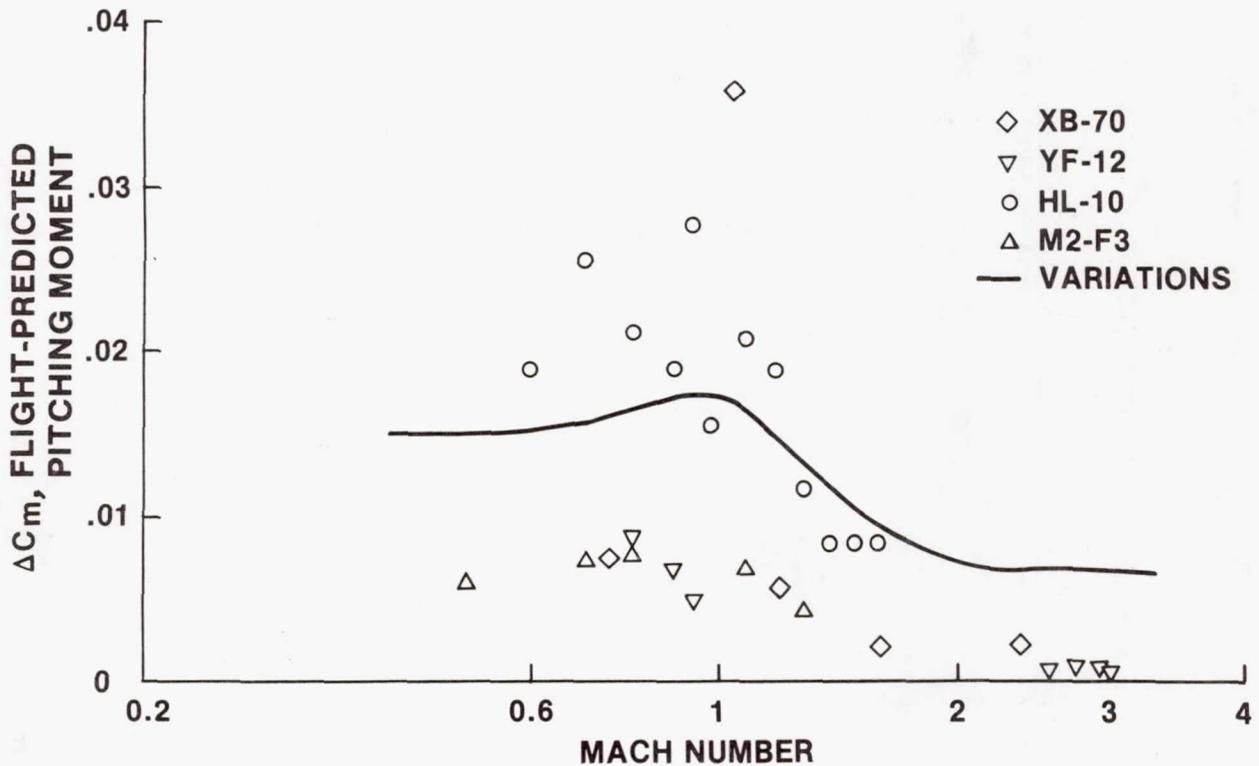
FIGURE 48.- CORRELATION OF FLIGHT AND PREDICTED PITCHING MOMENT
OF PREVIOUS AIRCRAFT.
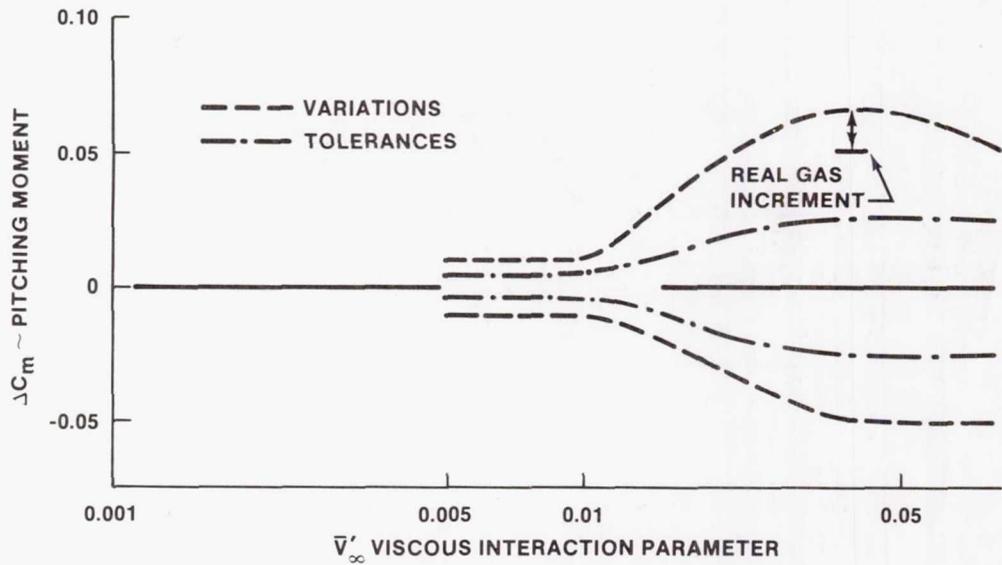
FIGURE 49.- HIGH ALTITUDE UNCERTAINTIES.
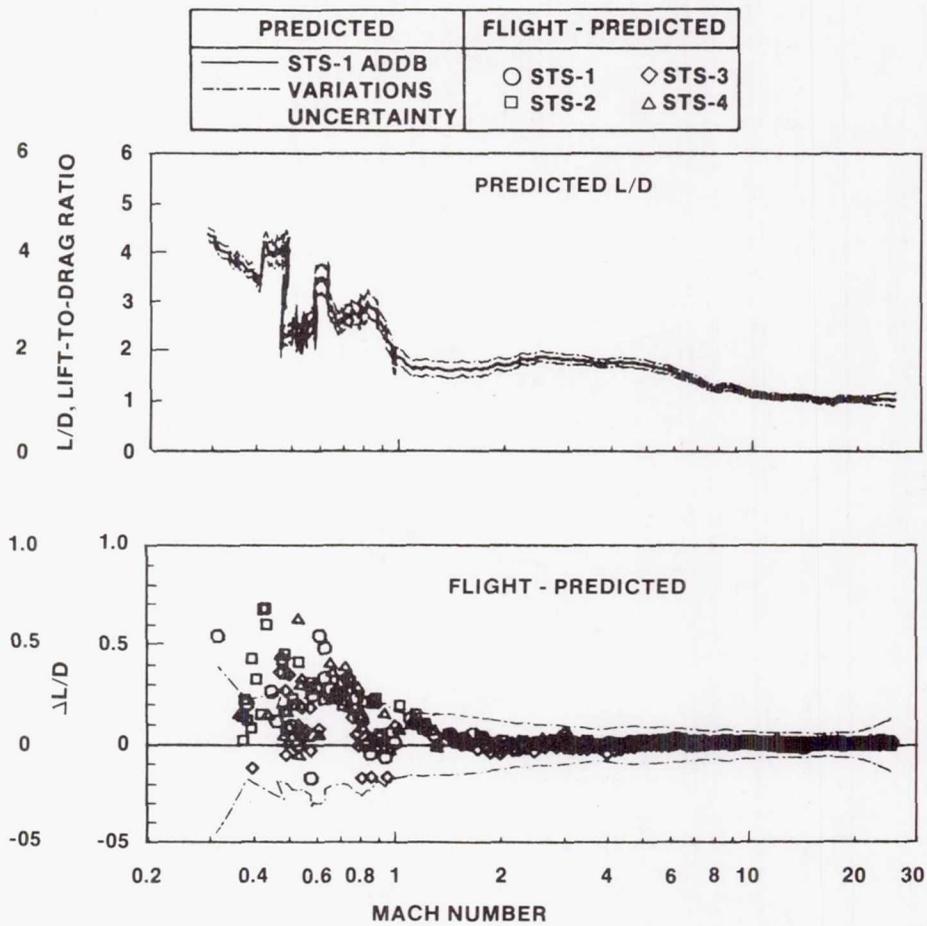
FIGURE 50.- CORRELATION OF FLIGHT WITH PREDICTED L/D.
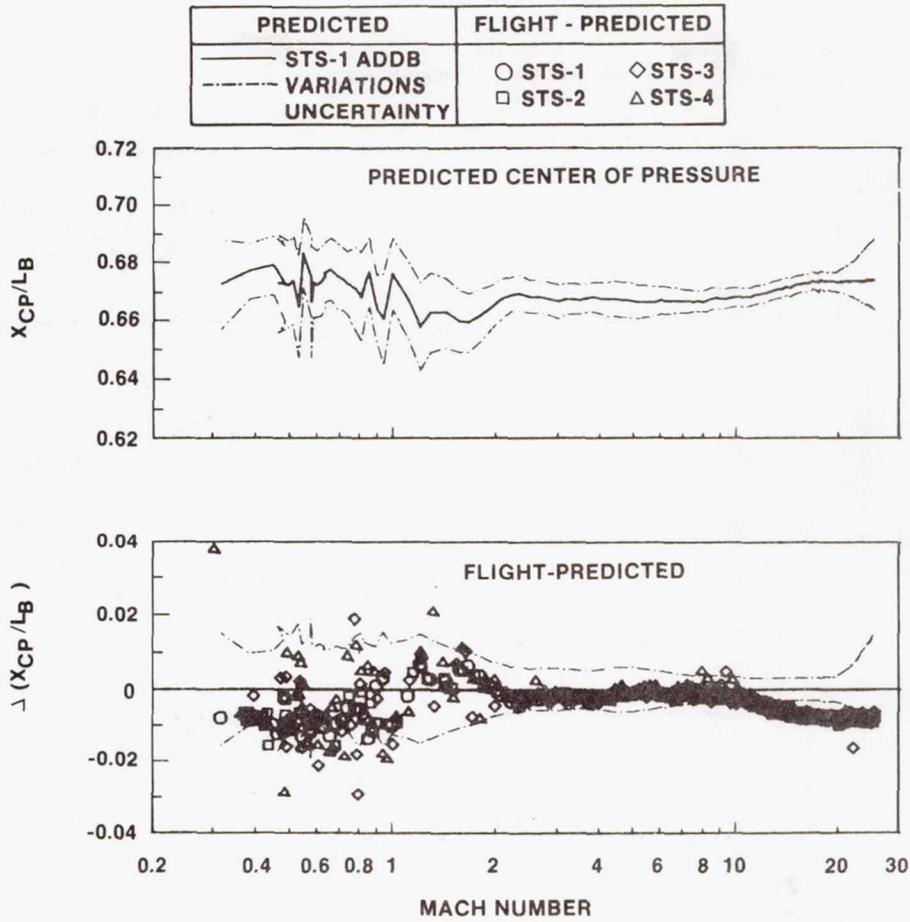
FIGURE 51.- CORRELATION OF FLIGHT WITH PREDICTED CENTER OF PRESSURE.
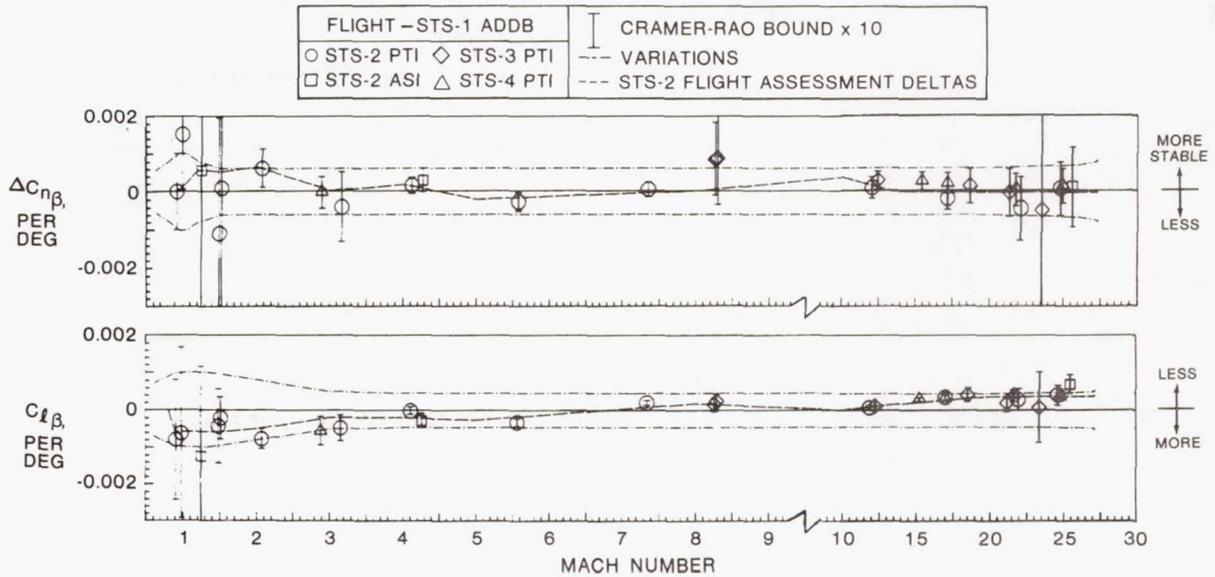
FIGURE 52.- CORRELATION OF FLIGHT WITH PREDICTED LATERAL-DIRECTIONAL STABILITY.
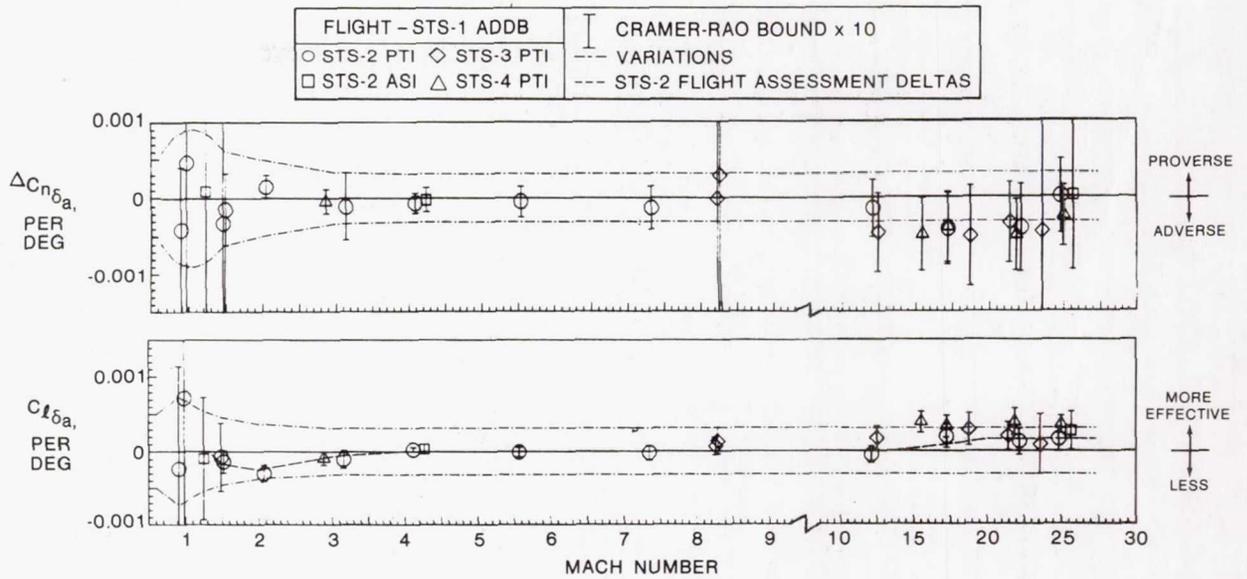
FIGURE 53.- CORRELATION OF FLIGHT WITH PREDICTED AILERON EFFECTIVENESS.
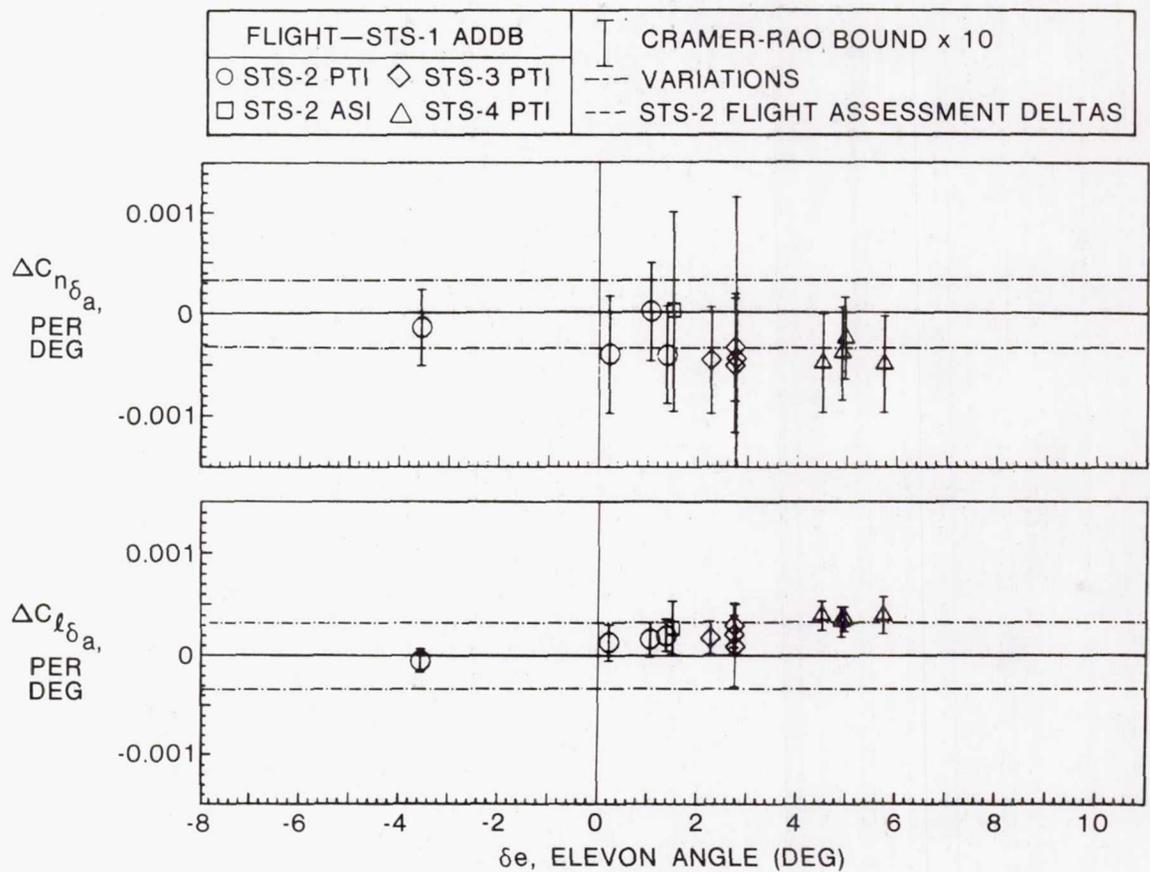
FIGURE 54.- CORRELATION OF FLIGHT WITH PREDICTED EFFECT OF ELEVON ON HYPERSONIC
AILERON EFFECTIVENESS.
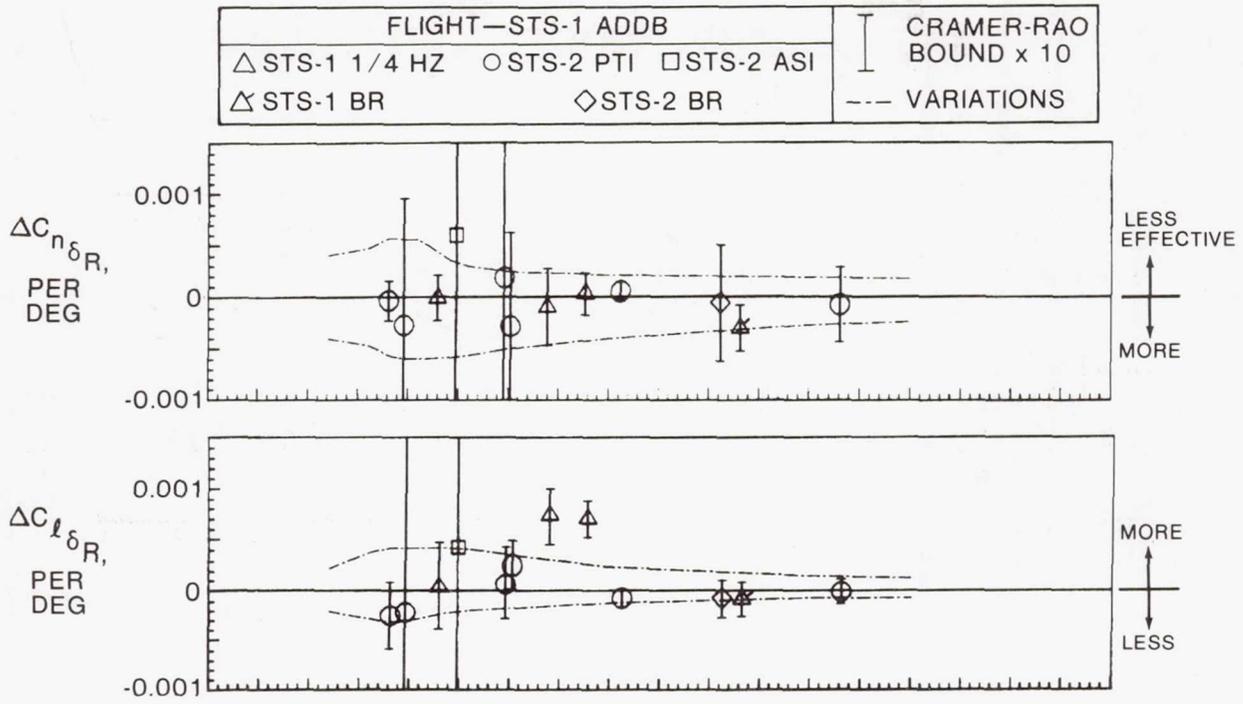
FIGURE 55.- CORRELATION OF FLIGHT WITH PREDICTED RUDDER EFFECTIVENESS.

MACH = 26   DYN PRESS = 14 PSF   ALT = 253 000 FT
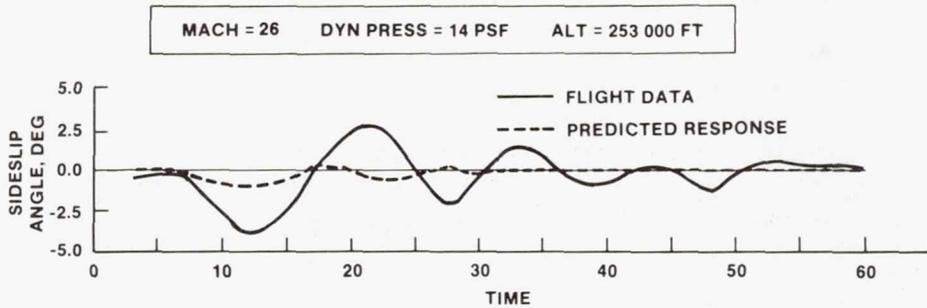
(a) OSCILLATIONS DURING STS-1 INITIAL BANK MANEUVERS.
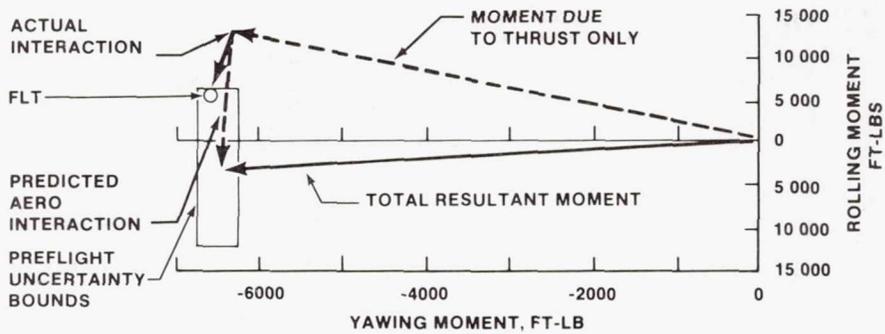
(b) EFFECT OF FLOWFIELD INTERFERENCE ON RCS JET EFFECTIVENESS.
FIGURE 56.- RCS JET INTERFERENCE DUE TO TWO SIDE-FIRING JETS.

261
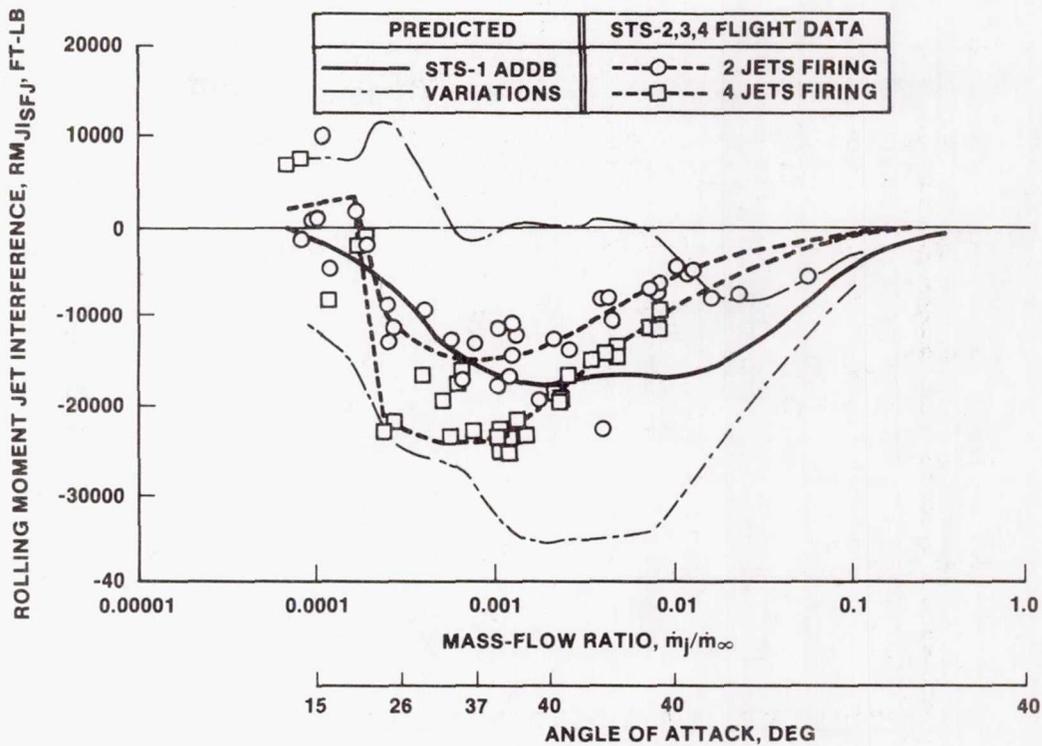
FIGURE 57.- CORRELATION OF FLIGHT WITH PREDICTED RCS
SIDE-FIRING JET INTERFERENCE.
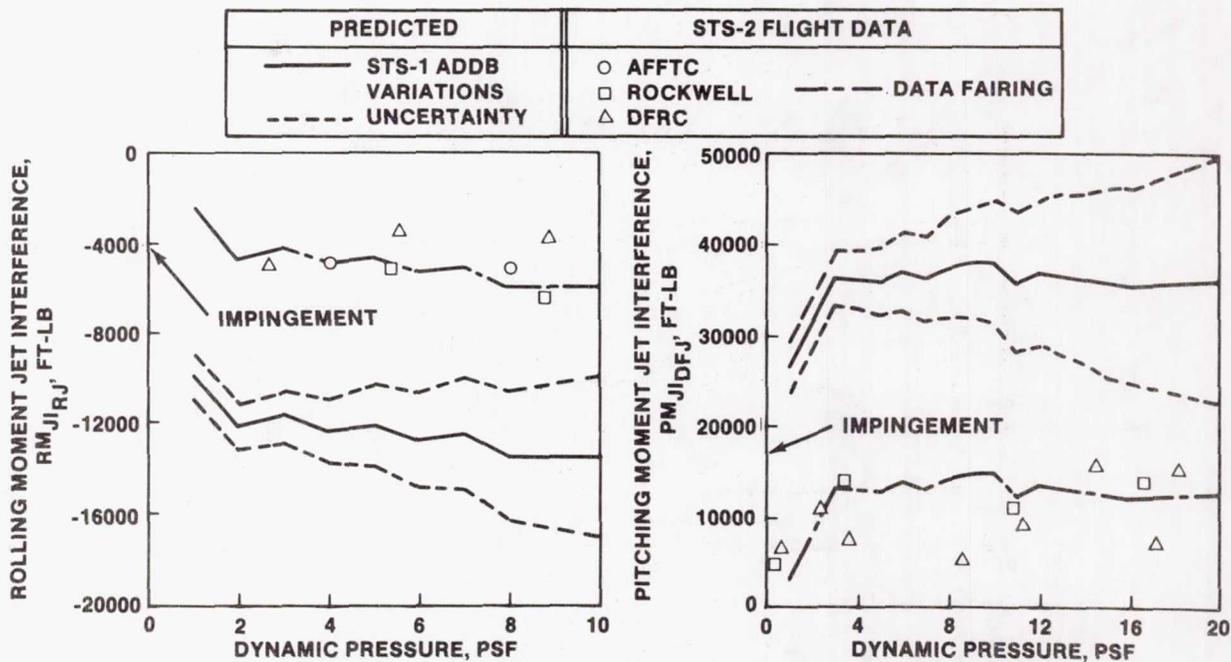
FIGURE 58.- CORRELATION OF FLIGHT WITH PREDICTED RCS JET INTERFERENCE
DUE TO UP AND DOWN FIRING JETS.

FIGURE 59.- HYPERSONIC MACH, REAL GAS, AND VISCOUS EFFECTS.

FIGURE 60.- TRIM BODYFLAP COMPARISON USING HYPERSONIC CORRECTIONS.

263

FIGURE 59.- HYPERSONIC MACH, REAL GAS, AND VISCOUS EFFECTS.

FIGURE 60.- TRIM BODYFLAP COMPARISON USING HYPERSONIC CORRECTIONS.